Synthesis of DMSO based silver nanoparticles for application in wound healing

UNIVERSITY *of the*
WESTERN CAPE

By

Zimkhitha Biancah Nqakala

(BSc Honours)

A mini thesis submitted in fulfilment of the requirements for the degree of Magister Scientiae Nanoscience in the Department of Chemistry, University of the Western
Cape.

Faculty of Science
University of the Western Cape
Cape Town / South Africa

Supervisor: Prof M.O Onani

Co-supervisor: Dr N.R.S Sibuyi

February 2021

DECLARATION

I hereby **declare** that *"**Synthesis of DMSO based silver nanoparticles for application in wound healing**"* is my own work, and that it has not been submitted for any degree or examination in any other university, and that all sources I have used or quoted have been indicated and acknowledged by complete references.

Zimkhitha Biancah Nqakala **Date: February 2021**

Signature..... .....

DEDICATION

I dedicate this thesis to my loving family “the Nqakalas”, my mother Bukelwa Nqakala, sisters Noniko Nqakala and Nombuyiselo Nqakala, brother Yamkela Nqakala and to my beautiful children Othandwayo Nqakala and Lunathi Nqakala. Your support, love and prayers have fuelled me with strength to successfully complete this project and for that I am eternally grateful.

ACKNOWLEDGEMENTS

First and foremost, I would like to thank the Almighty God for giving me the much-needed strength to complete this project, it was not easy. At times I wanted to give up but I was encouraged and motivated by his words in the book of Zechariah 4:6 " ***'Not by strength or by might, but by My Spirit**,' says the LORD of Hosts*". Indeed, it was his spirit that lifted me up, guarded and protected me throughout the course of this work and in all areas of my life.

To my supervisor **Prof Onani**, thank you so much for your guidance and direction. You are more than a supervisor, you are like a father that I never had. Thank you so much for trusting me with this work, I truly appreciate your eye for seeing potential in me.

To my co-supervisor **Dr Nicole**, I idolise you, you are the kind of scientist I aspire to be. Thank you for being patient with me and pushing me to work harder than I have ever before. Your honesty and constructive criticism fuelled me to complete this work.

To **Dr Fadaka**, my mentor, thank you so much "mntase" for all you have done for me. Working with you has truly been a blessing. Thank you for sacrificing your time and assisting me in the lab. Without your assistance and mentorship, I wouldn't have been able to successfully complete this project.

To **Prof Meyer**, I appreciate you for opening up your lab and allowing me to use the resources freely. In addition, I would like to show my deepest appreciation to the rest of the **NIC** and **Nanomaterials & Organometallic** groups for creating a positive working atmosphere.

I would also like to acknowledge the **DST** for funding this work through the **Nanoscience programme**. The contributions of the **chemistry**, **biotechnology**, **physics** and **pharmacy** department staff members at **UWC** for their analysis expertise is dully noted and appreciated.

To my grandmother **Nothandekile** and my cousins **Esekho**, **SipheSihle**, **Ntando**, **Myolisi**, **Bonakele**, **Lonwabo**, **Ayabonga** and **Anovuyo**, I love you all.

Last but not least, from the bottom of my heart, I would like to thank the real "gang gang", my siblings **Noniko**, **Nombuyiselo** and **Yamkela** for keeping me in their prayers and motivating me when I am weary. To my kids, **Othandwayo** and **Lunathi**, mommy loves you very much. Sincerely, special thanks and appreciation goes to my mother, my rock **Bukelwa Nqakala**, who is raising my kids and allowing me to be here and chase my dreams instead, mom you are a king.

Abstract

Silver nanoparticles (AgNPs) apart from being chemically significant, have shown a lot of health benefits, the most studied being their anti-bacterial and anti-inflammatory properties. These biological properties can be further enhanced by adding compounds with known medical properties giving rise to even more desired potent materials. Anti-bacterial and cytotoxicity studies show that these AgNPs can kill bacteria, prevent infections and regenerate skin cells. On the other hand, previous studies have reported dimethyl sulfoxide (DMSO) with attractive wound healing abilities specifically cell growth promotion. It was then envisaged that the combination of DMSO and AgNPs could lead to a potent wound healing agent. It is a well-known fact that non-healing wounds pose a socioeconomic threat to a large population worldwide. Thus, a formulation that can afford fast and complete wound healing would be highly significant. The combination of DMSO and AgNPs was proposed for this purpose since it is thought that it can afford better healing by accelerating the wound healing rate through the synergic effect of their individual properties.

Various concentrations of DMSO were used as solvents in AgNP synthesis through chemical reduction using sodium borohydride ($NaBH_4$) as a reducing agent. 3%, 4% and 100% DMSO-AgNPs along with Bare-AgNPs were characterized using various analytical techniques and evaluated for their biological applications. The presence of DMSO in the AgNPs caused a red shift in the SPR band when compared to the Bare-AgNPs, this shift increased with an increase in DMSO concentration. Overall, the 4% DMSO-AgNPs showed better anti-bacterial activity against both gram-negative and gram-positive bacteria i.e. *E. coli* and *S. aureus* compared to the other AgNPs. The 4% DMSO-AgNPs showed better biocompatibility with human skin cells (KMST-6 > HaCaT) compared with Chinese Hamster Ovary (CHO) cells at all tested concentrations in a time course of 72 hours. Darkfield (DF) microscopy also revealed that the 4% DMSO-AgNPs were better internalized by cells and localized in the cytoplasm than the other AgNPs in the following order: CHO > KMST-6 > HaCaT. Furthermore, the 4% DMSO-AgNPs showed an accelerated wound migration rate at 48 hours post treatment as well as higher cell viability. As a result, the 4% DMSO-AgNPs showed the synergic effect of DMSO and AgNPs by promoting cell proliferation, negligible cytotoxicity and anti-bacterial action resulting in a faster rate of healing. Therefore, the 4% DMSO-AgNPs can be potentially suitable for formulation of wound dressing agents for treatment of wounds. Further studies are warranted to validate these activities *in vivo*.

Keywords:

Cellular uptake

Cytotoxicity

Dimethyl sulfoxide

Membrane Mitochondrial Potential

Nanotechnology

Reactive oxygen species

Silver nanoparticles

Wound healing

Table of Contents

List of Figures

List of Tables

Thesis overview

The thesis is structured into four chapters as outlined below:

Chapter 1

This is an introductory chapter that gives a detailed literature review, it begins with the introduction to wounds, their types and classifications. A comprehensive explanation of wound healing as well as factors that impair the process. The history of silver and silver-based therapies for application in the wound healing process leading up to AgNPs is also discussed herein. Nanotechnology and nanomaterials are also briefly introduced, with the role of AgNPs in the wound healing as the focal point of this chapter. Also, the synthesis, and properties that make AgNPs excel in wound healing are discussed in detail, followed by a quick mention of their applications in various fields. The chapter closes off with the hypothesis as well as aims and objectives of the study.

Chapter 2

This chapter leads with a list of all the materials, reagents, cells lines and analytical techniques used throughout this study. Followed by a detailed procedure to synthesize AgNPs using DMSO and sodium borohydride as reducing agents. The analytical techniques employed to characterize and monitor the behaviour of the AgNPs are also explained. Lastly, the chapter describes the bioactivity assays of the AgNPs used to study their anti-bacterial effects through agar well diffusion method, cellular uptake using DF microscopy, cytotoxicity of the AgNPs using the MTT assay, wound healing studies using cell migration assay, and lastly the methods used to study their effect on the cell integrity using ROS and TMRE assays.

Chapter 3

The synthetic outcomes for the bare-AgNPs and DMSO-AgNPs are presented in this chapter followed by their characterization using various techniques; i.e. UV-vis, FTIR, SAXS, HR-TEM and DLS. The antibacterial activity of bare-AgNPs and DMSO-AgNPs against various

bacterial strands is also discussed in this chapter. The outcome of the MTT assay cytotoxicity and cellular uptake by DF microscopy studies of bare-AgNPs and DMSO-AgNPs on CHO, KMST-6 and HaCaT cells is also presented here. The chapter closes of with evaluation of wound healing, and cellular integrity of bare-AgNPs and DMSO-AgNPs on KMST-6 cells.

Chapter 4

This chapter summarized the findings obtained from the synthesis, characterization and biological applications of bare-AgNPs and DMSO-AgNPs. It also links the specific aims and objectives to the outcomes of the study. Furthermore, recommendations and future works are briefly discussed.

Problem statement and Rationale

Each year, the global market is flooded with new formulations which claim to have improved actions compared to the previously released wound treatment therapies (Berthet et al., 2017; Singla et al., 2017; Rajendran et al., 2018; Mihai et al., 2019). By this sole reason, it is clear that a problem exists with the conventional wound healing therapies. Furthermore, wound treatment and management products incur a huge economic burden on the healthcare system. For instance, in the US alone ≥6 million of its population is negatively affected by wounds every year and spends around 25 billion USD on wound treatment and management (Parani et al., 2016). Diabetes is among the major contributing factors to the financial strain caused by wounds, and one of the top 7% causes of deaths. Around 422 million people in the world are diabetic, (World health organization, 2016), of which 25% is estimated to develop a foot ulcer at least once in their life. Lower limb amputation is often considered to inhibit the infection and growth of the non-healing wounds (Parani et al., 2016; Kaur et al., 2019; Nethi et al., 2019). Roughly 9 billion USD per annum is spent on patients and surgeons to carryout lower limb amputations, an additional 15 billion USD is utilized for managing the wound scarring (Nethi et al., 2019). Prolonged hospital stay will also add to the costs. Lower limb amputation is associated with reduced quality of life, and increased mortality rates as 80% of the diabetic patients who undergo lower limb amputation are reported to die within 5 years (Parani et al., 2016; Kaur et al., 2019; Nethi et al., 2019).

Honey, maggots, propolis, larvae and plant extracts like aloe vera and vinca rosea are popularly used as conventional wound treatment therapies across the world (Mihai et al., 2019; Nethi et al., 2019). This stems from their vital roles in wound care and management such as re-epithelization, aiding wound debridement and skin regeneration. While current clinical wound treatment therapies include vascular surgery, bioengineered cell construct, hyperbaric oxygen therapy, negative wound pressure therapy and dressing materials (Kaur et al., 2019; Nethi et al., 2019). In spite of their potential, all of these wound treatment therapies are flooded with factors that limit their usage such as high risks of infection, allergic reactions, draining moisture in the wounded area, and batch to batch differences, etc (Kaur et al., 2019; Nethi et al., 2019). Furthermore, current wound treatment therapies are very costly and not readily available to low income areas and the elderly, which are the two main groups affected by health and socioeconomic factors associated with nonhealing wounds (Parani et al., 2016; Hamdan et al., 2017; Kaur et al., 2019; Nethi et al., 2019). Many other medications have also been explored for wound healing purposes such as chemotherapeutic drugs, glucocorticoid steroids and nonsteroidal anti-inflammatory drugs (Kaur et al., 2019; Nethi et al., 2019). These also impair wound healing in numerous ways including decreasing cellular movement to the harmed area, poor bone healing and obstruction of prostaglandin generation. Moreover, these drugs lower immunity, diminish the flow of oxygen in and out the wound, halt fibroblast production and tamper with collagen generation resulting in delayed wound healing (Nethi et al., 2019).

Therefore, new, innovative and practical strategies and/or formulations are required to address the limitations of existing wound treatment therapies (Nethi et al., 2019) . These novel materials need to be nontoxic, lower the rate of infection and speed up wound healing. Nanotechnology has taken centre stage in this movement ever since its discovery. It is an interdisciplinary field that deals with the fabrication, assembly and utilization of small materials with a diameter of 100 nm (Bansod et al., 2015; Bhatia, 2016; Ovais et al., 2018). Metallic nanoparticles have a high surface area to volume ratio which results in a variety of intrinsic properties that are not present in their bulk counterparts (Hasan, 2015; Mihai et al., 2019). Such physical, chemical, and biological properties make these nanoparticles feasible for many medical applications including wound healing (Vijayakumar et al., 2019). Their small size and high reactivity enable them to penetrate deeper into the wound site and afford better association with biological subjects as well as delivering other therapeutics, leading to accelerated healing process (Hamdan et al., 2017; Khan, Malik, et al., 2018). Moreover, metallic nanoparticles have

enhanced mechanical strength, controlled release and bactericidal effects against both fungi and bacteria, further making them excellent candidates for wound care and management (Parani et al., 2016). Among these, AgNPs are the most researched, highly utilized and commercialized nanomaterials for various medical purposes, more especially in the wound healing process (Hasan, 2015; Medici et al., 2019a). This stems from their excellent anti-microbial activity, since antiquity silver and its derivatives have been used to avert the occurrence of infections during wound healing (Konop et al., 2016; Medici et al., 2019a). Although prolonged exposure to silver therapies leads to adverse toxic outcomes such as skin discolouration; this issue is not encountered with AgNPs, especially when used at lower concentrations (Medici et al., 2019a). Thus, AgNPs are better wound healing agents than traditional silver compounds such as silver sulphadiazine and silver nitrate (Hamdan et al., 2017). AgNPs are effective against a broad spectrum of microbes such as bacteria, yeast and fungi, they are ideal for clearing infections at the wound bed. Little or no infection, faster healing and minimal scarring are the main desirable outcomes required from wound treatment therapies (Hamdan et al., 2017). AgNPs have shown these traits timeously in various in vitro, in vivo and clinical models as a result of both their anti-inflammatory and anti-microbial activities (Neibert et al., 2012; You et al., 2012; Franková et al., 2016; Naraginti et al., 2016; Berthet et al., 2017; Hamdan et al., 2017; Mugade, Patole & Pokharkar, 2017; Orlowski et al., 2018; Ovais et al., 2018; Sood & Chopra, 2018). Furthermore, they are affordable, easy to manufacture, and can be topically administered to minimize complications associated with internalizing AgNPs (Pacioni et al., 2015; Syafiuddin et al., 2017; Li et al., 2018). The above-mentioned reasons validate AgNPs as a better replacement to conventional and current therapies in wound healing.

On the hand, DMSO is an aprotic solvent that is utilized for many purposes such as stabilizing NPs and storing cells just to name a few (Astley & Levine, 1976; Rodríguez-Gattorno et al., 2002; Bhosale, Chenna & Bhanage, 2017). DMSO has shown remarkable cell growth and low toxicity towards numerous mammalian cells (Goldblum et al., 1983; ICH International Conference on Harmon, 2009; Wen, Tong & Zu, 2015). Furthermore, topical application of DMSO has been reported to promote wound healing and pain relief (Wen, Tong & Zu, 2015). DMSO potency towards the healing of the wound is due to its ease to penetrate biological membranes, great anti-inflammatory, analgesic, cryoprotective, prophylactic and

radioprotective properties (Jacob & Wood, 1967; ICH International Conference on Harmon, 2009; European Medicines Agency, 2019).

AgNPs have shown a synergic effect when coupled with various materials such as antibiotics (Parani et al., 2016; Berthet et al., 2017; Hamdan et al., 2017; Rajendran et al., 2018; Mihai et al., 2019). In fact, most AgNPs involved in clinical trials are often combined with polymers to enhance their activity (Hamdan et al., 2017). Therefore, in the present study it is envisaged that incorporating AgNPs with DMSO will result in improved wound healing activities. This is proposed because AgNPs have shown faster healing, minimal scarring as well as inhibition of pathogenic species, while DMSO exhibited increased cell growth, low toxicity and membrane permeability. Thus, DMSO-capped AgNPs might penetrate deeper into the wound site and they (DMSO and silver) can work in synergy leading to faster healing. The combination of these two materials (DMSO and silver) have not been explored for this purpose in the past and have a potential to shorten the rate of wound healing.

CHAPTER 1

1. Introduction

The skin is the largest organ in the human body and covers approximately 2 m^2 area of the entire body (Gupta et al., 2013; Chen et al., 2018). It maintains the body's homeostasis by serving as a protective barrier against invading infections such as microbial outbreaks ((Chen et al., 2018). When the skin or any other organ is attacked by various stimuli, the resulting injury is called a wound (Rajendran et al., 2018; Nethi et al., 2019). The most common external stimuli that are capable of creating a wound include; surgical operations, cuts, chemicals, pressure, friction, heat blow, stress, shear and certain diseases (Tejiram et al., 2016; Ovais et al., 2018). A wound is described as a damage in the epithelial integrity of the tissues, occasionally the damage can be extensive and involve deeper subepithelial tissues such as dermis, nerve, facia and muscle (Ather & Harding, 2009). Wound healing is a physiological process that voluntarily occurs as the skin's or other body parts response to the injury (Parani et al., 2016; Rajendran et al., 2018). There are many formulations and therapies systematically created or administered to aid wound healing. Among these are traditional medicines (aloe vera, honey, cotton, wool etc), which were replaced by conventional wound healing therapies due to their inadequate healing, lack of providing moisture to the wound site and many other limitations (Medici et al., 2019a; Mihai et al., 2019; Nethi et al., 2019). Conventional wound treatment therapies include wound dressings, creams, ointments, bandages, growth factors, surgery etc. Despite their potential usefulness, these too possess many limitations such as high cost, skin discolouration, disruption of nervous system and pneumothorax, and non-complete healing (Hamdan et al., 2017; Kaur et al., 2019; Mihai et al., 2019; Nethi et al., 2019). As a result of the limitations associated with current wound treatment therapies, new and innovative materials and strategies, some of which are already available are necessary to address these limitations to improve the quality of life, and afford better wound healing. In this study, AgNPs are proposed for this purpose, because they have antibacterial and anti-inflammatory properties that aid wound healing. However, these properties are also limited since AgNPs have been reported to be ineffective against resistant bacterial strains such as *P. aeruginosa*, which is very common in wounds. Also, AgNPs have been associated with high degrees of toxicity towards human cells (You et al., 2012). To address the shortcomings of AgNPs and maximize their wound healing properties, they can be incorporated with other compounds of known medical

benefits such as Dimethyl sulfoxide (DMSO). DMSO is an aprotic solvent that has shown remarkable cell growth and low toxicity towards numerous mammalian cells (Rodríguez-Gattorno et al., 2002). Furthermore, topical application of DMSO has been reported to promote wound healing and pain relief. DMSO potency towards the healing of the wound is due to its ease to penetrate biological membranes, great anti-inflammatory, analgesic, cryoprotective, prophylactic and radioprotective properties (Duimel-Peeters et al., 2003; Sciences, 2005; Capriotti & Capriotti, 2012; Atiba & Ghazy, 2015). Thus, a formulation of DMSO-AgNPs is proposed to address the limitations encountered with using AgNPs and has a potential to maximize wound healing.

1.1. Types of Wounds

Wounds are differentiated based on various properties such as their causative agent, healing period, depth of the injury, tissue involved, etc (Ather & Harding, 2009; Nethi et al., 2019).

1.1.1. Open Wounds

Open wounds are formed when the skin is torn, cut, or punctured through physical trauma (Ather & Harding, 2009). In an open wound, the injury occurs at the surface of the skin and there is external bleeding (Roddick, 2021). As shown in Figure 1.1, the skin is fractured, with the subepithelial tissues revealed onto the outside environment ("The Skin and Wound Healing - Physiopedia", 2020). There are five common types of open wounds, namely: incisions, puncture wounds, abrasion, laceration and avulsions. Most open wounds are minor and can be cured without medical attention (Roddick, 2021).

Figure 1. 1: Example of an open wound, the skin is cut open with underlying tissues exposed to the outside. The wound site is surrounded by blood, which indicates external bleeding. This type of open wound is referred to as a cut ("The Skin and Wound Healing - Physiopedia", 2020).

1.1.2. Closed Wounds

Close wounds occurs when the skin is subjected to blunt force trauma resulting in contusions (Ather & Harding, 2009; Nethi et al., 2019). In a closed wound, the damage to body tissue occurs underneath the skin and the bleeding occurs internally (Roddick, n.d.). The exterior layer of the skin is unscathed, but the subepithelial tissues are injured as illustrated in Figure 1.2 ("The Skin and Wound Healing - Physiopedia", 2020). The most common types of closed wounds include bruises, haematoma and crush injuries (Ather & Harding, 2009; Nethi et al., 2019).

Figure 1. 2: illustration of a bruise, which is a common type of closed wounds. The skin is still intact but underlying tissues are damaged as evident from the red and blue scarring underneath the skin. The bleeding occurred internally since blood is not visible outside but underneath the wounded area ("The Skin and Wound Healing - Physiopedia", 2020).

1.1.3. Acute Wounds

Acute wounds are fresh wounds that still need to advance via the coherent steps of the wound healing process (Ather & Harding, 2009). They heal in a timely manner, usually between 1 and 12 weeks, clearly depending on the nature of the wound (Parani et al., 2016). Frequently, they are characterized by little or no infection, scab formation and normal healing. Usually, the immune system fights off the infection when present, but in the event of serious microbial colonization, the immune system cannot clear the infection and the wound progresses to the chronic stage (Mihai et al., 2019). Surgical wounds, burns and traumatic wounds represent the majority of acute wounds (Tejiram et al., 2016; Nethi et al., 2019; Vijayakumar et al., 2019).

1.1.4. Chronic Wounds

Chronic wounds are those that fail to heal in a predicted time span and in a systematic manner, they also have a tendency of reoccurring (Ather & Harding, 2009; Vowden, 2011; Parani et al., 2016; Tejiram et al., 2016). They are more prone to infection and significantly difficult to maintain (Parani et al., 2016). Chronic wounds are characterized by an elevated degree of bacterial colonization, increased inflammation, declined oxygenation on the sub-epithelial tissues, damaged fibroblast and delayed re-epithelization (Hamdan et al., 2017; Mihai et al., 2019). The most common chronic wounds are illustrated in Figure 1.3, they are not limited to leg ulcers, fungating wounds, pressure ulcers, diabetic foot ulcers, etc. (Tejiram et al., 2016; Nethi et al., 2019; Vijayakumar et al., 2019).

Figure 1. 3: Examples of the most common chronic wounds and their characteristics. (a) venous leg ulcer, (b) arterial ulcer, (c) diabetic foot ulcer, (d) pressure sore, (e) hypertrophic scar and (f) keloid (Nethi et al., 2019).

1.2. Wound Healing

Following damage (wound) to the body tissue, the human body activates a physiological process to heal itself, known as "wound healing" (Kasuya & Tokura, 2014). Wound healing is defined as a dynamic process by which the skin or any affected body tissue involuntarily repairs itself after trauma (Naraginti et al., 2016; Rajendran et al., 2018; Chakrabarti et al., 2019). The process instantly begins after the injury has occurred and it progresses through four well-orchestrated and sometimes overlapping stages as summarized in Figure 1.4; homeostasis, inflammation, proliferation and remodelling (Kalashnikova & Seal, 2015; Franková et al., 2016; Ovais et al., 2018). Each stage is directed and controlled by a variety of particular factors such as cytokines, chemokines, enzymes and growth factors (Kalashnikova & Seal, 2015; Franková et al., 2016; Orlowski et al., 2018).

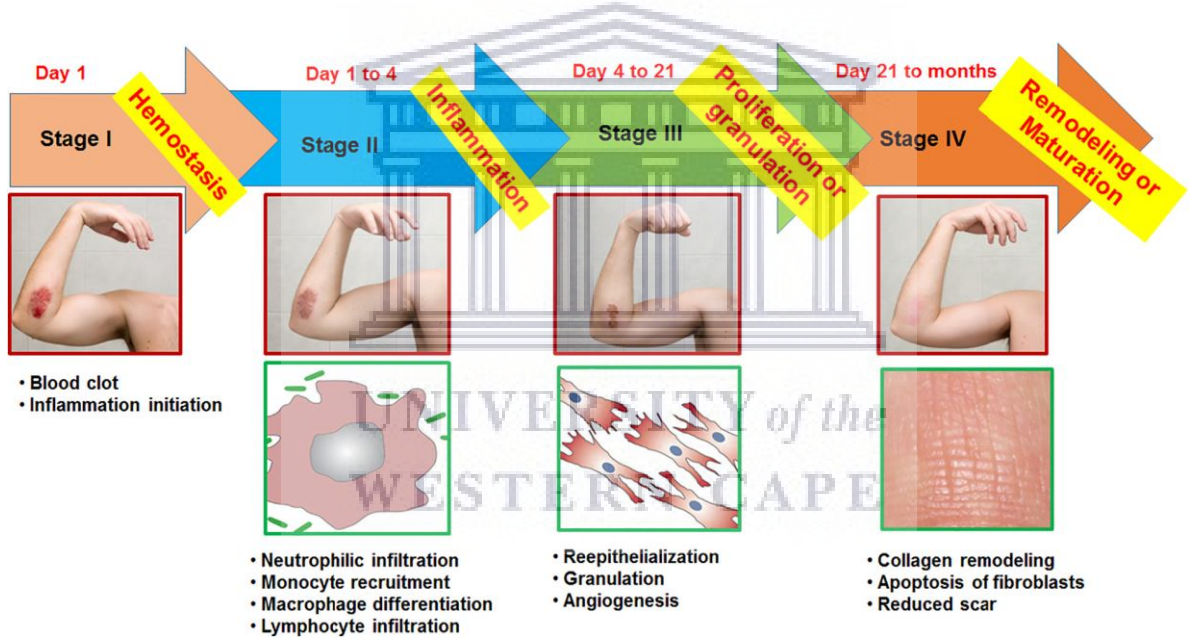

Figure 1. 4: The basic stages of wound healing, Stage (I) is the homeostasis phase and it occurs immediately after injury, stage (II) is inflammation, where a bunch of enzymes and growth factors are produced and fight off infection. Stage (III) represents the proliferation stage, this is where ECM and collagen are produced leading to reepithelization, the last stage (IV) is the remodelling stage where wound closure occurs (Vijayakumar et al., 2019).

1.2.1. Homeostasis

Homeostasis takes place promptly after skin damage, it is initiated by vasoconstriction and clotting cascade which halts bleeding and blocks microbes from invading the wound site (Berthet et al., 2017). The amount of thrombin present in the affected area leads to the

formation of platelet aggregation through which the platelets generate a variety of growth factors which sequentially promote the proliferation and migration of fibroblasts; followed by migration of the vascular endothelial cells to the wounded area (Rajendran et al., 2018).

1.2.2. Inflammation

Inflammation directly follows homeostasis. It is the most important stage of wound repair, because incomplete or extended inflammation impedes progression to the proliferative stages and impairs wound healing (Orlowski et al., 2018). Inflammatory stage is identified by the infiltration of the wound by the inflammatory cells (neutrophils, monocytes and macrophages), which are responsible for removing bacterial infection and dead tissues in the site of injury (Neibert et al., 2012).

1.2.3. Proliferation

In the proliferation stage, the fibroblasts from the nearby tissues start to proliferate towards the fibrin matrix to generate extracellular matrices such as collagen. The production of this glycoprotein is the determining step of this phase and at the same time epithelialization and angiogenesis also take place (Naraginti et al., 2016; Mihai et al., 2019). During epithelialization, the denuded epithelial surface is covered, through cellular and molecular processes which are vital for wound closure such as regulation of keratinocyte differentiation, migration and cross talk between various cells involved in wound contraction (Pastar et al., 2014). While angiogenesis involves the formation of new blood vessels from previous blood vessels generated in the prior homeostasis stage (Nethi et al., 2019). Lastly, the fibroblast found in the wound bed are activated by macrophages, and some of the fibroblast differentiate into myofibroblast which initiate wound closure (Berthet et al., 2017).

1.2.4. Remodelling

Remodelling is the last stage in the wound healing process, where the old collagen and protein molecules are crosslinked with the newly generated collagen molecules from the proliferation stage resulting in an increased tensile strength of the scar (Naraginti et al., 2016). In summary, this stage reinstate the morphology and function of the tissue (Mihai et al., 2019).

1.3. Factors affecting wound healing

Under normal circumstances, an acute wound should heal between 2-3 weeks at most, followed by the remodelling stage which occurs in a period of up to two years. If it fails to completely heal during that period, then it will progress to the chronic stage (Rajendran et al., 2018). Both external and internal factors which delay wound healing are well established, the former includes medication, malnutrition, lifestyle traditions such as smoking and excessive drinking, comorbidities such as diabetes and obesity (Kalashnikova & Seal, 2015; Nethi et al., 2019). While the internal factors include necrotic tissue, wound infection, entrapment of foreign species and pathogenic contamination (Parani et al., 2016; Rajendran et al., 2018; Mihai et al., 2019).

1.4. Current wound treatment therapies and their limitations

Although wound healing occurs naturally, there are many engineered materials that are used to aid the process in order to ensure that it progresses without interruptions or failure. Accelerated wound closure, preventing infections, complete healing and minimal scarring are the main goals of wound care and wound management (Parani et al., 2016; Berthet et al., 2017). In the past, a variety of plant extracts, natural products and materials such as honey, aloe vera, cottons and wools have been used for wound treatment for various individual benefits (Mihai et al., 2019). Unfortunately, they were associated with numerous limitations such as not providing enough moisture to the wound site, unpredicted allergic reactions and varied clinical outcomes (Hamdan et al., 2017). These factors limited their use and they were replaced by new therapies such as silver based therapy, stem cell therapy, artificial and biomaterial wound dressing materials, bioengineered skin substitutes, vacuum-assisted wound closure, growth factor therapy and vascular surgery (Rajendran et al., 2018; Chakrabarti et al., 2019; Mihai et al., 2019; Nethi et al., 2019).

Silver based therapies such as silver nitrate and silver sulphadiazine are frequently employed in burns dressings and for the treatment of infected nonhealing wounds. They are renowned for their antibacterial effect unleashed by silver ions which interact with thiol bearing groups. This interaction leads to DNA damage by ways of blocking respiratory enzyme pathways resulting in bacterial death (Hamdan et al., 2017; Mihai et al., 2019).

1.5. Medical properties of Silver

1.5.1. Brief History of Silver

Silver is a naturally occurring metal positioned at number 47 in the periodic table of elements, and have a characteristic white and shiny appearance (Chen & Schluesener, 2008; Barillo & Marx, 2014; Konop et al., 2016). It is denoted as Ag, which is short for "argentums" and belongs to the noble group of transition metals alongside, gold, copper and platinum (Chen & Schluesener, 2008; You et al., 2012; Medici et al., 2019b). In its pure form, it possesses extrinsic properties including high thermal and electrical conductivities than any other metal, while maintaining a very low contact resistance (Chen & Schluesener, 2008; You et al., 2012; Konop et al., 2016).

Since ancient history, the antimicrobial properties of silver were very well known, as a result this metal and its derivatives were widely used for various applications including (but not limited to) wound care, water disinfection and storage (Clement & Jarrett, 1869; Barillo & Marx, 2014; Alexander, 2009). The first reported use of silver was around 3500 BC in pre-dynastic Egypt, where silver coins were used as a currency (Russell & Hugo, 1994; Konop et al., 2016) carved with the head of king Ptolemy X or Aegis eagle (Figure 1.5).

Figure 1. 5: Ancient Egyptian silver coins carved with the head of king Ptolemy X. and Aegis eagle with closed wings ("Egypt, Ptolemy X (XI), ancient coins index with thumbnails - WildWinds.com", 2020).

Herodotus, the father of history reported that none of the Persian kings would drink water if it was not transported or stored in silver containers, because they believed that the silver retained the freshness and purity of the water (Clement & Jarrett, 1869; Konop et al., 2016). In 335 BC, Aristotle advised Alexander the great to store his drinking water in silver jars and to boil it before use when embarking on one of his many campaigns (Russell & Hugo, 1994). Throughout ancient civilization, the Greeks and Romans stored water and other beverages such

as wine in silver jars to avoid spoilage, this came in handy during the wars as there was a lack of fresh water in the battlefields (Alexander, 2009). Furthermore, silver coins were not only used for currency but as disinfectants as well, they were placed in water vessels with other liquids in order to sterilize the liquids (Jm et al., 2007). Even during the times of exploring new places and frontiers, the Australians and American settlers inserted either silver coins or tableware in their drinking water and milk barrels for preservation (Alexander, 2009; Barillo & Marx, 2014; Medici et al., 2019). Since it was known that silver prevents decay and spoilage, the wealthy adapted that notion and started using it in their cutlery, even to date silverware is used for serving food (Medici et al., 2019a). However, the rich often developed a blue-grey discolouration of the skin and other mucosal body parts as a result of prolonged usage or contact with silver or silver containing compounds (Alexander, 2009). This discolouration condition is better known as argyria and it is less common nowadays due to the decrease in usage of silver based therapies (Russell & Hugo, 1994).

1.5.2. Silver in Medicine

The medicinal usage of silver dates back to 1000 BC, where ancient civilizations used it as a prophylactic and treatment for various diseases (Jm et al., 2007). Silver nitrate (*lapis infernalis*) or lunar caustic as referred to by the alchemists was the commonly used silver salt according to The Merck Index First Edition published in 1889 amongst other salts listed for pharmaceutical purposes (Medici et al., 2019a). A Roman published pharmacopeia was the first to mention silver nitrate in 69 BC, but the first information about the medicinal use of this silver salt for the treatment of wounds is attributed to Gabor in 702-705 (Alexander, 2009; Konop et al., 2016). In 980 A.D., Avicenna applied silver filings to prevent heart palpitations and foul breath. It was also believed that silver can cure epilepsy, because when an epileptic man accidentally swallowed a large silver coin that was placed in his mouth to stop him from biting his tongue during a seizure, it completely cured his epilepsy (Alexander, 2009). In the late 19th century, the very first scientific paper detailing the medicinal use of silver was written by F. Crédé, who used 1% silver nitrate solution as eye drops to cure blindness caused by postpartum eye infections in infants (Maillard & Hartemann, 2012). This therapy was highly effective in decreasing the occurrence of *ophthalmia neonatorium* in new-borns from 7.8% to 0.13% in a period of 13 years. As a result, this therapy was accepted in many countries across the world, some even mandated it by law and it continued until it was taken over by the discovery and use of antibiotics (Alexander, 2009). F. Crédé's son followed in his tracks and

investigated the effect of metallic silver on *Staphylococci* and *Streptococci* via *in vitro* studies. He found that when slivers of silver were taken out of an inoculated dish after 24 hours, no microorganisms would grow in the place that was previously occupied by the silver (Jm et al., 2007). Furthermore, Credé developed two silver salts namely silver lactate and silver citrate as delivery mechanisms of silver ions during in vitro antibacterial studies (Klasen, 2000; Jm et al., 2007). The medical use of silver salts was not only limited to the treatment of bacteria such as gonorrhoea and syphilis, but extended to the treatment of mental health illness as well as nicotine addictions (Medici et al., 2019a).

Silver also played a major role in battlefield surgery, where Ambrosie Pare, a royal surgeon successfully used silver clips in facial reconstructions (Konop et al., 2016). Another impressive medicinal use of metallic silver in the 19th century is attributed to Konrad Röntgen for his discovery of the X-ray. He realized that X-rays activated silver halide crystals, making it possible to record radiographic images (Alexander, 2009). Older editions of the British National Formulary also reported the use of silver nitrate in a body lotion (Russell & Hugo, 1994), other silver based personal care products have also been reported as early as 1996, with neither signs of toxicity nor hypersensitivity (Maillard & Hartemann, 2012). By the beginning of the 20th century, numerous advances in the medicinal use of silver had already been made since the antimicrobial mode of action of silver was better understood through research (Jm et al., 2007). In this era, silver was mainly used in colloidal form for numerous applications such as germicides in hospitals. The efficacy of colloidal silver is described as a bactericide with no serious limitations by many prestigious medical journals (Medici et al., 2019a). Currently, silver and its derivatives are used at large in the medical industry as coating for catheters and other bodily implants, with the most important use as a microbicide to prevent long term and recurrent infections in burns, diabetic ulcers and traumatic wounds (Maillard & Hartemann, 2012).

1.5.3. Silver in wound care

Silver is the most studied precious metal in the bacterial infection combat (Bell & Dn, 2017). The very first time silver was used in wound care was when the Macedonians used silver plates to treat and prevent surgical infections, and by doing so achieved better wound healing (Alexander, 2009). The Surgeons Mate, a textbook published in 1617, was one of the earliest publications to mention the wound healing abilities of silver, where a solution containing 1:3 silver to nitric acid ratio was used to treat wounds such as leg ulcers (Jm et al., 2007). In 1895,

Halstead successfully used silver wires to suture surgical wounds and silver foil dressings in his surgery in an attempt to avoid postoperative infections (Jm et al., 2007). Furthermore, during World War I, a silver leaf was placed onto the wounds of soldiers to prevent infections and to promote healing (Medici et al., 2019a), this was also commonly practiced in Ancient Mediterranean and Asiatic cultures (Barillo & Marx, 2014). The initial topical use of silver nitrate in wound treatment is attributed to Moyer and his co-workers, who used 0.5% of this silver compound to control the growth of *P. aeruginosa* in severely burnt patients (Maillard & Hartemann, 2012). Grawits also reported on the antimicrobial properties of silver when he used a highly diluted silver nitrate solution to stop the growth of *S. aureus* (Jm et al., 2007). Unfortunately, the bacteria later developed resistance against silver nitrate, prompting a change in formulation which resulted in the introduction and application of silver sulphadiazine (Maillard & Hartemann, 2012). Silver sulphadiazine is a manmade complex that was synthesized in the 1960s by complexing a silver ion (Ag^+) to a sulphonamide antibiotic (Figure 2.6) (Medici et al., 2019), and is still commercially available today (Bell & Dn, 2017).

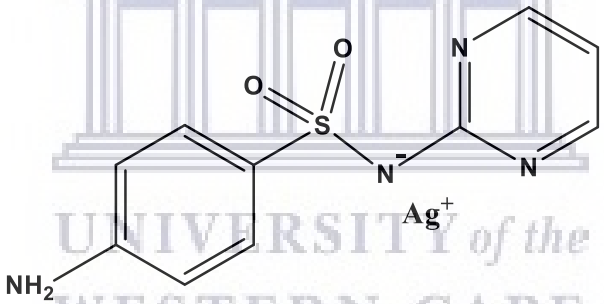

Figure 1. 6: Structural configuration of silver sulphadiazine.

Silver sulphadiazine was created in an attempt to retard the absorption of sulphadiazine since it was observed that a few water soluble compounds such as sodium sulphadiazine are quickly absorbed from wounds and excreted in urine (Russell & Hugo, 1994). As a result, the combination of both the silver and sulphadiazine achieved a synergic effect against bacteria (Clement & Jarrett, 1869). The complex (silver sulphadiazine) was indeed a far better alternative because it did not produce argyria, which was a serious side effect associated with the silver nitrate based products (Maillard & Hartemann, 2012). The silver sulphadiazine was highly effective against a broad spectrum of bacteria because it slowly delivered the Ag^+ ions to the wound site (Konop et al., 2016). This claim was proven correct by an experiment where

silver sulphadiazine against other silver compounds were all incubated with sodium chloride, nutrient broth, DNA, human serum and bacteria. Other salts, for example silver nitrate dissolved immediately and disappeared in the solution and reappeared as a silver chloride precipitate. The other salts showed a poor dissociation of the silver ions releasing a very limited amount of silver over several hours. On the other hand, the silver sulphadiazine released silver ions in uniform concentrations at a controlled intermediate rate (Clement & Jarrett, 1869). Hence, it rapidly became the gold standard for the treatment of burns, chronic ulcers and other skin wounds in general (Clement & Jarrett, 1869; Medici et al., 2019a).

It has been used as one of the main ingredients at 1% in many topically administered wound therapies such as creams, ointments and dressings (Medici et al., 2019). One of the most common 1% silver sulphadiazine containing cream, Flamazine™, has been a mainstay topical therapy for the treatment of infections in burns, acute and chronic wounds (White & Cooper, 2003). Another 1% silver sulphadiazine cream, Silvadene™ was successfully used to treat wounds in pigs and increased epithelialisation by almost 30% (White & Cooper, 2003). Although silver sulphadiazine has proven to have antimicrobial activity against a broad spectrum of bacteria, some bacteria developed resistance to it. The bacterial resistance was attributed to the antibiotic component of the compound (Maillard & Hartemann, 2012). This led to the investigation of a combination of silver sulphadiazine with other compounds as topical wound therapies for example, Flammacerium, a combination of 1% silver sulphadiazine and cerium nitrate (Ross, Phipps & Clarke, 1993), while Silvazine™ is a mixture of 1% silver sulphadiazine and chlorhexidine digluconate (Maillard & Hartemann, 2012). Fraser and his colleagues conducted a series of *in vitro* studies using Acticoat™, Silvazine™ and Flamazine™ against eight bacterial strains namely, *MRSA, P. aeruginosa*, *E. coli*, *S. aureus*, *Enterococcus faecalis*, *Enterobacter cloacae*, *Proteus mirabilis* and *Acinetobacter baumannii*. Acticoat™ is a wound dressing that consist of a rayon-polyester core sandwiched in between two layers of high density polyethylene mesh coated with nanocrystalline silver (Bell & Dn, 2017). Silvazine™ was the most effective in killing all the bacteria within 30 minutes while the other two dressings had similar efficacy against many of the isolates. Furthermore, Acticoat™ was successful only against *Enterococcus faecalis* and *MRSA*, as a significant amount of *S. aureus* was still present after 24 hours. Bacterial resistance to Acticoat™ was observed with the *Proteus mirabilis* and *Enterobacter cloacae* between 8 and 24 hours (Fraser et al., 2004). Despite the limitations associated with the clinical use of silver sulphadiazine such as the breakout of resistant strains, impairment of wound healing and development of

systemic side effects (White & Cooper, 2003), it is still listed as an essential medication by the World Health Organisation that is highly recommended in the market for wound treatment (Medici et al., 2019a).

A number of topically applied silver based therapies have been extensively evaluated on chronic wounds in many controlled clinical trials with favourable outcomes (White & Cooper, 2003; Bell & Dn, 2017). As a result, a variety of silver based dressings including (but not limited to) Acticoat™, Aquacel™ Ag, Contreet™, Actisorb™ Silver 220, Urgotul SSD™ and Avance™ have been commercially introduced (Bell & Dn, 2017). Although, recent therapeutic agents were able to overcame a number of setbacks associated with silver based wound treatment therapies, they too have limitations of their own. They are expensive, have limited safety and hazardous impact on the healthy neighbouring cells or tissues around the wound site (Ovais et al., 2018). As a result, science is faced with a burden of developing new and innovative wound treatment technologies that will tackle these issues head on, for the betterment of human health and well-being. Nanotechnology is an emerging branch of science that has the potential competency of solving these problems at the molecular and submolecular level (Bansod et al., 2015; Bhatia, 2016; Ovais et al., 2018).

1.6. Nanotechnology

Nanotechnology is an interdisciplinary field that deals with the production, manufacturing, characterization and application of nanosized materials (Bansod et al., 2015; Bhatia, 2016; Ovais et al., 2018). Nanotechnology is coined from the Latin word “nanos” which means dwarf because it deals with significantly smaller objects. Ideally, the size ranges from one thousand millionth of a metre which is equal to one nanometre (10^{-9} m =1 nm) (Bhatia, 2016). This technology is developed in numerous levels such as nanomaterials, nanosystems and nanodevices, with nanomaterials being the highly utilized level in both commercial application and scientific knowledge. This stems from their novel size dependant properties, which make nanomaterials exceptional and essential for various aspects of human life (Hoet, Brüske-Hohlfeld & Salata, 2004). Remarkable research in this field has already created the possibility of developing advanced potential therapeutic agents for wound healing (Ovais et al., 2018).

1.6.1. Nanomaterials

Nanomaterials refers to specimens which have at least one dimension that is less than 100 nm (Becaro et al., 2015). They are divided into four different classes that is, zero, one, two and three dimensions and come in various shapes and sizes, examples include quantum dots, nanowires, nanometre thick films and nanoparticles belonging to each of the classes, respectively (Hong, 2019). Nanomaterials have distinctive biological and physicochemical properties that are not observed in their bulk counterparts (Srikar et al., 2016). These unique features are attributed to quantum confinement effects and large surface areas that are not present in the macro compounds of the same composition (Srikar et al., 2016; Hong, 2019). As a result, nanomaterials have attracted a great deal of scientific research due to their remarkable optical, electrical, magnetic, catalytic, biological, or mechanical properties (Capek, 2019). These special features make them excellent candidates for numerous applications in a variety of fields such as electronics, drug delivery, environmental remediation, biological labelling, chemical sensing and imagining, information storage, photonics and catalysis (Nath & Banerjee, 2013). There are generally two types, organic and inorganic nanoparticles, the former includes carbon bearing particles such as liposomes amongst others, while the latter consists of semiconducting nanoparticles such as titanium dioxide and metallic nanoparticles made from noble transition metals (Khan et al., 2017). However, the study will only focus on the metallic nanoparticles (MNPs), specifically the silver nanoparticles (AgNPs).

1.6.1.1. Silver nanoparticles and synthesis

AgNPs are without a doubt the extensively commercialized nanomaterials among all (Hasan, 2014), and reported by the Nanotechnology Consumer Products Inventory to be the most used MNPs as it appears in 24% of the registered products for various applications (Medici et al., 2019). This is because AgNPs can circumvent the previously mentioned limitations of silver compounds, importantly, they are effective at very low concentrations. Some of their essential properties that make them highly useful in wound healing processes (Gunasekaran, Nigusse & Dhanaraju, 2011), treatment and management (Vijayakumar et al., 2019) are listed in Table 2.1.

Table 1. 1: Various properties of AgNPs that make them useful in wound healing

Number	Property
1	AgNPs are easy to fabricate with a variety of methods to choose from
2	Size and morphology can be easily altered for a desired application
3	Surface modification is very achievable with AgNPs, which is very useful in targeted drug delivery
4	AgNPs have a high antibacterial efficacy against a broad spectrum of bacteria
5	Bacterial resistance with AgNPs is very rare, thus they have multi antibacterial synergy
6	AgNPs can easily be impregnated into dressings with no side effects
7	AgNPs possess anti-inflammatory properties that aid tissue regeneration.

Like most nanomaterials, AgNPs synthesis follow either the top down or the bottom up approaches as shown in Figure 1.7 (Lee & Jun, 2019). The top down approach involves the physical reduction of a bulk compound to its smaller constituents. In this method, a heavy force is used to crush the macromolecule into nanoparticles through physical and mechanical processes such as UV irradiation, lithography, laser ablation, ultrasonic fields, and photochemical reduction (Medici et al., 2019a; Sasidharan, Raj & Sonawane, 2019). The most common top down methods are evaporation-condensation and laser ablation techniques (Lee & Jun, 2019). In the bottom up approach, small particles such as atoms and molecules are utilized as the building blocks to obtain nanoparticles. Self or assisted assembly of these smaller particles results in the production of a complex nanoparticle (Sasidharan, Raj & Sonawane, 2019). The bottom up approach is subdivided into: biological, gaseous, liquid and solid phase methods; where biological materials such as plants or fungi, chemical vapour deposition, reduction using metal salts and spinning among others, are respectively used for reduction of the metal salts (Pacioni et al., 2015).

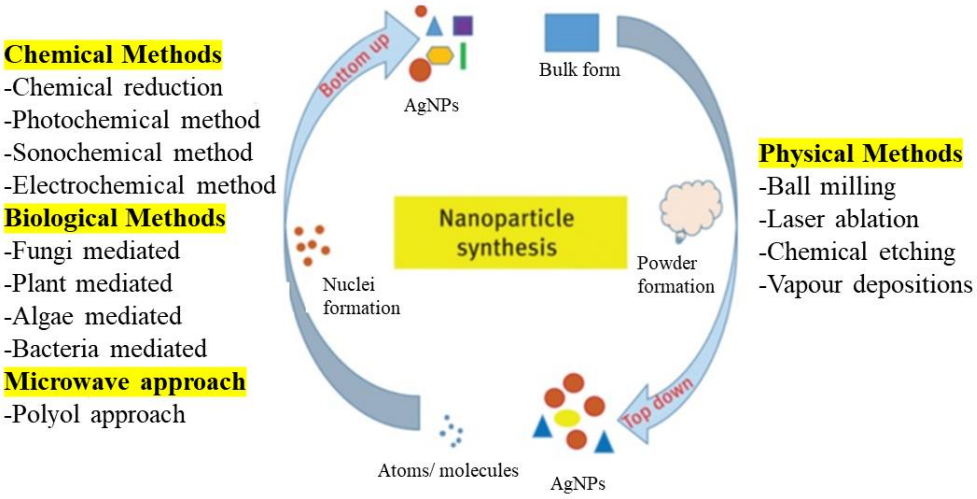

Figure 1. 7: Approaches for nanoparticle synthesis (Mukherji et al., 2019).

Synthetic methods that use wet chemistry for the production of nanoparticles such as chemical reduction, sol gel and polyol synthesis are classified as chemical methods (Sasidharan, Raj & Sonawane, 2019). Lastly, the biological methods also referred to as "green synthesis", involve the use of a biological component such as fungi, plant extract or microorganisms as reducing and stabilizing agents (Hasan, 2015).

It is important to note that most physical methods belong in the top down approach while the chemical and biological methods form part of the bottom up approach. Although the physical methods produce AgNPs with a narrow size distribution range and usually have fast processing times, they have many adverse effects including large space requirement, taking long to reach thermal stability, uses a lot of energy to increase the temperature of the source material, and cannot be employed for scaling up purposes (Syafiuddin et al., 2017; Medici et al., 2019). Chemical methods are widely used for the production of AgNPs in solution, they are either prepared in water or other organic solvents (Pacioni et al., 2015). Chemical methods are fast and efficient, however the use of toxic chemicals as reducing agents or production of toxic by-products is a major concern (Hasan, 2015; Medici et al., 2019). Therefore, new alternative methods that are eco-friendly, cost effective and energy efficient are emerging very quickly (Srikar et al., 2016). This emerging of green or biological synthesis and has been widely reviewed in literature (Hasan, 2015; Srikar et al., 2016; Khan et al., 2017; Syafiuddin et al., 2017; Medici et al., 2019a; Sasidharan, Raj & Sonawane, 2019).

Green synthesis works exactly like chemical reduction methods, however the capping/stabilizing and reducing agents are replaced by environmentally benign materials like fungal and bacterial enzymes; plant extracts from leaves, roots, barks, flowers, fruits, peels and seeds. These biological entities make the nanoparticles useful candidates for pharmaceutical and biomedical applications due to their eco-friendly nature (Lee & Jun, 2019). Although it seems like green synthesis is more favourable than chemical and physical methods, using microorganisms like mediated fungus and bacteria as reducing agents in nanoparticle synthesis is very complicated. These microorganisms first have to be isolated and then grown; both processes are complex and require numerous steps. The aforementioned problems resulted in the consideration of plant extracts for AgNP production because they are abundantly available, easily extracted and do not require complicated procedures. Leaves are used the most for nanoparticle production mainly because they are vastly accessible since they are naturally discarded into the environment. It is very challenging to produce AgNPs of uniform shapes and sizes with plant-based synthesis (Syafiuddin et al., 2017). Furthermore, the reduction mechanism of biological methods is poorly understood (Sasidharan, Raj & Sonawane, 2019).

1.6.1.2. Properties and bio-medical application of AgNPs

Physical and chemical properties of AgNPs such as surface chemistry, shape, morphology, composition, coating/capping, size, surface charge, and reactivity amongst many others, are very important in downstream application of the AgNPs (Zhang et al., 2016; Medici et al., 2019). AgNPs are highly utilized in various applications due to their many biological properties such as anti-fungal (Kotakadi et al., 2014), anti-cancer (Li et al., 2018), anti-viral (Wei et al., 2015), anti-angiogenic (Gurunathan et al., 2009), anti-leishmanial (Khan, Saleh, et al., 2018) anti-inflammatory (Hebeish et al., 2014) and anti-bacterial (Murugan et al., 2014) activities, amongst others (Figure 1.8).

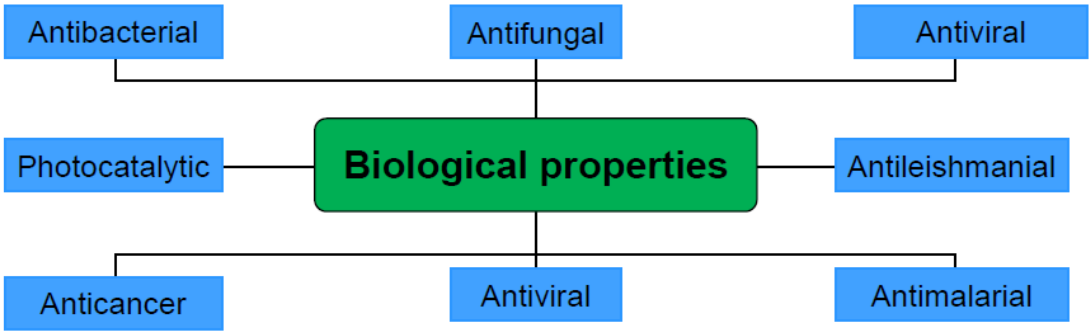

Figure 1. 8: Biological properties of AgNPs (Khan, Saleh, et al., 2018).

Due to their remarkable size dependant physicochemical properties such as optical, thermal, catalytic and electronic characteristics, AgNPs are utilized in many applications including but not limited to pharmaceuticals, cosmetics, water purification, biosensors and electronics (Syafiuddin et al., 2017). However, it is their biological activities (Figure 1.8) that make AgNPs attractive in medical applications. Due to the global increase of life threatening diseases and the multidrug resistance of pathogens against antibiotics (Shanmuganathan et al., 2019), AgNPs are used in multiple medical applications such as sensors for disease diagnosis, nanocarriers for drug delivery, sensitizers in radiation therapy, electro spin resonance Dosimetry, etc.(Srikar et al., 2016). And also have other applications in different fields as listed Figure 1.9. In this study, the interest is on the wound healing property of AgNPs.

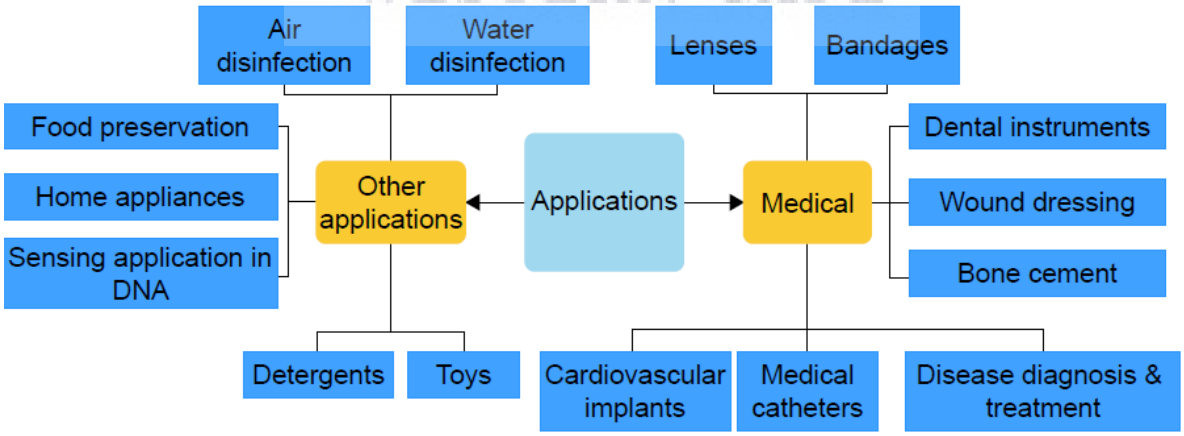

Figure 1. 9: Applications of AgNPs in various fields (Khan, Saleh, et al., 2018).

1.6.1.3. Properties of AgNPs That Aid Wound Healing

Bare AgNPs (chemically synthesized AgNPs) are used as therapeutic agents for wound healing purposes mainly because of their remarkable anti-inflammatory and anti-bacterial properties (Berthet et al., 2017), shown in Figure 1.10. AgNPs initiate neutrophil apoptosis which reduces the activity of the mitochondrial membrane potential by lowering cytokine modulated inflammatory response, resulting in faster healing (Chakrabarti et al., 2019).

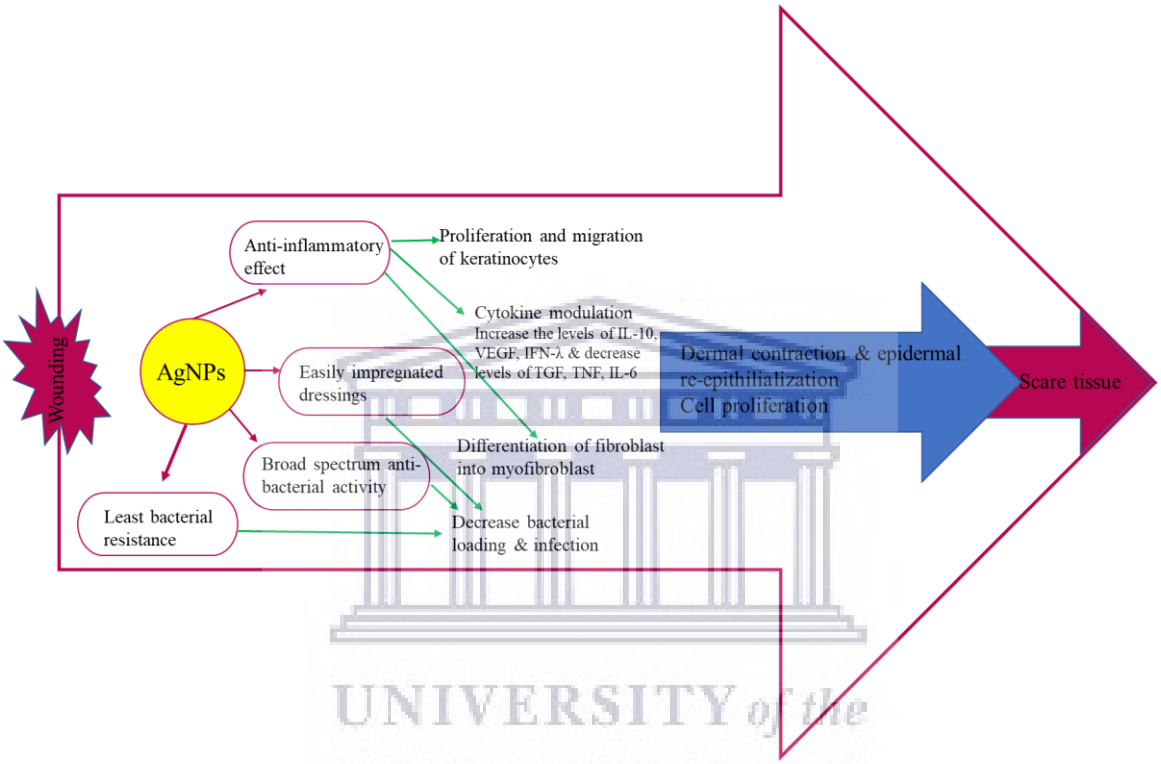

Figure 1. 10: Antibacterial, anti-inflammatory, least bacterial resistance and ease of loading into dressing abilities make AgNPs a force to be reckoned with in wound healing (Gunasekaran, Nigusse & Dhanaraju, 2011).

1.6.1.3.1. Anti-inflammatory Properties

When foreign particles invade the body, tissues trigger an early immunological response i.e. inflammation to fight off these disturbances by producing an excessive amount of pro-inflammatory cytokines, activate the immune system and release chemotactic and prostaglandins species. The released factors include the complement factors, interleukin-1 (IL-1), tumour necrosis factor (TNF)-α, and transforming growth factor (TGF-β). AgNPs are bio-compatible and are able to escape this involuntary inflammatory action, hence they can be used as anti-inflammatory agents (Zhang et al., 2016). Nanocrystalline silver, in the form of AgNPs, has exhibited excellent anti-inflammatory activities in animal models as well as clinical trials

by enhancing the expression of pro-inflammatory cytokines via a mechanism that includes the transformation of growth factor-α and TNF -α (Medici et al., 2019b). Through the AgNP-based anti-inflammatory properties, topical application of the AgNPs in the wound area will reduce the release of cytokine, and lymphocyte and mast cell infiltration which will then promote wound healing with minimal scarring (Gunasekaran, Nigusse & Dhanaraju, 2011; Rajendran et al., 2018; Mihai et al., 2019). Similarly, in diabetic wounds, AgNPs accelerate the rate of wound healing by activating the proliferation and migration of keratinocytes. Moreover, they aid in the differentiation of fibroblast to myofibroblast which accordingly promotes wound contraction and speeds up the healing of diabetic ulcers (Vijayakumar et al., 2019).

Two different doses (0.25 and 0.50 mL) of 250 ppm AgNPs were tested *in vivo* against saline (control) and a commercially available drug, indomethacin. Both doses of AgNPs exhibited a decrease in inflammation in the animal models. It was reported that the 0.50 mL dose was more effective than the 0.25 mL, indicating that the anti-inflammatory activity of AgNPs was dose dependant. Furthermore, the AgNPs had similar activity to the indomethacin reference drug in reducing the degree of rat bow oedema (Hebeish et al., 2014). A recent *in vitro* experiment utilizing dermal fibroblast and human keratinocytes revealed that treating the cells with AgNPs remarkably lowered inflammation by lowering the cytokines levels, oxidative stress and promoted healing. While topical application of the same AgNPs in mice with burn wounds showed decreased counts of neutrophils and low levels of IL-6, accompanied with an increased in levels of IL-10, TGF-β, vascular endothelial growth factor (VEGF), and interferon gamma (IFN-γ) (Rajendran et al., 2018). As a result of their anti-inflammatory activity and ability to promote cell growth, AgNPs are useful tools in wound healing (Gunasekaran, Nigusse & Dhanaraju, 2011). They are responsible for the differentiation of fibroblast into myofibroblast, which encourages wound contraction, fast healing duty, and quicken the proliferation and relocation of keratinocytes (Paladini & Pollini, 2019). The effect of AgNPs on keratinocytes and fibroblasts of rodents was studied in an excisional wound model, the histological and ex vivo tests showed that AgNPs enhance proliferation and movement of keratinocytes from the corners to the middle of the wound and stimulated the differentiation and maturation of keratinocytes and hence prompted wound contraction. The group of mice that was treated with AgNPs showed better wound closure than the control group treated with the reference drug i.e. silver sulfadiazine (Liu et al., 2010).

1.6.1.3.2. Antibacterial Properties

Compared to other silver derivatives such as salts and complexes, AgNPs exhibit higher antibacterial efficacy (Medici et al., 2019). This is due to their ultrafine size, large surface areas and more fractions in their surface atoms which gives them greater contact with microorganisms (You et al., 2012; Konop et al., 2016; Shanmuganathan et al., 2019). AgNPs are utilized in wound care management to avoid secondary infections, as they are active against various strains that can delay the normal healing process (Gunasekaran, Nigusse & Dhanaraju, 2011; Pal et al., 2017). The antibacterial activity of AgNPs is very complicated and its mechanism is only recently being explained in literature (Srikar et al., 2016; Medici et al., 2019). Nevertheless, the mode of antibacterial action initially involves the AgNPs binding to the cell membrane and penetrating the cytoplasm of the bacteria where they interact with proteins, DNA, and enzymes that contain phosphorus or thiol groups (Mihai et al., 2019). Once the AgNPs are inside the bacterial cell, the oxidation of AgNPs in aqueous medium triggers the release of Ag ions under acidic conditions that carry out the bactericidal effect and not the AgNPs themselves (Parani et al., 2016). The AgNPs attack and destroy the respiratory chain resulting in cell death (Rajendran et al., 2018).

AgNPs have exhibited remarkable antibacterial activity against an astonishing number of pathogenic bacteria, both Gram-positive and Gram-negative specimens (Tran, Nguyen & Le, n.d.). This activity was influenced by many parameters, most especially their size, morphology, concentration, surface charge, and coating. Also, many resistant and multi-resistant strains have also been treated with AgNPs and yielded positive outcomes (Medici et al., 2019). One common problem associated with wound closure is the colonization with an infectious agent. Even though the bacteria present in the skin's microbiota are useful in preventing colonization of other infectious pathogens, they can also impair wound healing if it reaches a critical threshold at the wound site. Additionally, external pathogens can infiltrate the wound, resulting in delayed wound healing. Out of these, the frequently detected are *S. aureus* and *MRSA*, which are found at the beginning stages of wound healing, while *P. aeruginosa* and *E. coli* are observable in chronic wounds since they infect deep skin layers (Mihai et al., 2019). The anti-bacterial activity of AgNPs against *E. coli* was reported in previous studies, the AgNPs formed holes in the bacterial cell wall and accumulated in their membrane resulting in bacterial death (Singh, 2016). *S. aureus*, *MRSA*, *P. aeruginosa* and *E. coli* were all reported to be susceptible to chemically fabricated 8 – 50 nm sized AgNPs *in vitro* (Lee, Song & Lee, 2010). Another

study evaluated the antibacterial efficacy of 26 nm sized green synthesized AgNPs against three strains, they exhibited impressive activity against *S. aureus*, *E. coli* and *P. aeruginosa* (Khan, Saleh, et al., 2018). It is the antimicrobial efficacy of AgNPs that aid in the removal of these microbes especially bacteria that might disturb and impair the normal stages of wound healing (Rajendran et al., 2018).

1.6.2. Other nanoformulations of AgNPs in Wound Healing

AgNPs as single units have demonstrated potential wound healing abilities, but when combined with other wound dressing materials, they impressively killed microbes that might cause infections at the wound site (Rajendran et al., 2018). Furthermore, owing to their very small size, they have a very high surface area to volume ratio which enables surface functionalization, which allows them to be decorated with other biomolecules. Beneficial biomolecules such as DNA and drugs, can be incorporated to enhance their activity and prolong their circulation time (Bhatia, 2016). As a result of the aforementioned properties together with the inherent broad-spectrum antimicrobial activity of the AgNPs, they are highly utilized as topical agents in wound healing applications in combination with other materials (Khan, Saleh, et al., 2018). The main categories of the nanohybrids employed in wound treatment are depicted in Figure 1.11 (Mihai et al., 2019).

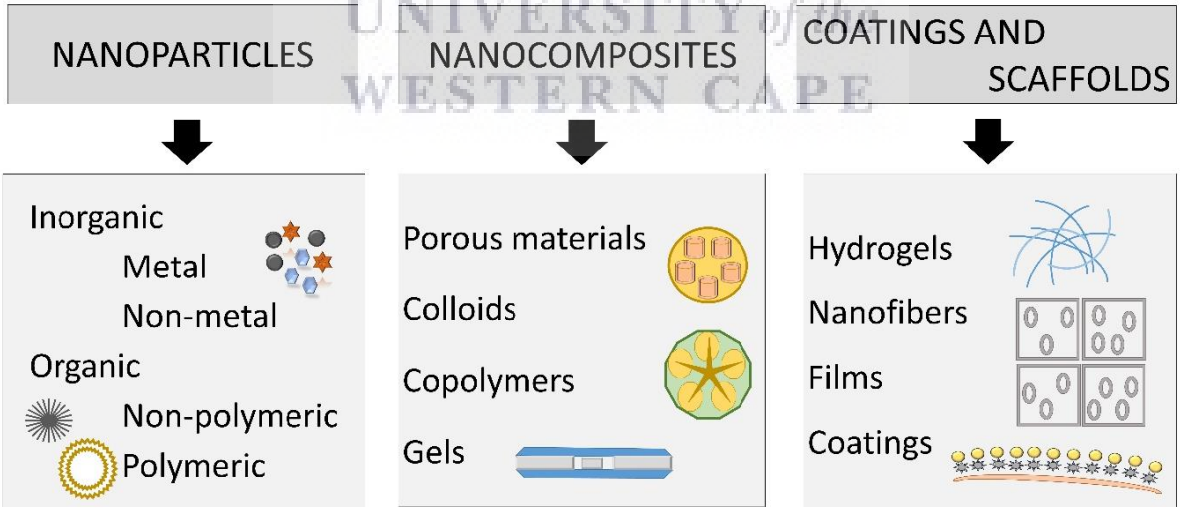

Figure 1. 11: main types of nanomaterials explored in wound treatment (Mihai et al., 2019).

In wound therapy, mainly two types of nanomaterials are used: (1) nanomaterials that show distinctive characteristics which are instrumental for wound treatment and (2) nanomaterials used as delivery channels for therapeutic agents (Hamdan et al., 2017; Mihai et al., 2019). (1)

includes various type of MNPs such as AgNPs, metal oxides, non-metal, and metalloid based nanoparticles used in various stages of the wound healing process, while (2) includes organic nanoparticles that have therapeutic benefits (Nethi et al., 2019). As previously mentioned AgNPs are easily coated with different useful functional groups and incorporated into various materials to fabricate nanocomposites and scaffolds which afford them a synergic activity in the treatments of wounds (Singh, 2016; Mihai et al., 2019).

Colloids (Lee et al., 2011; Niska et al., 2018; Mihai et al., 2019), gels (Wu et al., 2014; Sood & Chopra, 2018; Chakrabarti et al., 2019), porous (Wu et al., 2014; Liang et al., 2016; Tonda-Turo et al., 2016; Pal et al., 2017; Mihai et al., 2019) and polymeric (Liang et al., 2016; Lu et al., 2017; Oryan et al., 2018; Biranje et al., 2019; Loan Khanh et al., 2019) materials embedded with AgNPs all belong to the subclass of nanocomposites. These materials are enriched with many useful groups such as amino acids, proteins, phenols and alkaloids which are used for the reduction and stabilization of AgNPs. The antibacterial property of AgNPs works in synergy with the low toxic, biocompatible, biodegradable and moisture retaining phytochemicals present in these materials leading to faster healing.

Scaffolds such as hydrogels (Ghavaminejad, Park & Kim, 2016; Makvandi et al., 2019; Pham et al., 2020), coatings (Xu et al., 2013; Mekkawy et al., 2017; Baygar, 2020), nanofibers (Neibert et al., 2012; GhavamiNejad et al., 2015; Mohseni et al., 2019), and films (Kinam Park, 2014; Singla et al., 2017; Yu et al., 2017) have the ability to imitate properties of extracellular matrix (ECM) and highly utilized in formulations for wound healing (Berthet et al., 2017). ECMs are fibrous in nature and possess nanoscale features that are attractive for wound healing purposes, that is why researchers are using materials such as polymers to mimic these structures (Hamdan et al., 2017). Impregnation of AgNPs on these scaffolds achieves synergic effects that aid accelerated wound healing (Gunasekaran, Nigusse & Dhanaraju, 2011). Among these scaffolds dressings, hydrogels have exhibited tremendous wound healing abilities (Mihai et al., 2019). Hydrogels are made up of a network of polymers that have a vast number of hydrophilic groups with cross-interactions, which form a 3-dimensional matrix capable of trapping liquids like water or wound exudates (Mihai et al., 2019). They can rehydrate necrotic skin tissues and advance autolytic debridement as a result of their high moistening abilities (Berthet et al., 2017). Not only do they provide the wound site with sufficient moisture but also enable gas diffusion and absorb wound exudates, thereby preventing secondary infections (Mihai et al., 2019).

1.6.3. Toxicity of AgNPs

Despite the global accelerated increase in manufacturing and commercialization of nanotechnology-based products, there are still issues in question such as their exposure, long and short term toxicity towards animals, humans and the ecosystem (Tran, Nguyen & Le, n.d.). As previously mentioned, prolonged contact with conventional silver products causes argyria, thus it is crucial to study the toxicity effects of silver at the nanoscale since at this dimension the inert metal bursts with energy due to confinement effects. AgNPs pose a more harmful threat compared to their bulk counterparts because of their significantly smaller size and larger surface area to volume ratios which give rise to enhanced chemical and physiological performances (Roy et al., 2013). For this reason, the interaction of this nanometal with humans and the environment needs to be explicitly investigated, so that unfavourable consequences can be known without ambiguity to ensure that proper steps can be taken to overcome the implicated health risks and potential cytotoxicity in cases of accidental and prolonged exposure (Loomba & Scarabelli, 2013).

AgNPs may be administered orally, absorbed by the skin through direct contact or inhaled (Adeyemi & Adewumi, 2014; Golinska et al., 2014), the latter being the most common route of exposure among employees who fabricate and deal with nanomaterials (Nymark et al., 2013). Once they enter the body, they can travel and become toxic to many other organs (Adeyemi & Adewumi, 2014; Ceresa et al., 2019). If AgNPs are exposed to the skin, they can get internalized by macrophages and cause inflammation, pronounced neovascularization and unusual generation of extracellular matrix. And can use a different route when ingested, and accumulate in the liver since it is the main metabolic organ in the human body, where they can induce reactive oxygen species (ROS), lower mitochondrial function and the consumption of glutamine levels. When inhaled, AgNPs may attack the respiratory system through oxidative stress (Golinska et al., 2014). There are many proposed mechanisms for AgNPs toxicity, Figure 1.12 summarises four of the proposed mechanisms. AgNPs are suspected to induce cellular toxicity by one of the four mechanisms: (i) adherence of AgNPs to the cell membrane resulting in physical destruction and cell membrane impairment; (ii) internalization of AgNPs can cause malfunction of intracellular organelle (mitochondria, vacuoles and ribosomes), and biomolecules (proteins, enzymes, lipids and DNA); (iii) induced cytotoxicity and oxidative stress by generation of ROS and free radicals which also disrupts activity of biomolecules and

intracellular micro organelles; and lastly by (iv) modulation of intracellular signal pathways (Lee & Jun, 2019; Medici et al., 2019b).

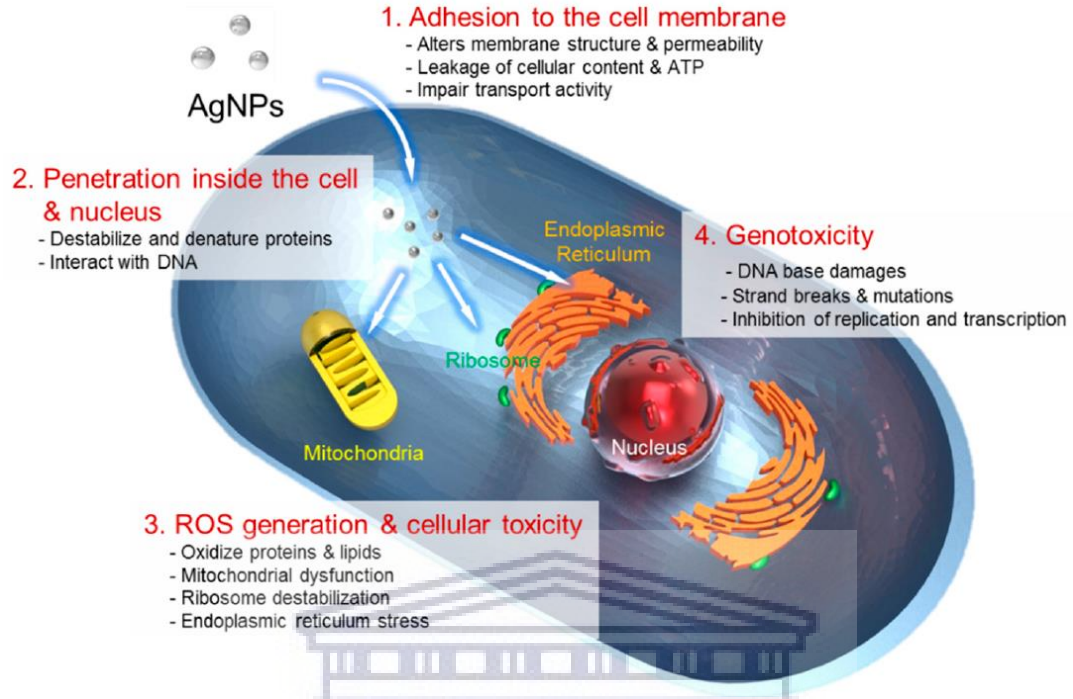

Figure 1. 12: Routes of cytotoxicity action of AgNPs (1) Adhesion to cell wall; (2) Cellular internalization; (3) ROS generation; (4) Genotoxicity (Lee & Jun, 2019).

The release of Ag^{+} ions inside the cell, has been identified as the biologically active agent responsible for inducing cytotoxicity of AgNPs, however this does not explain why AgNPs have improved cytotoxicity than other silver bearing compounds (Medici et al., 2019a). Many scientists proposed that this toxicity is a result of highly exposed surface area and surface energies of the nanoparticles that allow for improved interaction with the cells, and they increase with a decrease in particles size, that is why AgNPs of smaller sizes have a higher toxicity effect compared to larger ones (Roy et al., 2013). However, these toxicity effects depend on the study areas for different groups. Numerous papers reported that AgNPs are less toxic towards animal cells compared to bacterial cells, creating a curative opening that can kill bacteria without posing a threat to animal cells (Shao et al., 2019). This stems from the highly complex structure and functionality of the former which is not present in the latter, thus higher Ag ions concentrations are needed to exert the same toxic effect of bacterial cells on animal cells (Ceresa et al., 2019). That is why most identified IC_{50} AgNPs concentration kill bacteria but pose no cytotoxic effect on animal cells as reported by (Mohanty et al., 2012) that 2 µM of the starch stabilized AgNPs had no notable cytotoxicity towards macrophages while the same

concentration was lethal to various gram-positive and gram-negative bacteria. Another paper reported that various AgNPs/chitosan dressings enhanced cell growth on both human embryonic kidney cells (HEK293) and human normal hepatocyte cells (L02) while they imposed a toxic effect on drug sensitive *S. aureus* and *E. coli* and drug-resistant *MRSA* and drug-resistant *E. coli* at increasing AgNPs content inside the dressings (Liang et al., 2016).

1.7. Hypothesis

DMSO-capped AgNPs could accelerate the wound healing process due to the individual medical properties of DMSO and silver.

1.8. Aims and Objectives

The purpose of this study was to exploit the antibacterial properties of AgNPs and cell growth promoting abilities of DMSO to probe wound healing properties.

The general objectives were as follows:

- Synthesize various AgNPs in different solvents i.e water and DMSO denoted bare-AgNPs and DMSO-AgNPs, respectively.
- Characterize the size, surface morphology, optical properties, structural composition and stability of bare-AgNPs and DMSO-AgNPs with different analytical techniques such as UV-vis, FTIR, DLS, SAXS and HR-TEM.
- Investigate the anti-bacterial properties of bare-AgNPs and DMSO-AgNPs using the agar well diffusion method on gram-negative and gram-positive bacterial strains which frequently colonialize non-healing wounds, i.e. *E. coli*, *P. aeruginosa*, *S. aureus* and *MRSA.*
- Evaluate cytotoxic effects of bare-AgNPs and DMSO-AgNPs on epithelial (CHO), fibroblasts (KMST-6) and keratinocytes (HaCaT) using MTT assay.
- Measure cellular uptake of bare-AgNPs and DMSO-AgNPs using DF microscopy.
- Evaluate the wound healing activity of bare-AgNPs and DMSO-AgNPs on KMST-6 cells through wound scratch assay by measuring the wound closure rate.
- Investigate changes in cellular integrity of KMST-6 cells after treatment with bare-AgNPs and DMSO-AgNPs by measuring generation of intracellular ROS and depolarization of MMP using cell permeant florescent dyes CM-H_2DCFDA and TMRE, respectively.

CHAPTER 2

Methods and Materials

2.1. Materials

Table 2.1 contains relevant information about the different cell types and bacterial strains used to test the biological activities of the AgNPs.

Table 2.1: Cell types and their supplier

Cell line	Abbreviations	Cell type	Tissue of origin	Company and location
Chinese Hamster Ovary	CHO	Normal	Ovary	ATCC, Manassas, USA
Adult Human Keratinocyte	HaCaT	Normal	Skin (dermis)	ATCC, Manassas, USA
Human Fibroblast	KMST-6	Normal	Skin (dermis)	ATCC, Manassas, USA
Escherichia coli	*E. coli*	Bacterial	-	ATCC, Manassas, USA
Methicillin-resistant Staphylococcus aureus	*MRSA*	Bacterial	-	ATCC, Manassas, USA
Staphylococcus aureus	*S. aureus*	Bacterial	-	ATCC, Manassas, USA
Pseudomonas aeruginosa	*P. aeruginosa*	Bacterial	-	ATCC, Manassas, USA

Table 2.2 lists all the chemicals and solvents used for the, preparation, synthesis, analysis and activity of the nanoparticles. All the chemicals used in this study were of good quality and grade, they were used as provided by the supplier without modifications.

Table 2. 2: List of chemicals and suppliers

Chemical Name	Common Name	Chemical formula	Company
1-cyclopropyl-6-fluoro-4-oxo-7-piperazin-1-ylquinoline-3-carboxylic acid	Ciprofloxacin	$C_{17}H_{18}FN_3O_3$	Sigma Aldrich, St Louis, USA
3-(4,5-Dimethyl-2-thiazolyl)-2,5-diphenyl-2H-tetrazolium bromide	MTT	$C_{18}H_{16}BrN_5S$	Sigma Aldrich, St Louis, USA
4´,6-Diamidino-2-phenylindole dihydrochloride	DAPI	$C_{16}H_{15}N_5 \cdot 2HCl$	Sigma Aldrich, St Louis, USA
Acetone	-	C_3H_6O	Kimix Chemical and Lab supplies, Cape Town, SA
Allantoin	Glyoxylic diureide	$C_4H_6N_4O_3$	Sigma Aldrich, St Louis, USA
CM-H_2DCFDA	ROS indicator	$C_{27}H_{19}Cl_3O_8$	Invitrogen, Carlsbad, USA
Deionized Water	d(H_2O)	H_2O	-
DMSO	DMSO	C_2H_6OS	Kimix Chemical and Lab supplies, Cape Town, SA
DMSO	DMSO	C_2H_6OS	Sigma Aldrich, St Louis, USA
Doxorubicin	Dox	$C_{27}H_{29}NO_{11} \cdot HCl$	Sigma Aldrich, St Louis, USA
Dulbecco Buffered Phosphate Saline	DBPS	-	Biochrom, Cambridge, UK
Dulbecco Modified Eagle medium	DMEM	-	Biochrom, Cambridge, UK
Ethanol	-	C_2H_5OH	Kimix Chemical and Lab supplies, Cape Town, SA
Foetal Bovine Serum	FBS	-	Biochrom, Cambridge, UK
Ham's F12 Medium	Ham's F12	-	Biochrom, Cambridge, UK
Hydrogen Peroxide	-	H_2O_2	Sigma Aldrich, St Louis, USA
Paraformaldehyde	Polyoxymethylene	$HO(CH_2O)_nH$	Sigma Aldrich, St Louis, USA
Penicillin/streptomycin	Pen-strep	-	Lonza, Basel, Switzerland
Silver Nitrate	-	$AgNO_3$	Sigma Aldrich, St Louis, USA
Sodium Borohydride	-	$NaBH_4$	Sigma Aldrich, St Louis, USA
Tetramethylrhodamine, ethyl ester	TMRE	$C_{26}H_{27}ClN_2O_7$	Invitrogen, Carlsbad, USA
Trypsin-EDTA	-	-	Biochrom, Cambridge, UK

Table 2.3 lists all the equipment used in the study, their supplier and company location.

Table 2. 1: Analytical instruments involved in the study

Technique	Common Name	Machine	Supplier	Location
UltraViolet Visible Spectroscopy	UV-Vis	POLARstar Omega Plate reader	BMG Labtech	Offenburg, Germany
Fourier Transforms Infrared Spectroscopy	FTIR	PerkinElmer spectrometer	Anton Paar	Graz, Austria
Dynamic Light Scattering	DLS	Malvern Zetasizer Nano-ZS90	Malvern Instruments	Malvern, UK
High Resolution Microscopy	HR-TEM	F20 Tenai EDAX G^2	FEI	Eindhovea, Netherlands
Small Angle X-ray Scattering	SAXS	SAXSpace Spectrometer	Anton Paar	Graz, Austria
Darkfield and Florescent Microscope	DF Microscope	Axioplan-2 Imaging Fluorescent Microscope	Zeiss	Jena, Germany
Flow Cytometer	-	Accuri™ C6 flow cytometer	BD Biosciences	Belgium
Centrifuge	-	Eppendorf mini spin plus	Eppendorf	Hamburg, Germany
Thermomixer	-	Eppendorf thermomixer comfort	Eppendorf	Hamburg, Germany
Light Microscope	-	EVOS™ XL core Imaging system	ThermoFisher scientific	Massachusetts, USA

2.2 Methods

2.2.1 Glassware Preparation

All the glassware was thoroughly washed with soap and warm water, followed with 70% ethanol and then rinsed with acetone and placed in the oven to dry before use.

2.2.2 Synthesis of AgNPs

AgNPs were synthesized following the chemical reduction method by (Rashid, Bhuiyan & Quayum, 2013) with slight modifications, using $NaBH_4$ and DMSO as reducing agents. The DMSO-AgNPs were synthesized by DMSO and the combination of $NaBH_4$ and DMSO. The methods are described below.

2.2.2.1 $NaBH_4$ as a reducing agent

The successful synthesis of AgNPs was carried out using the chemical reduction method of silver in the presence of $NaBH_4$.

The $AgNO_3$ solutions were prepared by adding different masses of $AgNO_3$ into 25 mL distilled water in order to obtain the following concentrations: 0.25 mM, 0.50 mM, 0.75 mM, 1 mM, 1.25 mM, 1.50 mM and 1.75 mM. The $AgNO_3$ solutions were then added drop wise (about 1 drop per second) to 30 mL of 2 mM $NaBH_4$ solution prepared in distilled water that had been chilled in an ice bath. The reaction mixture was stirred gently on a magnetic stirrer. The solution turned to light yellow after the addition of 2 mL of $AgNO_3$ and to brighter yellow after adding 10 mL of the $AgNO_3$ solution. The entire addition process took about 3 minutes, after which the stirring was stopped and the stir bar was removed.

2.2.2.2 DMSO as a reducing Agent

DMSO-AgNPs were synthesized following the method described in 2.2.2.1 with some modifications. DMSO was used as a reducing agent instead of $NaBH_4$, and the $AgNO_3$ solution was prepared in (a) DMSO and (b) dH_2O.

The synthesis of DMSO-AgNPs was attempted by adding 1.5 mL of 1 mM $AgNO_3$ solution prepared in DMSO to 500 mL of increasing percentages of DMSO solutions (1,2,3,4,5,20,40,60,80 and 100%). The samples were covered with foil and placed in the dark to investigate the spontaneous reduction of $AgNO_3$ into DMSO-AgNPs. Similarly, the same reaction was done with 1 mM of $AgNO_3$ solution prepared in dH_2O. This reaction was also performed at 70 ºC while shaking at a speed of 700 rpm for 6 hours in an Eppendorf thermomixer comfort.

2.2.2.3. Synthesis of $NaBH_4$-reduced DMSO-AgNPs

The solutions used in the synthesis of NaBH4-reduced DMSO-AgNPs were prepared in 100% DMSO, i.e. and 2 mM $NaBH_4$. To the 30 mL $NaBH_4$ solution (2 mM) gentle stirring at room temperature for about 3 minutes, 25 mL solution of 1 mM $AgNO_3$ was added dropwise. After adding 10 mL of the $AgNO_3$ solution, the colour changed from clear to pale yellow and finally reddish-brown, and the reaction was stopped and the stirring bar removed from the reaction vessel. The same procedure was repeated for synthesis of 1,2,3,4,5,20,40,60 and 80% $NaBH_4$ reduced DMSO-AgNPs. The different percentages of DMSO were diluted in dH_2O.

All the prepared AgNPs were spun down at 14,500 rpm for 30 minutes using an Eppendorf mini spin plus centrifuge machine and the pellets were resuspended in dH_2O.

2.2.2.4. Storage of the AgNPs

The AgNPs were covered in foil and stored in the fridge until further analysis.

2.3. Characterization of the AgNPs

Knowing the physicochemical properties of AgNPs is very crucial in understanding their behaviour, safety, efficacy and biodistribution (Zhang et al., 2016). Various characterization techniques that give specific information such as size, stability, chemical composition and distribution are employed for this purpose. In this study, UltraViolet-visible (UV-vis) spectroscopy, Fourier Transforms Infrared (FTIR) spectroscopy, Dynamic Light Scattering (DLS), High-Resolution- Transmittance Electron Microscopy (HR-TEM) and Small Angle X-ray Spectroscopy (SAXS) were used to analyse the bare-AgNPs and DMSO-AgNPs

2.3.1. UV-vis spectroscopy

The absorption spectra of all the prepared AgNPs was obtained using UV-vis Spectroscopy through a POLARstar Omega plate reader at the Life sciences building, University of the Western Cape (UWC). The samples were added in a 96 non-sterile well plate, which was inserted in the plate reader and the absorbance measurements were made over the wavelength range of 300-600 nm at 100 µL of each sample.

2.3.2. FTIR spectroscopy

The structural composition of bare-AgNPs and DMSO-AgNPs (3% DMSO-AgNPs, 4% DMSO-AgNPs and 100% DMSO-AgNPs) was evaluated by FTIR spectroscopy through identification of functional groups present in each sample by observing the vibrational spectra of molecules between 4000-600 cm^{-1}. The FTIR spectra were recorded on the PerkinElmer spectrometer at UWC, pharmacy department. The analysis was performed by dropping liquid samples with a 200 µL pipette on the surface at an angle of 15, the surface and the knob were thouroghly cleaned with ethanol and wiped dried with a tissue after each measurement.

2.3.3. HR-TEM

Sizes and surface morphologies of bare-AgNPs, 3% DMSO-AgNPs, 4% DMSO-AgNPs and 100% DMSO-AgNPs were probed using HR-TEM with a resolution of ~0.2 nm at 200 keV on a F20 TECNAI EDAX G^2 microscope by drop coating ~ 2 ml of each samples on ultrathin carbon-film-coated copper grids. HR-TEM was used in conjuction with ImageJ software to determine the diameter of the particles. HR-TEM analysis was perfomed at the electron microscope unit at UWC.

2.3.4. SAXS

The particle sizes and size dispersions of the prepared bare-AgNPs and DMSO-AgNPs (3% DMSO-AgNPs, 4% DMSO-AgNPs and 100% DMSO-AgNPs) were evaluated using a SAXSpace system with an X-ray beam of 8-keV at sensorlab, UWC. All the resulting measurements from the analysis were Fourier transformed using GIFT software into a pair distance distribution function (PDDF) by volume, intensity and size distribution by number function. For each measurement, 100 µL liquid samples were loaded into the system via a 1 mm diameter quartz capillary positioned at a distance of 305.3 mm from the CCD and temperature-controlled at 22 °C. After each use, the cappillary was thoroughly cleaned with ethanol and vacuum dried.

2.3.5. DLS

Particle sizes and distributions (polydispersity index, PDI) as well as the zeta potentials were further investigated using a Zetasizer elicited on the DLS technique. Particle size, PDI and zeta potentials of bare-AgNPs and DMSO-AgNPs (3% DMSO-AgNPs, 4% DMSO-AgNPs and

100% DMSO-AgNPs) were determined using a Zetasizer by placing specific cuvettes which contain a 10:1 dilution of the solvent dH_2O and the sample in question in the machine. For each measurement, appropriate settings on the machine were set. DLS analysis was done at life science building, UWC.

2.4. Biological Activity of the AgNPs

The bio-activity of the AgNPs was performed at the Biolabels Node research labs (Department of Biotechnology, UWC) following the biosafety level 2 regulations. The biological waste was disposed according to the laboratory's disposal protocol indicated in their standard operating procedures.

2.4.1. Antimicrobial Activity of the AgNPs

Antibacterial activity of various AgNPs was evaluated on four bacterial strains of . *E. coli*, *P. aeruginosa*, *S. aureus* and *MRSA* using agar well diffusion method as described (Loan Khanh et al., 2019).

2.4.1.1. Bacterial culture

A single colony was picked from an agar plate containing each of the selected bacterial strains and tranferred into a 15 mL tube that contains Muller Hinton broth. The cultures were incubated at 37 ^oC with shaking at 250 rpm for 6 hours.

2.4.1.2. Agar Well Diffusion Method

A cotton swab was then dipped into the bacterial suspension and spread over the entire surface area of the agar. Then 50 µL of the positive control (10 mg/L ciprofloxacin), negative control (dH_2O) and 100 µg/mL AgNPs were deposited into the wells that been punctured and clearly labelled in the agar. The plates were then incubated at 37 ^oC for 24 hours after treatment. The zones of inhibitions were observed and quantified.

2.4.2. Investigation of the wound healing effects of the AgNPs

2.4.2.1. Cell culture

Cell culture experiments were carried out using CHO, KMST-6 and HaCaT cell lines. The cells were cultured in their respective media; Ham's F12 for CHO cells, and DMEM for KMST-6

and HaCaT cells. All the media were supplemented with 1% pen-strep and 10% FBS, unless stated otherwise. The cells were cultured at 37 °C in a humidified atmosphere of 5% CO_2, the media was changed every three days until the cells reached ~80% confluency before sub-culturing.

For cytotoxicity studies, the cells were seeded in 96 well plates at a density of 1 x 10^5 cells/mL, 100 µL per well. For cellular uptake, all the cell lines were seeded in 12 well plates at a density of 2 × 10^5 cells/mL in their respective medium, 500 µL per well.

2.4.2.1.1. Cytotoxicity Assay

Cytotoxicity of the AgNPs was evaluated using the MTT reduction assay as previously described (Gurunathan et al., 2013). Briefly, the cells were seeded in a 96 well plate in their respective medium at 1 x 10^5 cells/mL, 100 µL per well and incubated for 24 hours. After 24 hours, the culture media was discarded and replaced with fresh media consisting of various treatments. The treatments include: DMSO (0 – 6%) and Allantoin (0-3.5 µg/mL), Dox (0-3.5 µg/mL), DMSO-AgNPs (3% DMSO-AgNPs, 4% DMSO-AgNPs and 100% DMSO-AgNPs) and bare-AgNPs (0-3.5 µg/mL). The cells were incubated for 24, 48 or 72 hours, after each treatment the media was replaced with fresh media containing 10 μL of MTT (5mg/mL in dH_2O) was added to each well, and the plate was incubated for a further 3 hours at 37 °C. After that, the MTT containing media was removed and the resulting formazan was solubilized in 100 μL of DMSO with gentle shaking at 37 °C for another 10 minutes. The optical density at 570 and 700 nm was measured in the POLARstar Omega plate reader. Cell viability was calculated as a percentage of the absorbance of the treated cells versus untreated controls * 100.

2.4.2.1.2. AgNP Cellular Uptake by Dark Field Microscopy

Darkfield florescent microscopy was used to investigate the cellular uptake of various AgNPs by the CHO, KMST-6 and HaCaT cells as previously described (S Sibuyi et al., 2017). A cell density of 2×10^5 cells/mL was seeded in 12 well plates containing round coverslips, and the cells were allowed to attach to the coverslips in the wells. The following day, the media was aspirated and replaced with fresh media consisting of 3.5 µg/mL of bare-AgNPs, and DMSO-AgNPs (3% DMSO-AgNPs, 4% DMSO-AgNPs and 100% DMSO-AgNPs). After 24 hours post treatment, the culture media was discarded and the cells were washed three times with 1×PBS to remove any non-internalized AgNPs. Followed by fixation with 1000 µL of 4%

paraformaldehyde solution for 15 minutes. After that, the solution was removed and the cells were washed twice with 1×PBS. After washing, the coverslips were mounted on glass slides using nuclear staining Fluoroshield-DAPI mounting media which stains the nucleus of the cells. The coverslips were stored in the dark and allowed to dry for another 24 hours. Lastly, the cells were imaged under a darkfield and fluorescence using Axioplan-2 imaging fluorescent microscope.

2.4.2.1.3. Wound Scratch Assay

The *in vitro* wound scratch assay was used to investigate the rate of cell migration on KMST-6 cells after exposure to various treatments as described (Kumar, Houreld & Abrahamse, 2020). Briefly, the cells were seeded at a density of 2×10^5 cells/mL in a 12 well plate in DMEM. The medium was replaced with starvation medium (DMEM containing 1% FBS) followed by incubation at 37 °C and 5% CO_2, then 48 hours later, they were treated with 1% DMSO and 3.5 µg/ml of allantoin, AgNPs (bare AgNPs, 3% DMSO-AgNPs, 4% DMSO-AgNPs and 100% DMSO-AgNPs) prepared in starvation media. 24 hours later, the cells were washed two times with PBS to remove any sample material that was not internalized. A 200 µL sterile yellow pipette tip was used to create a wound on the cells, PBS was again used to wash the cells twice to get rid of the detached cells and the cells were kept in starvation medium for up to 72 hours. Wound closure was monitored by taking images of the scratch at the same spot for 0, 24, 48 and 72 hours with an EVOS™ XL core imaging system. The step by step wound scratch protocol is outlined in figure 2.1.

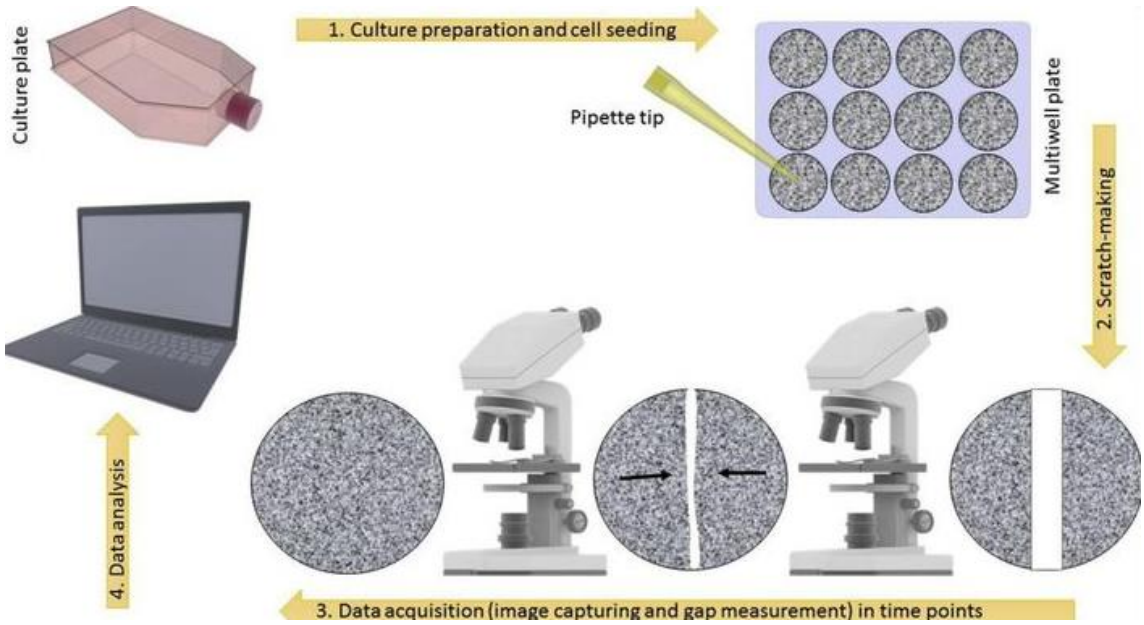

Figure 2. 1: Detailed protocol for wound scratch assay (Grada et al., 2017).

The wound area was measured at 0, 24, 48 and 72 hours post treatment and analysed using MRI wound healing tool on the imageJ software. The rate at which the cells migrated expressed as pixels/ hour was calculated based on the procedure explained by (Kumar, Houreld & Abrahamse, 2020) using the following equation:

$$Rate\ of\ Migration\ \left(\frac{pixels}{hour}\right) = \left[\frac{(Pre\text{-}migration\ area)-(Migration\ area)}{Time}\right] \quad (1)$$

Where pre-migration area is the initial wounded area at T = 0 hours and the migration area is the wounded area at a specific time point.

2.4.2.1.4. Trypan blue exclusion assay

After 72 hours of the wound scratch assay, cell viability of KMST-6 was evaluated using Trypan blue exclusion assay as described (Aueviriyavit, Phummiratch & Maniratanachote, 2014). The media was discarded and the cells were washed twice with 1×PBS and detached from the plates using trypsin-EDTA. The detached cells were spun down at 2,500 rpm for 5 minutes. 10 µL of the suspension cells were mixed with 10 µL of trypan blue dye and counted on a hemacytometer. Dead cells appeared blue while live cells had a clear appearance. The cell

viability was determined as a percentage of live cells and demonstrated relative to the untreated control.

2.5. Flow cytometer analysis

For the flow cytometer studies, only the KMST-6 cells were used evaluate reactive oxygen species (ROS) and depolarization of the mitochondrial membrane potential as described (Aueviriyavit, Phummiratch & Maniratanachote, 2014). In both cases, the cells were seeded at 2×10^5 cells/mL in 12 well plates. The cells were treated with 1% DMSO, and 3.5 µg/mL of allantoin and AgNPs (bare-AgNPs, 3% DMSO-AgNPs, 4% DMSO-AgNPs and 100% DMSO-AgNPs) for 24 hours. Then the media was aspirated and the cells were washed twice with 1×PBS, detached using trypsin-EDTA. The cell suspension was centrifuged at 2,500 rpm for 5 minutes, the pellets were used in the following assays.

2.5.1. Measurement of intracellular ROS

Investigation of the intracellular ROS was performed using CM-H_2DCFDA compound. Following the steps described above, 200 μL of 7.4 µM CM-H_2DCFDA (prepared in PBS) was added to the cells and incubated for 30 minutes. The cells were washed by adding 4 mL of 1×PBS, and centrifuged as before. The pellets were resuspended in 300 µL of DMEM and further incubated at 37 °C for 30 minutes followed by analysis using an Accuri™ C6 flow cytometer.

2.5.2. Measurement of depolarization of MMP

Mitochondrial damage analysis was done using TMRE. 200 µL of TMRE was added to the tubes and the cells were further incubated for 30 minutes. The cells were washed once by addition of 1×PBS, followed by centrifugation at 2,500 rpm for 5 minutes. The media was aspirated, 300 µL of 1× PBS in each tube. The cell suspension was analysed using an Accuri™ C6 flow cytometer.

CHAPTER 3

RESULTS AND DISCUSSION

3.1. Synthesis of bare-AgNPs

Synthesis of AgNPs follows a sequential process, which is thoroughly described for AgNPs formed by reduction of silver perchlorate ($AgClO_4$) with $NaBH_4$. The reaction mechanism is presented in Figure 3.1, it starts with the reduction of Ag^+ ions into Ag° forming dimers, trimmers and clusters in milliseconds. The second step is the first coalescence and it involves the generation of smaller particles with radii between 2 and 3 nm from the clusters generated in the previous step. In the metastable state, which is the third step, the formed AgNPs maintain their uniform size for a couple of minutes. The last step is the second coalescence and formation of the AgNPs with the final size (Polte et al., 2012). This reaction mechanism might hold for other silver salt, since $AgClO_4$ only served as the source of silver. $AgNO_3$ was chosen as the silver salt for this study because it is relatively cheaper and readily available than $AgClO_4$. Further, the former is relatively environmentally friendlier than the latter.

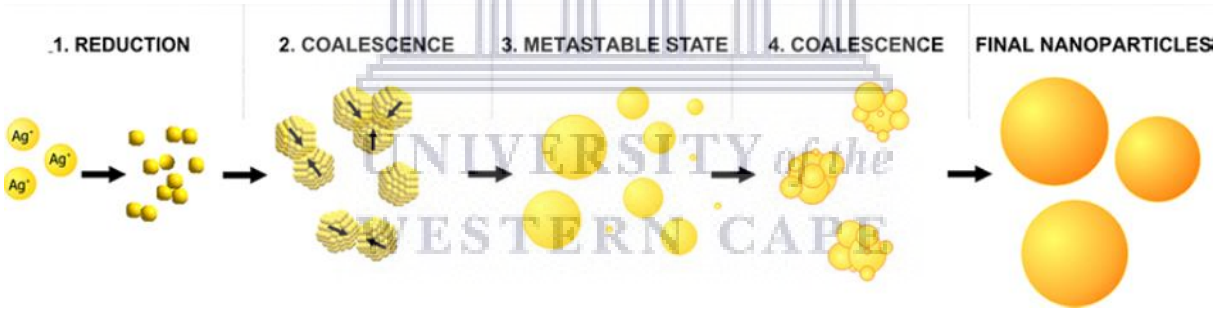

Figure 3. 1: Proposed reaction mechanism for the formation of AgNPs through the reduction of $AgClO_4$ using $NaBH_4$. Step 1 indicates the reduction of Ag^+ into Ag°, Step 2 is the first coalescence step 3 metastable state of AgNPs Step 4 is the second coalescence step leading to the formation of AgNPs with the final size (Polte et al., 2012).

Bare-AgNPs were synthesized by drop-wise addition of various concentrations of $AgNO_3$ solution into an ice cold $NaBH_4$ solution. The colour changes observed throughout the course of the reaction are represented in Figure 3.2. These changes in colour have a direct link to the proposed mechanism in Figure 3.1. Figure 3.2(A) represents the reduction step, where Ag^+ is transformed into Ag° resulting in the formation of clusters, dimers and trimers. At this step, the reaction mixture is still colourless. Figure 3.2(B) is the first coalescence step, where AgNPs with small radii are formed, this is characterized by the pale-yellow colour. In Figure 3.2(C),

the slightly darker yellow indicates the formation of AgNPs with uniform size from the smaller AgNPs generated in Figure 3.2(A). This colour is observed for a few minutes indicating metastable state of the formed AgNPs. The darker yellow colour observed in Figure 3.2(D) indicates the presence of overall larger AgNPs which were formed through the second coalescence step. Lastly the colour observed in Figure 4.2(E) represents the final AgNPs.

Figure 3. 2: Reaction of $AgNO_3$ and $NaBH_4$ leading to the formation of bare-AgNPs. Different stages of bare-AgNPs formation are as follows: (A) reduction, (B) first coalescence, (C) metastable state, (D) second coalescence and (E) final AgNPs.

3.1.1 Effect of Concentration

Various concentrations of $AgNO_3$ (0.5 – 1.75 mM) were utilized for the synthesis of bare-AgNPs through the $NaBH_4$ reduction method, the AgNPs are represented in Figure 3.3. AgNPs synthesized from 0.25 mM $AgNO_3$ appeared pale yellow in colour followed by the ones synthesized at 0.5 mM $AgNO_3$ which were slightly darker compared to the former. The colour intensity became darker with increasing concentrations of $AgNO_3$, from 0.75 mM to 1.75 mM. Thus, the content of $AgNO_3$ was directly proportional to the amount of the AgNPs. Furthermore, since the observed colour of the AgNPs is characteristic of the size of the AgNPs as deduced from the reaction mechanism by Polte et al, lighter colours of the AgNPs suggest that they are smaller in size compared to darker AgNPs. Thus, the 0.25 mM AgNPs were smaller in size compared to the AgNPs made from 0.5 - 1.75 mM $AgNO_3$.

Figure 3. 3: AgNPs prepared by utilizing 0.25, 0.50, 0.75, 1, 1.25, 1.5 and 1.75 mM concentrations of $AgNO_3$, the colour of the prepared AgNPs intensifies with an increase in concentration of the $AgNO_3$.

3.1.2. DMSO as a reducing agent

DMSO has been reported to possess wound healing properties such as cell growth, pain relief and low toxicity at lower concentrations. Moreover, the solvent can easily permeate cell membranes and interact with biological components leading to better wound healing outcomes (Astley & Levine, 1976; Goldblum et al., 1983; Rodríguez-Gattorno et al., 2002; ICH International Conference on Harmon, 2009; Bhosale, Chenna & Bhanage, 2017; European Medicines Agency, 2019). Therefore, it was used as the solvent of choice in the present study.

Reduction of silver salts into AgNPs in the presence of some reducing solvents such as certain alcohols, formamides and sulfoxides has been previously reported (Rodríguez-Gattorno et al., 2002). The present study investigated the spontaneous reduction of $AgNO_3$ into AgNPs using DMSO. When 100% DMSO or DMSO diluted in dH_2O was added into 1 mM $AgNO_3$ solutions, no colour change was observed in the solutions at room temperature (Figure 3.4 (A) and (B)). Lack of colour suggested that no reduction and no AgNP formation had occurred, since AgNPs are characterized by a yellow-brown colour. Thus, DMSO alone cannot be used to form AgNPs, and was ruled out as a potential reductant of the $AgNO_3$ salt. This result concurs with report made by Rodrı´guez-Gattorno and his colleagues where they investigated the voluntary reduction of Ag^+ ions into Ag° using several silver salts such as silver 2-ethylhexanoate [Ag(ethex)], $AgNO_3$, $AgClO_4$ and silver metavanadate (AgO_3V) at room temperature in DMSO via the co-precipitation method. They reported that it was only Ag(ethex) that was reduced by DMSO forming AgNPs, and not the other silver salts. $AgNO_3$ managed to form AgNPs in the presence of another reducing agent, (trisodium citrate) (Rodríguez-Gattorno et al., 2002). Thus, in this study, $NaBH_4$ was the reductant of choice because the synthetic procedure that involves $NaBH_4$ is very simple, well established, does not require heating or excessive temperatures, inert conditions or any other complicated apparatus (Pacioni et al., 2015).

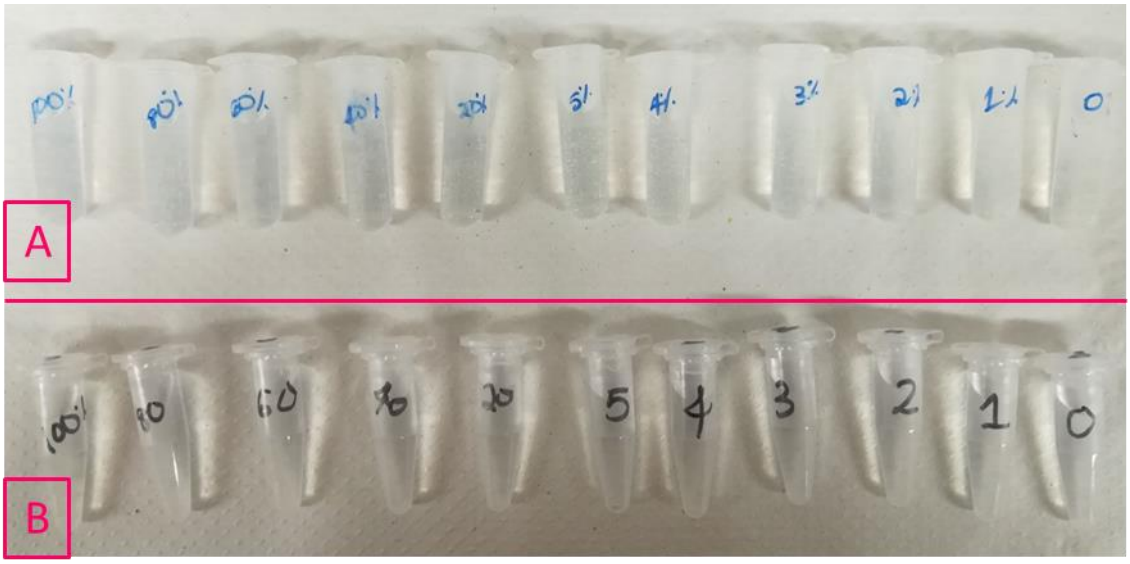

Figure 3. 4: Reaction mixtures of 1 mM $AgNO_3$ dissolved in 0-100% DMSO-dH2O dilutions with (a) just DMSO and (b) dH2O, in both instances no reduction of $AgNO_3$ to AgNPs occurred since the solutions retained their colourless nature.

3.1.3 Synthesis of $NaBH_4$ reduced DMSO-AgNPs

During the dropwise addition of $AgNO_3$ into the $NaBH_4$ solution in presence of DMSO, colour changes were observed as the reaction progressed as demonstrated in Figure 3.5. It was also suggested that the formation of DMSO-AgNPs also follows the mechanism proposed by Polte et al in Figure 3.1. Hence, the reduction of Ag^+ into Ag° occurs in Figure 3.5 (A), the absence of colour in this stage indicates that DMSO-AgNPs have not formed yet, followed by the first coalescence in Figure 3.5 (B) characterized by the light orange-brownish colour which represents the formation of DMSO-AgNPs with small radii. Figure 3.5 (C), is the metastable state where the formed DMSO-AgNPs maintain a uniform size for a few minutes, the notable colour difference between the former and the later steps indicated that at this state, the DMSO-AgNPs are larger in size compared to the former step. The second coalescence step in Figure 3.5 (D) is identified by the darker brown colour of the DMSO-AgNPs, which is also the final size of the DMSO-AgNPs (Figure 3.5 (E)).

Figure 3. 5: Reaction of $AgNO_3$ and $NaBH_4$ in the presence of DMSO leading to the formation of DMSO-AgNPs. Different stages of DMSO- AgNPs formation are as follows: (A) reduction, (B) first coalescence, (C) metastable state, (D) second coalescence and (E) final AgNPs.

Following the successful synthesis of DMSO-AgNPs through the $NaBH_4$ reduction route, the present study also aimed to investigate the role of the concentration of DMSO in the synthesis. Hence, 20, 40, 60 and 80% DMSO solutions were also utilized for the synthesis of DMSO-AgNPs presented in Figure 3.6. The 20% DMSO-AgNPs appeared colourless, indicating that the reduction of Ag^+ into Ag° did not occur at this concentration. DMSO-AgNPs were synthesized at 40, 60 and 80% DMSO, as indicated by the different shades of brown colour in each. However, the DMSO-AgNPs were quite unstable and aggregated instantly and were not used any further. This high degree of instability and aggregation behaviour could be caused by the high content of DMSO in the miscible solution. Thus, it was suggested that lower concentrations of DMSO such as 1, 2, 3, 4 and 5% be explored instead.

Figure 3. 6: Synthesis of DMSO-AgNPs using 20 % to 80 % DMSO.

The 1 – 5% DMSO-AgNPs did not aggregate immediately, suggesting they have improved stability compared to the 20, 40, 60 and 80% DMSO-AgNPs. The 1 – 5 % formation of DMSO-AgNPs was confirmed by the yellow colour as illustrated in Figure 3.7. The yellow colour of 5% DMSO-AgNPs was more intense followed by 4% DMSO-AgNPs, 3% DMSO-AgNPs 2 % DMSO-AgNPs and 1% DMSO-AgNPs. This means that the percentage of DMSO used in the

synthesis has a direct correlation to the amount of DMSO-AgNPs formed, and their sizes increased with the increase in concentration of DMSO. Furthermore, the colour of the 1 – 5% DMSO-AgNPs appeared similar to the bare-AgNPs presented in Figure 3.2 rather than the DMSO-AgNPs (Figures 3.5 and 3.6).

Figure 3. 7: Synthesis of DMSO-AgNPs using 1 - 5% of DMSO.

3.2. Characterization of the AgNPs

3.2.1. UV-vis Spectroscopy analysis of the AgNPs

UV-vis spectroscopy is very helpful and valid for early characterization of nanomaterials as it can be used to monitor and confirm their synthesis and stability (Zhang et al., 2016). AgNPs have special optical properties that are dependent on factors such as concentration, aggregation level, shape, size and the refractive index close to the surface of the nanoparticles. All this make UV-vis spectroscopy a suitable technique for characterizing, identifying and studying AgNPs (Prakash et al., 2013; Khorrami et al., 2018). The UV-vis absorption spectra were used to confirm the formation of the bare and DMSO AgNPs. According to literature, the maximum extinction of the Surface Plasmon Resonance (SPR) band for AgNPs occurs in the range between 380 and 450 nm (Lee & Jun, 2019). Thus, it was also expected that the bare-AgNPs and DMSO-AgNPs would also have a peak (SPR) in that range, that would indicate that the AgNPs were formed successfully. The absorption spectra for bare-AgNPs at different $AgNO_3$ concentrations are shown in Figure 3.8.

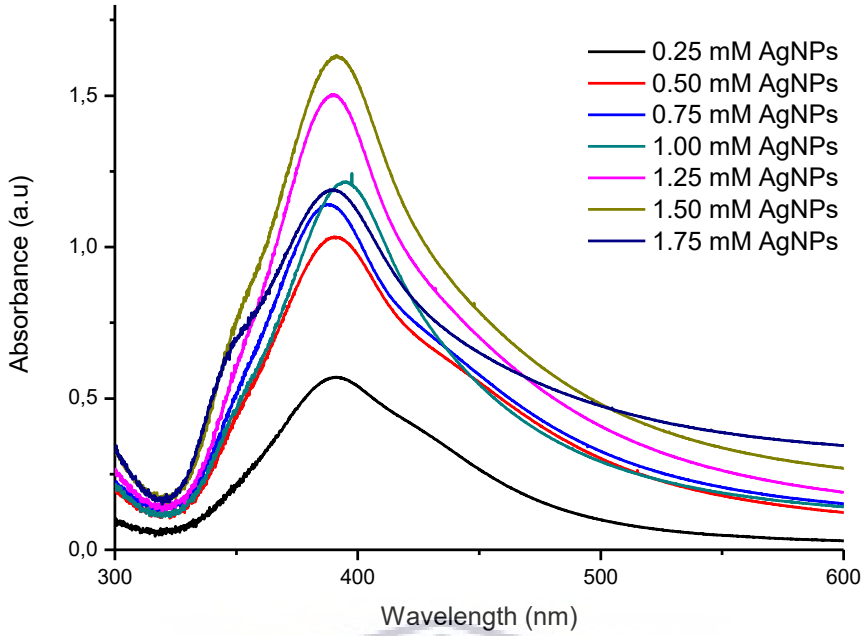

Figure 3. 8: UV-vis absorption spectra of bare-AgNPs at 0.25, 0.50, 0.75, 1, 1.25, 1.5 and 1.75 mM $AgNO_3$.

The 0.25 mM, 0.50 mM, 1.25 mM, and 1.5 mM AgNPs had a peak at 390 nm with absorbances of 0.56 a.u, 1.02 a.u, 1.50 a.u, and 1.63 a.u respectively. The 0.75 mM AgNPs had a peak at 388 nm, with an absorbance of 1.14 a.u; 1 mM AgNPs had a peak at 395 nm, with an absorbance of 1.22 a.u, and the 1.75 mM AgNPs had a peak at 389 nm, with an absorbance of 1.18 a.u. The SPR bands were all in the region specified for AgNPs, confirming the successful synthesis of bare-AgNPs at all concentrations of $AgNO_3$ (0.25, 0.5, 0.75, 1, 1.25, 1.5 and 1.75 mM).

Concentration is one of the key factors linked to variations in the SPR bands (Prakash et al., 2013; Khorrami et al., 2018). The change in concentrations of $AgNO_3$ did not change the characteristics of the bare-AgNPs since only slight variations were observed in their SPR band. More so, the SPR band was not shifted to longer or shorter wavelengths with a change in concentration. However, the concentration of the AgNPs greatly impacted the absorbance of the AgNPs, the AgNPs with lowest concentration resulted in the lowest absorbance. An increase in absorbance was observed with an increase in concentration, in the following order: 0.25 mM <0.5 mM < 0.75 mM < 1.75 mM < 1 mM < 1.25 mM < 1.5 mM AgNPs. The absorbance of 1.75 mM AgNPs was slightly lower than expected, this could due to the observed colour of the AgNPs since they appeared darker than the rest. For further synthetic purposes, the 1.00 mM $AgNO_3$ solution was used.

The absorption spectra for 100% DMSO-AgNPs and their resulting colour change is shown in Figure 3.9. The SPR band for 100% DMSO-AgNPs was observed at 422 nm which is characteristic of AgNPs. Moreover, this band is similar to the 424 nm band that was reported for DMSO-AgNPs derived from the spontaneous reduction of DMSO in Ag(ethex) (Rodríguez-Gattorno et al., 2002). This peak was at higher wavelengths compared to the bare-AgNPs synthesized using 1 mM of $AgNO_3$. This red shift was expected due to the higher refractive index of DMSO than water in classical silver colloid dispersions at 20°C of 1.4170 and 1.333, respectively (Rodríguez-Gattorno et al., 2002). Thus, the shift arises due to the change in surrounding medium, since the molecules around the surface of the DMSO-AgNPs are different than that of the bare-AgNPs. This was further confirmed by investigating the functional groups present in the AgNPs via FTIR spectroscopy. Furthermore, the observed colour for 100% DMSO-AgNPs was more on the reddish-brown side compared to the bare-AgNPs which were yellowish in colour. Also, the absorbance at their SPR was slightly lower for 100% DMSO-AgNPs with 1.10 a.u compared to the 1.20 a.u for bare-AgNPs. These differences arise from differences in features like size, shape, chemical composition and surrounding medium (Prakash et al., 2013; Khorrami et al., 2018).

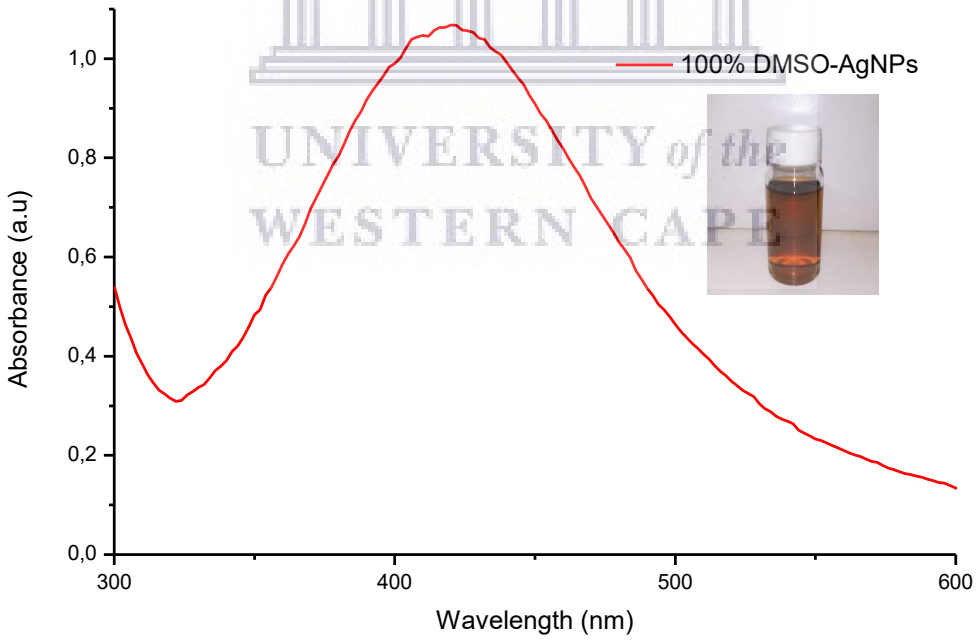

Figure 3. 9: UV-vis spectra and colour change for 100 % DMSO-AgNPs.

The 20, 40, 60 and 80% DMSO solutions were also utilized for the synthesis of DMSO-AgNPs following the successful synthesis with the 100% DMSO solution. From the spectra, it can be

deduced that AgNPs were not formed, due to the absence of the SPR band between 380 and 450 nm. The 20, 40, 80% DMSO solutions (Figure 3.10) were quite unstable and aggregated instantly as their UV-Vis graph showed absorption spectra that was not characteristic of the AgNPs. Although the 60% DMSO-AgNPs showed a spectral profile of AgNPs, the broadness of the peak was characteristic of aggregating AgNPs and the AgNPs were unstable (Rodríguez-Gattorno et al., 2002) and were not used any further.

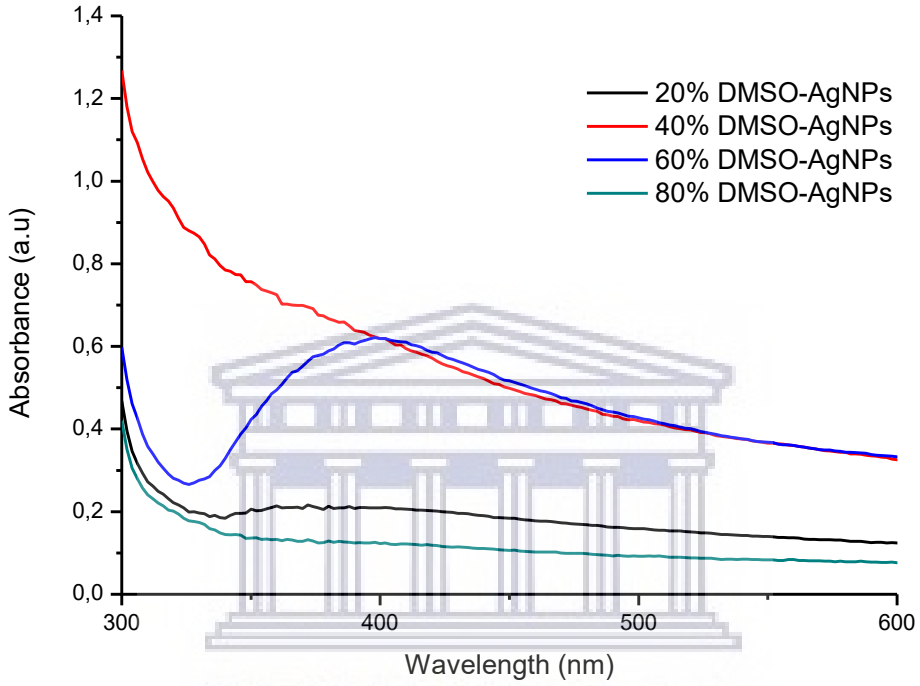

Figure 3. 10: UV-vis spectra of 20% to 80% DMSO-AgNPs.

The UV-vis absorption spectra of 1 – 5% DMSO-AgNPs is shown in Figure 3.11. All the absorbance spectra were within the SPR band range specified for AgNPs, indicating that the 1 – 5% DMSO-AgNPs were synthesized successfully. 1% and 2% DMSO-AgNPs had an SPR band peak at 398 nm, with an absorbance of 0.34 a.u and 0.59 a.u, respectively. , The 3% DMSO-AgNPs had an SPR band peak at 400 nm, with an absorbance of 0.71 a.u, 4% DMSO-AgNPs had an SPR band peak at 402 nm, with an absorbance of 1.88 a.u and the 5% DMSO-AgNPs had an SPR band peak at 396 nm, with an absorbance of 0.65 a.u. At this point in time, no relationship was observed between the SPR band, absorbance and DMSO concentration in the synthesis of the DMSO-AgNPs. The variations in both the SPR and absorbance were not proportional to the DMSO concentration. The 3% and 4% DMSO-AgNPs were selected for further analysis and investigation because they had a higher absorbance compared to the 1, 2 and 5% DMSO-AgNPs.

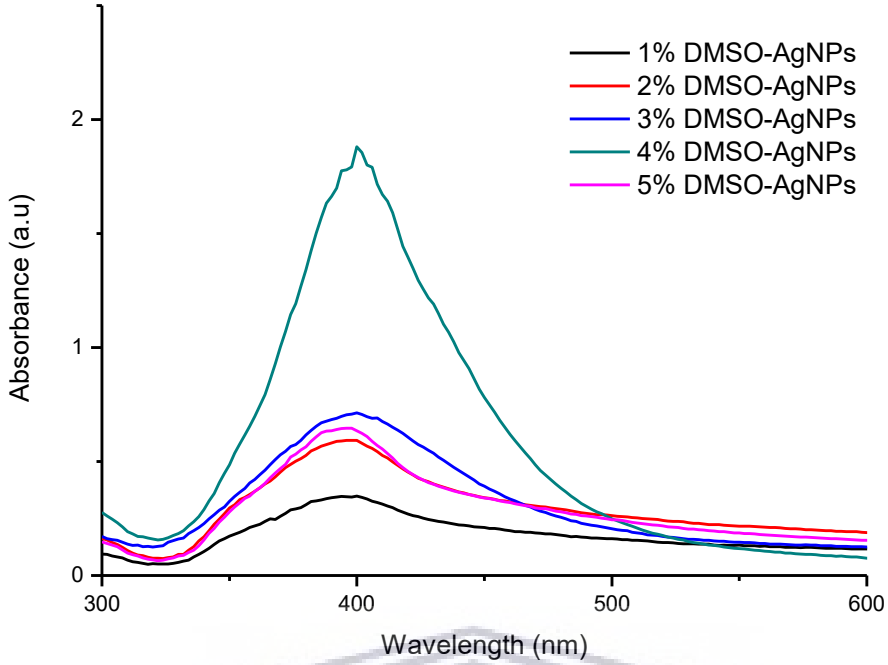

Figure 3. 11: UV-Vis absorption spectra of 1% to 5% DMSO-AgNPs.

The 1 mM bare AgNPs, 3% DMSO-AgNPs, 4% DMSO-AgNPs and 100% DMSO-AgNPs were chosen to conduct further characterization and their combined UV-vis spectra is presented in Figure 3.12. The relationship between the SPR and concentration of DMSO can be established from their spectra, the bare-AgNPs (no DMSO used) peaks at lower wavelengths of 395 nm compared to the 3% DMSO-AgNPs, 4% DMSO-AgNPs and 100% DMSO-AgNPs with the SPR bands at 400, 402 and 422 nm, respectively.

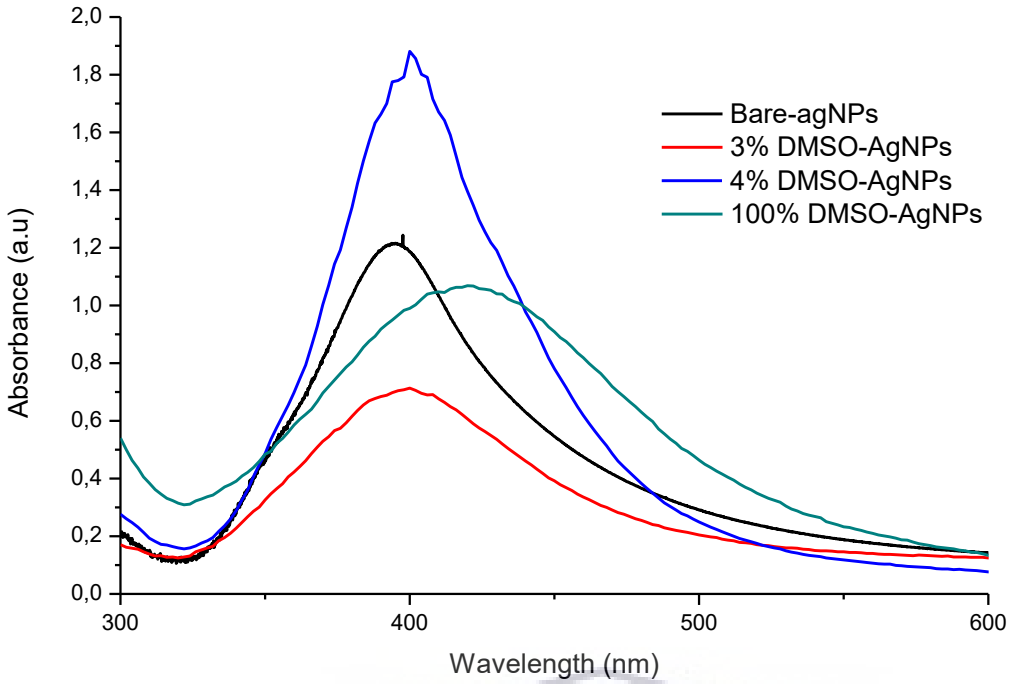

Figure 3. 12: UV-Vis spectra of bare-AgNPs, 3% DMSO-AgNPs, 4% DMSO-AgNPs and 100% DMSO-AgNPs chosen for further analysis and testing.

3.2.2. FTIR analysis of the AgNPs

FTIR spectroscopy was used to identify the structural composition of bare-AgNPs, 3% DMSO-AgNPs, 4% DMSO-AgNPs and 100% DMSO-AgNPs, the results are presented in Figure 3.13 and 14. The spectra of bare-AgNPs, 3% DMSO-AgNPs and 100% DMSO-AgNPs had a similar FTIR profile, broad peaks at 3327 cm^{-1}, 3320 cm^{-1} and 3308 cm^{-1} were observed for the AgNPs, respectively. The peaks were assigned to the O−H stretch of alcohols or phenols. While the peaks at 1636 cm^{-1} for bare-AgNPs, 1637 cm^{-1} for 3% DMSO-AgNPs and 1637 cm^{-1} for 4% DMSO-AgNPs were assigned to an (O−H) bend out of plane (Coates, 2006). Most FTIR spectra of AgNPs in literature also reported on these two peaks, with slight shifts in wavenumbers, it was thus, concluded that they are characteristic of the functional groups that were involved in the synthesis of the AgNPs (Jeyaraj et al., 2013; Rosarin et al., 2013; Rangasamy et al., 2016; Huq, 2020; Martínez-Rodríguez et al., 2020; Raj et al., 2020). The presence of these identified functional groups then confirmed the successful reduction of $AgNO_3$ into AgNPs using $NaBH_4$ in the different medium (water and DMSO).

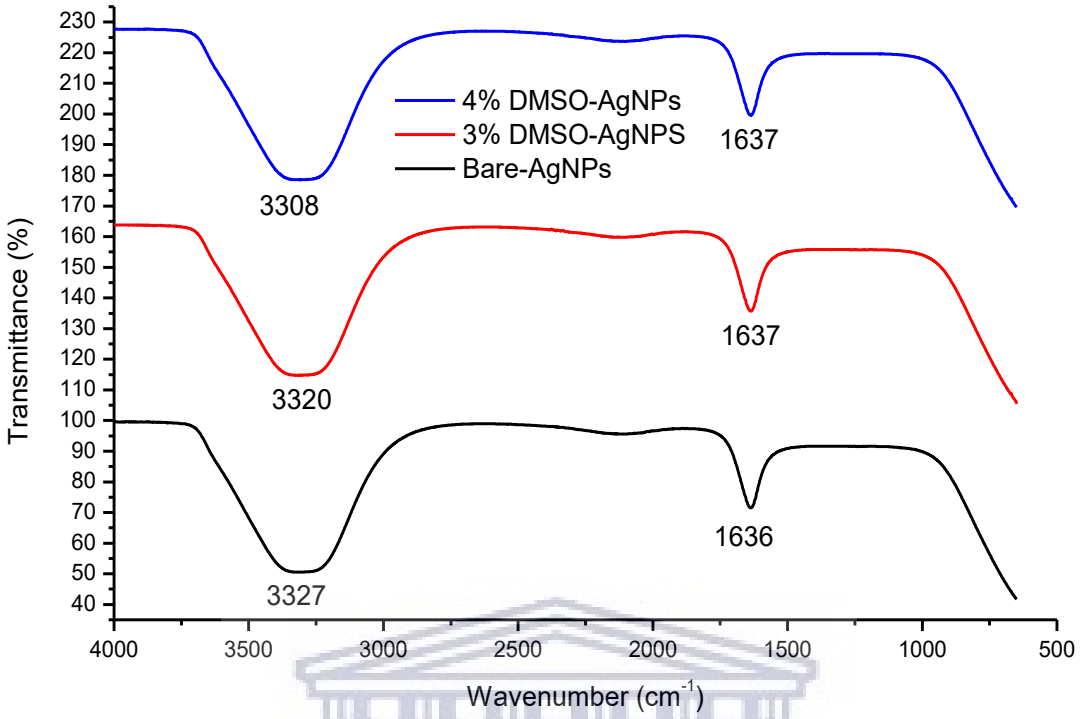

Figure 3. 13: FTIR spectra of bare-AgNPs, 3% DMSO-AgNPs and 4% DMSO-AgNPs.

The IR spectra of DMSO has been thoroughly discussed elsewhere (Crowley, 2020), the focus was on a few peaks that were of importance to this study. The peak at 1042 cm^{-1} was attributed to the S=O stretch and the symmetric vibrations of $-CH_3$ groups which gave rise to a peak at 1310 cm^{-1}. The bands at 1661 and 1436 cm^{-1} was attributed to the asymmetric vibrations of $-CH_3$ groups, and the peak split was attributed to the vibration coupling effects (Lai et al., 2015). Furthermore, the peaks at 952 cm^{-1} and 697 cm^{-1} were attributed to C−S stretching/bending vibrations respectively (Crowley, 2020). These peaks are important because they were also observed in the IR spectra of 100% DMSO-AgNPs with a slight shift in wavenumbers. The peak at 1011 cm^{-1} was assigned to the S=O bond vibration stretching modes, Also, the bands at 1320 and 1438 cm^{-1} were assigned to the symmetric and asymmetric vibrations of $-CH_3$ groups, respectively (Lai et al., 2015). The peaks at 951 and 675 cm^{-1} were also assigned to C−S stretch or bend (Crowley, 2020). This information suggested that the aprotic solvent was adsorbed on the surface of the 100% DMSO-AgNPs since it possesses functional groups identical (slightly shifted) to that of DMSO (Lai et al., 2015). This was not observed with the 3% and 4% DMSO-AgNPs, this could be due to the fact that the concentration of the DMSO was very low and could not be picked up during IR analysis thus another more sensitive technique such as NMR could be used to give information about the

structure of the DMSO-AgNPs. Moreover, the IR spectra of the 100% DMSO-AgNPs showed an O−H stretch and to an (O−H) bending out of plane at 3320 and 1637 cm^{-1}, respectively (Coates, 2006). Which are characteristic of AgNPs and have been observed in the other AgNPs in the previously discussed spectra of Figure 3.13 (Jeyaraj et al., 2013; Rosarin et al., 2013; Rangasamy et al., 2016; Huq, 2020; Martínez-Rodríguez et al., 2020; Raj et al., 2020).

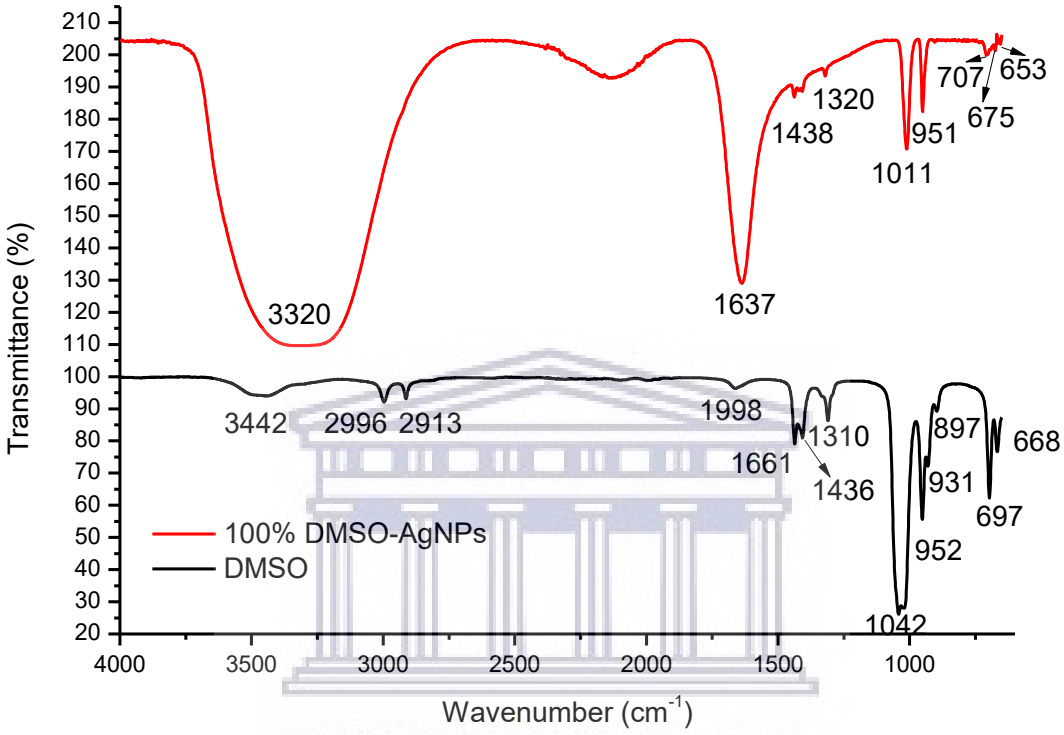

Figure 3. 14: FTIR spectra of 100% DMSO-AgNPs and DMSO.

3.2.3. SAXS analysis of the AgNPs

From a SAXSpace experiment, the analysis can be Fourier transformed using GIFT software into a pair distance distribution function (PDDF) either by intensity, volume or size distribution by number of the AgNPs as presented in Figures 3.15 and 3.16.

The free model PDDF of the bare-AgNPs, 3% DMSO-AgNPs and 4% DMSO-AgNPs had a similar shape. From 0 to 50 nm, the graphs showed a profile characteristic of globular AgNPs which are spherical in nature, followed by a sharp decrease between 50 and 60 nm which is always observed for the hollow spheres (Schnablegger & Singh, 2013). This indicated that the AgNPs are not uniform because they contained features for both spheres and hollow spheres. This could mean that the particles are polydispersed in nature, and that the highest particle in each graph had a mean radius of 55 nm. This was not the actual size of the AgNPs since the

PDDF of hallow nanoparticles has a maximum diameter that is shifted towards values larger than $D_{max}\backslash 2$ (Schnablegger & Singh, 2013). The predicted shape of the 100% DMSO-AgNPs was globular with two shoulders at 10 nm and 50 nm, indicating that the particles are spherical in nature (Worsch, 2015) with agglomerates at those radii since SAXS can also give information about a particle's agglomeration state by exhibiting shoulders in their PDDF graphs (Schnablegger & Singh, 2013). The graph also had a dip in the negative direction which suggest the AgNPs had a core shell structure (Schnablegger & Singh, 2013), and was concluded that the DMSO was adsorbed on the surface of the AgNPs, hence the (S=O) group could be protecting the particles by forming a cushion around it. This claim can be investigated further on the HR-TEM images. The largest radius was 60 nm for 100% DMSO-AgNPs. Thus, according to the PDDF, 100% DMSO-AgNPs were larger in size compared to the bare-AgNPs, 3% DMSO-AgNPs and 4% DMSO-AgNPs.

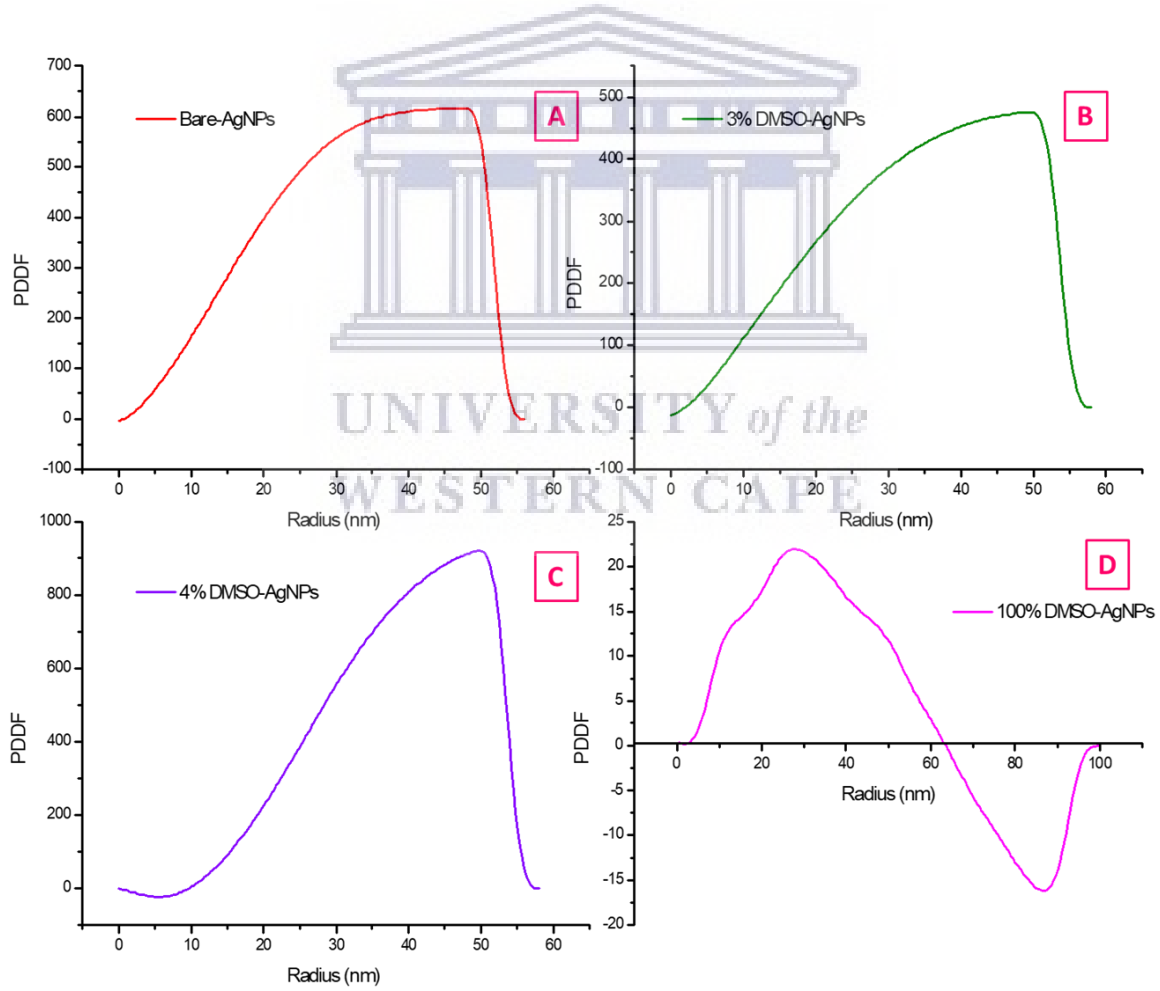

Figure 3. 15: Free model PDDF of (a) bare-AgNPs, (b) 3% DMSO-AgNPs, (c) 4% DMSO-AgNPs and (d) 100% DMSO-AgNPs by SAXS.

The distribution by number curve in Figure 3.16 (A) showed the average number of AgNPs that had a specific size in terms of their radii. For bare-AgNPs, 3% DMSO-AgNPs and 4% DMSO-AgNPs, the peak was more intense at around 13 nm, this meant that for these AgNPs, most particles had a radius of 13 nm, since the data followed a normal distribution curve, the AgNPs were said to be monodispersed (Schnablegger and Singh, 2013). For 100% DMSO-AgNPs, this intensity was observed at r = ±18 nm, however there was also another peak at r =± 32 nm, meaning that another portion of the AgNPs had a radius of 32 nm. Since the second peak was less intense, then it can be concluded that the AgNPs with a size of ±18 nm are the most dominant in terms of size distribution by number. As a result, the particles were said to be polydispersed (Schnablegger & Singh, 2013).

AgNPs with a size of 15 nm occupy the most volume as demonstrated by the size distribution by volume curve in Figure 3.16 (B) in the bare-AgNPs, 3% DMSO-AgNPs and 4% DMSO-AgNPs. While it was 18 nm and 32 nm radii AgNPs that took up more space in the 100% DMSO-AgNPs, with the former being dominant. The distribution by volume also gave information about the crystallinity of the particles. If a second peak at further radii was observed, thus the material was crystalline in nature, if a shoulder appears then the AgNPs have agglomerated (Schnablegger & Singh, 2013). For all the evaluated AgNPs, these peaks were not observed, however that does not mean the AgNPs were amorphous or non-crystalline in nature, rather another sensitive technique such as the Selected Area Electron Diffraction (SAED) imaging can be used to give information about the crystallinity of these materials.

The most intense particles (Figure 3.16 (C)) had a radius of ± 20 nm for bare-AgNPs, 3% DMSO-AgNPs, 4% DMSO-AgNPs, while intensity curve for 100% DMSO-AgNPs was very broad with a maximum between ± 20 and 40 nm, indicating that the most intense AgNPs had a radius within that range. Since the particles are polydispersed in nature, it was expected that the larger particles will have the highest intensity according to the following relationship:

$$r \propto I^6$$

This explains why the curve shifted to higher radii compared to the size distribution by number which suggested that a large number of AgNPs hada radius of ±13 nm for bare-AgNPs, 3% DMSO-AgNPs, 4% DMSO-AgNPs. This could be explained better for 100% DMSO-AgNPs, since a large fraction of the AgNPs had a radius of ±18 nm, one would expect that these AgNPs would have a higher intensity, however it was AgNPs with radii between 20 and 40 nm which

were more intense because of the relationship between intensity and the gyroradius of the AgNPs (Schnablegger & Singh, 2013).

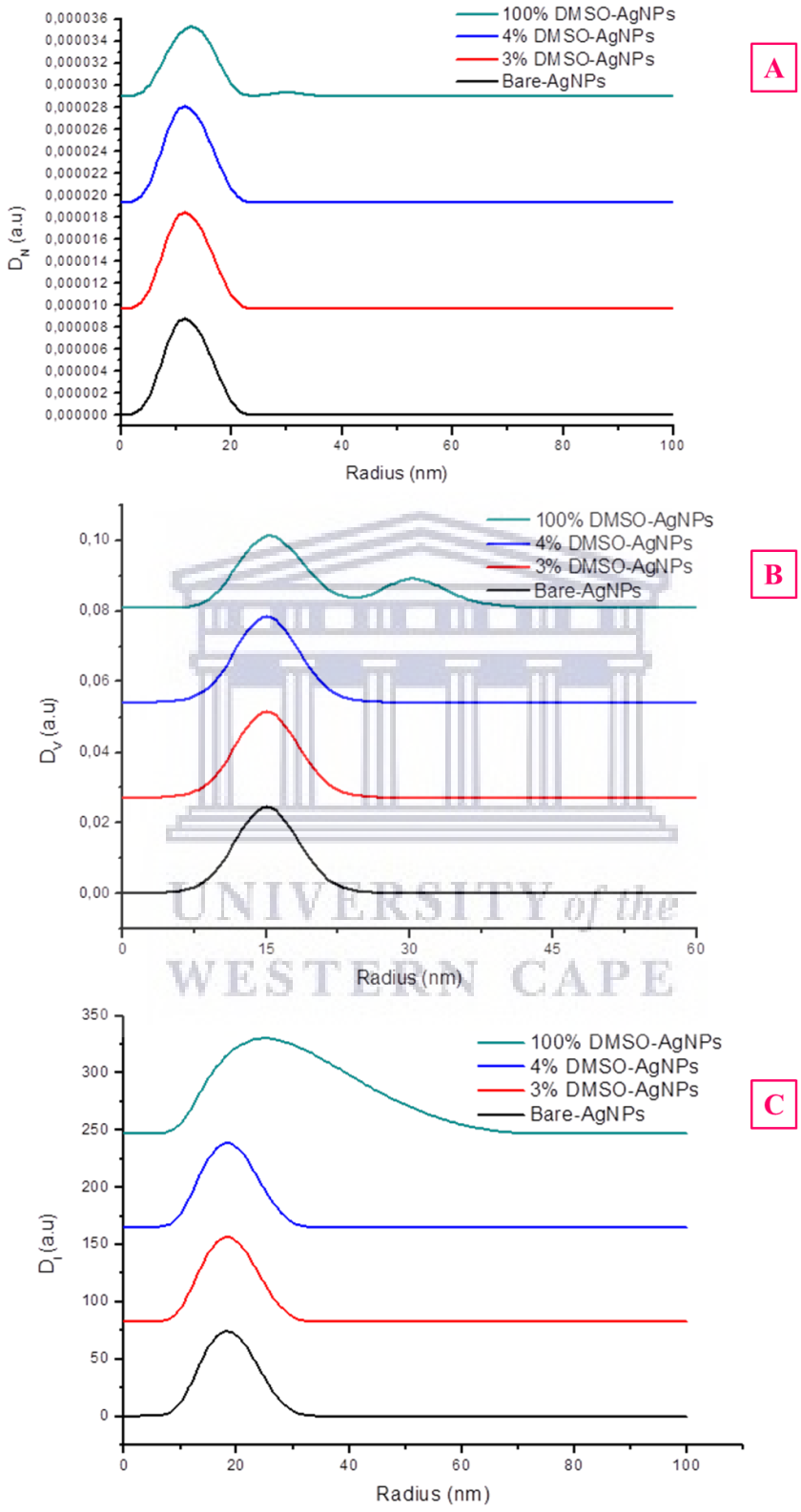

Figure 3. 16: Size distribution by (A) number, (B) volume and (C) intensity of bare-AgNPs, 3% DMSO-AgNPs, 4% DMSO-AgNPs and 100% DMSO-AgNPs as determined by SAXS.

3.2.4. HR-TEM analysis of the AgNPs

Particle size, morphology and further assessment of crystallinity were evaluated using HR-TEM together with SAED imaging. Image J software was used to analyse the size distribution of the AgNPs for the bare-AgNPs, 3% DMSO-AgNPs, 4% DMSO-AgNPs and 100% DMSO-AgNPs which are presented in Figures 3.17 and 18.

The bare-AgNPs were mostly spherical in shape as shown in Figure 3.17 (A) although other shapes such as elongated structures were visible from certain individual nanoparticles. This could be due to aggregation of two or more particles. This data supported the free model PDDF structure of the bare-AgNPs which suggested that the AgNPs were spherical in nature (Figure 3.15(A)). Their sizes ranged between 8 and 24 nm, with 15 nm as the most frequent size. This data also agrees with the size distribution by number and volume as illustrated in Figure 3.16 (A). This meant that the bare-AgNPs were polydispersed in nature because they consist of particles which have more than one shape and size. The SAED pattern of the bare-AgNPs suggested that the particles were polycrystalline in nature since their SAED pattern showed concentric rings with intermittent dots characteristic of materials with a polycrystalline background (Egerton, 2016). This diffraction pattern was reported throughout literature for AgNPs respective of the synthetic route, starting materials, concentration and/or size (Gonzalez-Carter et al., 2017; Venugopal et al., 2017).

The electron microscope image in Figure 3.17 (A) reveal that the 3% DMSO-AgNPs were spherical in nature, with most individual particles having a size of 14 nm. This data further supported the size distributions by number and volume (Figure 3.16 (B) and (C)). Furthermore, the spherical shape predicted (Figure 3.15 (B)) by SAXS data also agreed with the size observed on the HRTEM images. The diffraction pattern from SAED also suggested that the particles have a polycrystalline nature by reasons already mentioned in above (Egerton, 2016).

As in the case of the bare-AgNPs and 3% DMSO-AgNPs, the 4% DMSO-AgNPs were also polydispersed in nature as exhibited by the HRTEM images (Figure 3.17 (A) and size distribution data in Figure 3.16 ((A), (B) and (C)) of the SAXS experiment. Their size range was between 6 and 24 nm, with 14 nm AgNPs being the most common. This result was in line with the SAXS data. The spherical structure proposed by the free model PDDF in Figure 3.15 (C) can be observed from the HR-TEM image in Figure 3.17 (A). Furthermore, the 4% DMSO-AgNPs were also polycrystalline in nature for the same reason as bare-AgNPs and 3% DMSO-AgNPs (Egerton, 2016).

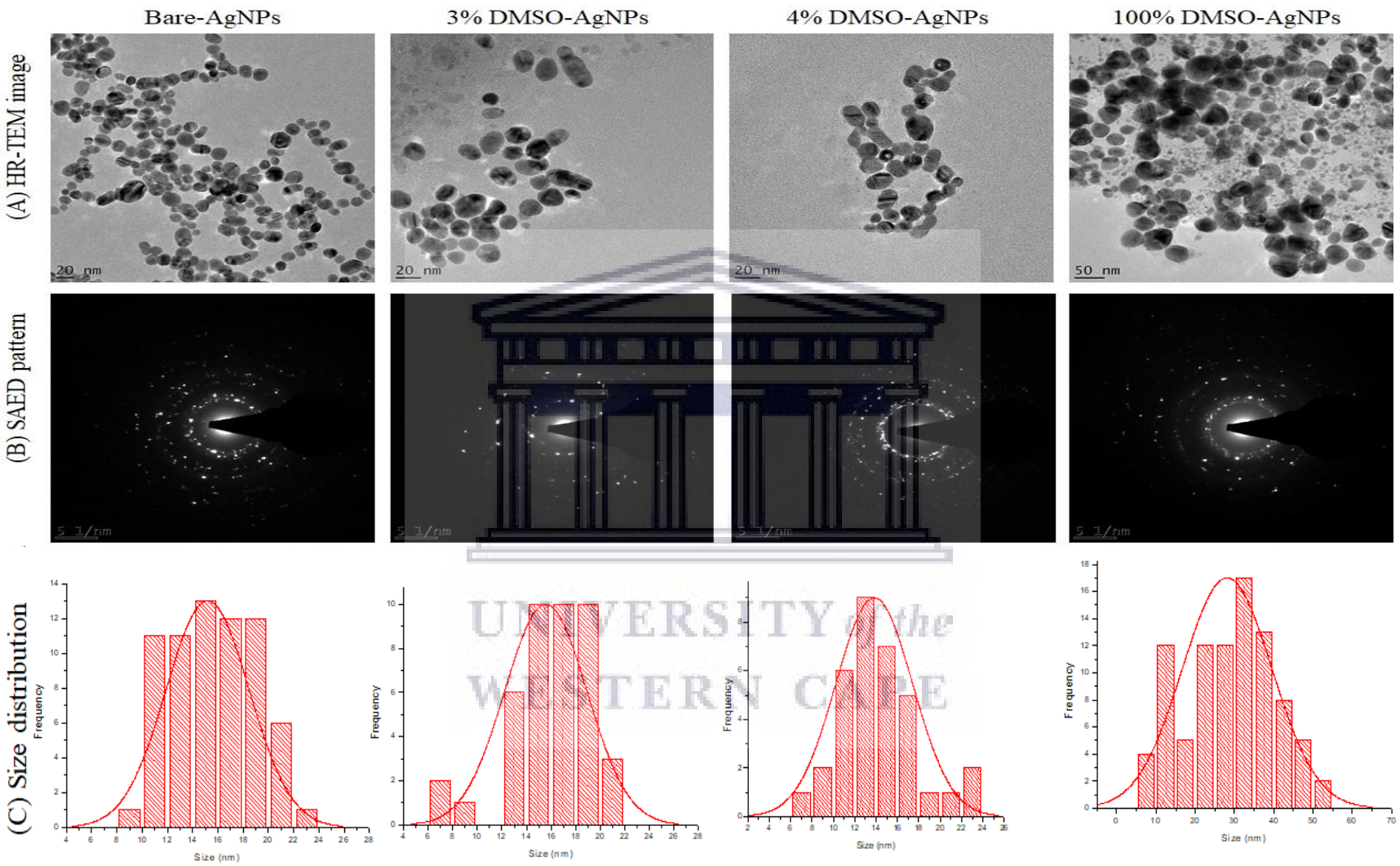

Figure 3. 17: (A)HR-TEM images of bare-AgNPs, 3% DMSO-AgNPs, 4% DMSO-AgNPs and 100% DMSO-AgNPs. (B) SAED patterns of bare-AgNPs, 3% DMSO-AgNPs, 4% DMSO-AgNPs and 100% DMSO-AgNPs. (D) size distribution of bare-AgNPs, 3% DMSO-AgNPs, 4% DMSO-AgNPs and 100% DMSO-AgNPs images.

The 100% DMSO-AgNPs were also spherical in nature as shown in the HR-TEM images in Figure 3.17 (A), this information was consistent with the shape predicted by the free model PDDF in Figure 3.16(D) which suggested that the 100% DMSO-AgNPs had spherical structures. However, the 100% DMSO-AgNPs had a number of defects such as twinning and stacking of multiple particles, an observation also made by (Rodríguez-Gattorno et al., 2002). Smaller individual 100% DMSO-AgNPs, typically around 5 nm in size were the most dominant particles, but they combine either by twinning or stacking resulting in larger particles or smaller particles trapped inside larger ones. This was illustrated with pink arrows in Figure 3.18 (A) and (B). This phenomenon was also predicted as aggregates (shoulders) in the free model PDDF of the 100% DMSO-AgNPs in Figure 3.15 (D). This also led to quite a huge size distribution as seen in Figure 3.17 (C), since the particle sizes ranged between 5 and 55 nm with an average of 26 nm. However, from the size distribution curves by number and volume in Figure 3.16 (B) and (C), it was suggested that the more intense particles are the smaller ones as shown in the HRTEM images (Figure 3.17 (A), Figure 3.18 (A) and (B)) that they were more dominant, it was unfortunate that their size distribution could not be represented in frequency curve (Figure 3.17(C)) curve because image J software is a limiting technique and cannot measure particle sizes of very small materials, thus a more sensitive software is needed to measure the particle size of those small AgNPs. The above-mentioned defects can be best explained by carefully studying the growth mechanism of AgNPs formation as described by (Henglein & Giersig, 1999), who observed similar defects including dislocations in the AgNPs as well as lamella twinning and staple faults when using high and lower concentrations of the citrate ion solution for AgNP formation. They credited these faults to the spontaneous reaction of the free radical of their reducing agent which results in the formation of larger particles formed by several coalescence, indicating that new nuclei are generated throughout all the stages of silver reduction. This notion also served as an explanation for the broad size distribution in the present study, since there are particles with a size of 5 nm in the same time frame as those with 55 nm. The SAED pattern also suggested that the 100% DMSO-AgNPs were also polycrystalline in nature by the visible dots around the concentric rings (Venugopal et al., 2017).

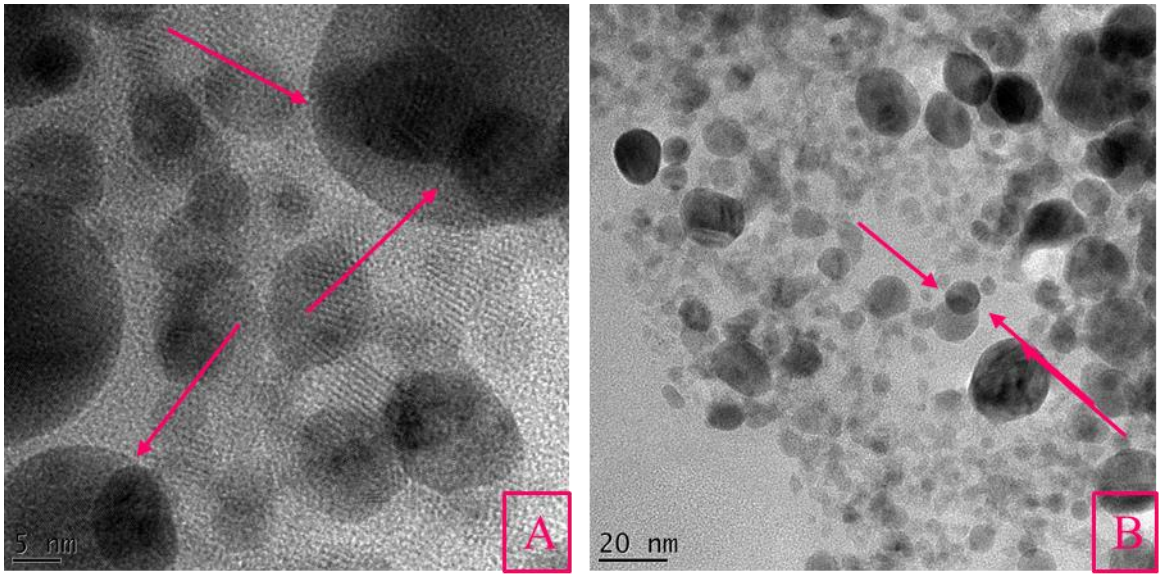

Figure 3. 18: HR-TEM images of 100% DMSO-AgNPs illustrating stacking ang twinning defects at resolutions of (A) 5 and (B) 20 nm.

3.2.5. DLS analysis of AgNPs

The light scattering information as well as ζ-potentials of the AgNPs are tabulated below (Table 3.1). The mean hydrodynamic size of the AgNPs ranged from 13 nm, 19 nm, 57 nm and 74 nm for 3% DMSO-AgNPs, 4% DMSO-AgNPs, bare-AgNPs and 100% DMSO-AgNPs, respectively. For both the bare-AgNPs and 100% DMSO-AgNPs, the sizes obtained from the DLS was much greater than the sizes from the HR-TEM because the former uses light scattering based on the Brownian motion of AgNPs while the later measures the metallic core of the AgNPs (Mukherji et al., 2019). Hence, the variation in size was highly expected. The PDI is a dimensionless number that describes the broadness of the size distribution obtained from the cumulants analysis. It is scaled in a manner such that a PDI of zero represent a monodisperse distribution while a PDI of one represents a polydisperse distribution in terms of particle sizes. A PDI value of ≥ 0.7 indicates that the size distribution is very broad and the sample is likely not suitable for analysis with the DLS principle. While PDI values ≤ 0.05 represent extremely monodispersed systems (Khorrami et al., 2018).

In this study, PDI values of 0.992, 0.959, 0.937 and 0.436 were obtained for bare-AgNPs, 3% DMSO-AgNPs, 4% DMSO-AgNPs and 100% DMSO-AgNPs, respectively. The PDI values indicated that the bare-AgNPs, 3% DMSO-AgNPs and 4% DMSO-AgNPs had a very broad size distribution, hence an extremely high degree of polydispersity since all these values were >0.7. This high dispersity was in conjunction with the HR-TEM data in Figure 3.17, the AgNPs

had different sizes and shapes. The 0.436 PDI value obtained for 100% DMSO-AgNPs was within the range since it was <0.7, however it also represented a polydisperse systems as suggested by the previous analysis with the HRTEM and SAXS.

The calculation of the size of electrostatic repulsive or attractive forces between the particles in a solution is referred to as Zeta potential. Zeta potential values can be used to predict the stability of particles in colloidal solutions (Khorrami et al., 2018). From Table 3.1, it can be concluded that the AgNPs had a negatively charged surface in stable medium since it was reported that NPs which have a zeta potential between ±30 mV possess high stability. 3% DMSO-AgNPs were highly stable than the rest of the prepared AgNPs with a zeta potential of -26.1 mV followed by -25.5 mV, -20.8 and -16.1 mV for 4% DMSO-AgNPs, AgNPs and 100% DMSO-AgNPs, respectively. A zeta potential value of − 27.8 ± 0.1 mV was also reported for AgNPs capped with citrate in a previous study (Gonzalez-Carter et al., 2017). This value was slightly similar to that recorded for both the 3 and 4% DMSO-AgNPs. These values were not that far from those reported by (Vanitha et al., 2017) who prepared AgNPs from various concentrations (including 1.00 mM) of $AgNO_3$ solutions. It was also worth noting that, although the AgNPs were prepared in different media, the size had an inversely proportional relationship with the stability (zeta potential) since the smaller particles had the higher stability. This is opposition with the observation made by (Jeong, Lim & Choi, 2014), who reported that the smaller AgNPs (10 nm) had a lower stability compared to the larger AgNPs (100 nm).

Table 3. 1: Particle size, PDI and Zeta potential values of bare-AgNPs, 3% DMSO-AgNPs, 4% DMSO-AgNPs and 100% DMSO-AgNPs were analysed immediately after synthesis.

Sample	Particle size	PDI	Zeta Potential (-)
Bare-AgNPs	56.35 ± 1.51	0.992 ± 0.008	20.8 ± 0.52
3% DMSO-AgNPs	13.32 ± 0.23	0.959 ± 0.001	26.1 ± 0.29
4% DMSO-AgNPs	18.50 ± 3.46	0.937 ± 0.06	25.5 ± 1.92
100% DMSO-AgNPs	74.97 ± 0.34	0.399 ± 0.03	16.1 ± 0.37

3.3. Antibacterial Activity of AgNPs

Bacterial inhibition plays an important role in the rate of wound healing, since non-healing wounds are usually characterized by colonization with bacteria. Antibacterial properties of AgNPs equips them with the ability to inhibit bacteria causing infections at the wound site. Upon internalization of the AgNPs by the bacteria, the AgNPs are presumed to release the Ag^+

ions in the aqueous media. The AgNPs are usually via passive bacterial channels, one involves AgNP interaction with the thiol bearing enzymes and proteins in the bacterial cell membrane. The cell membrane permeability becomes compromised by the build-up of the AgNPs on the bacterial wall. This results in the leakage of the bacterial elements causing cell death (Dhapte et al., 2014; Martínez-Rodríguez et al., 2020). Death of the bacteria in the wound sites leads to better wound healing as demonstrated in Figure 3.19. Once the AgNPs are introduced to the wound site, they inhibit bacterial growth and cause their death, with no bacteria present, epithelization on the wound site occurs effortlessly. The collagen fibres are generated in abundance, resulting in minimal scarring and quick healing. Furthermore, the AgNPs enhances the immune modulation in the wounded area leading to quicker wound closure with minimal scarring (Ovais et al., 2018).

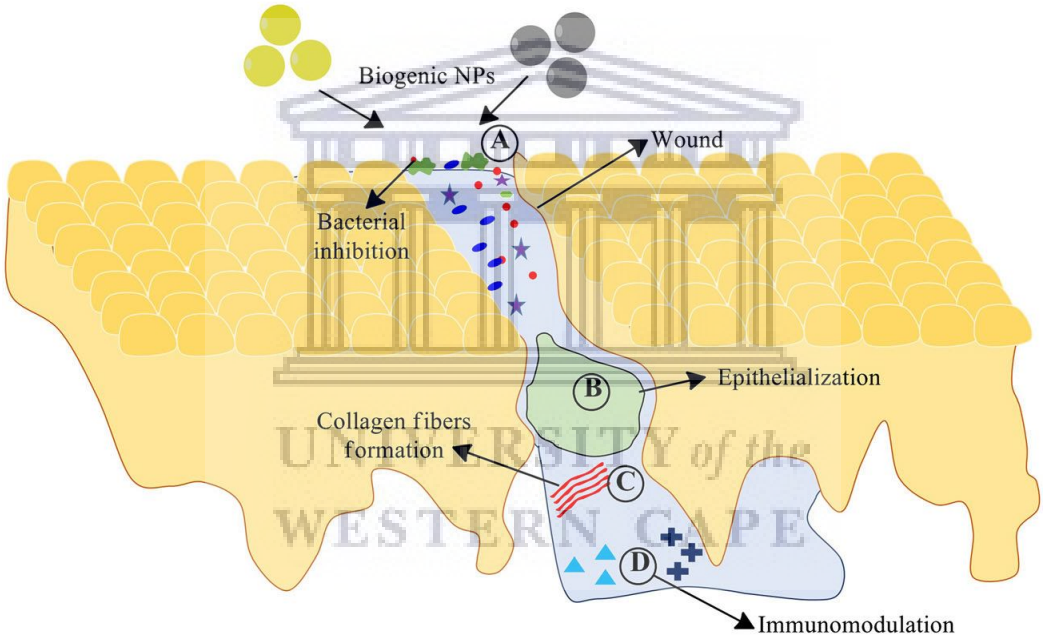

Figure 3. 19: Suggested wound healing route of biogenic AgNPs by inhibiting bacterial growth leading to improved wound healing. (A) Biogenic NPs such as AgNPs and gold nanoparticles at the wound, (B) improves epithelization, (c) enhances collagen regeneration and (d) immunomodulation (Ovais et al., 2018).

In this study, the antibacterial activity of the AgNPs was tested against 4 human pathogenic strains i.e *E. coli*, *P. aeruginosa*, *S. aureus* and *MRSA* which have been identified as the most common bacteria in the infected wounds (Mihai et al., 2019). The presence of the clearing zones (ZOIs) around the wells was used as a measure for the anti-bacterial effect of the AgNPs, All the AgNPs had no activity against the multidrug resistant strains i.e the *P. aeruginosa* and *MRSA* as evident from the absence of zones of inhibitions in Figure 3.19 (B) and (D). Although majority of the AgNPs have broad anti-bacterial activities, other studies have also reported on

the inability AgNPs to inhibit the growth of bacteria such as *P. aeruginosa*. Furthermore, the resistance of *P. aeruginosa* towards silver compounds was documented as early as 1996 (Maillard & Hartemann, 2012). ZOIs were only seen around the wells that contained ciprofloxacin (positive control), which is an antibiotic with known anti-bacterial activity against a broad range of bacterial strains.

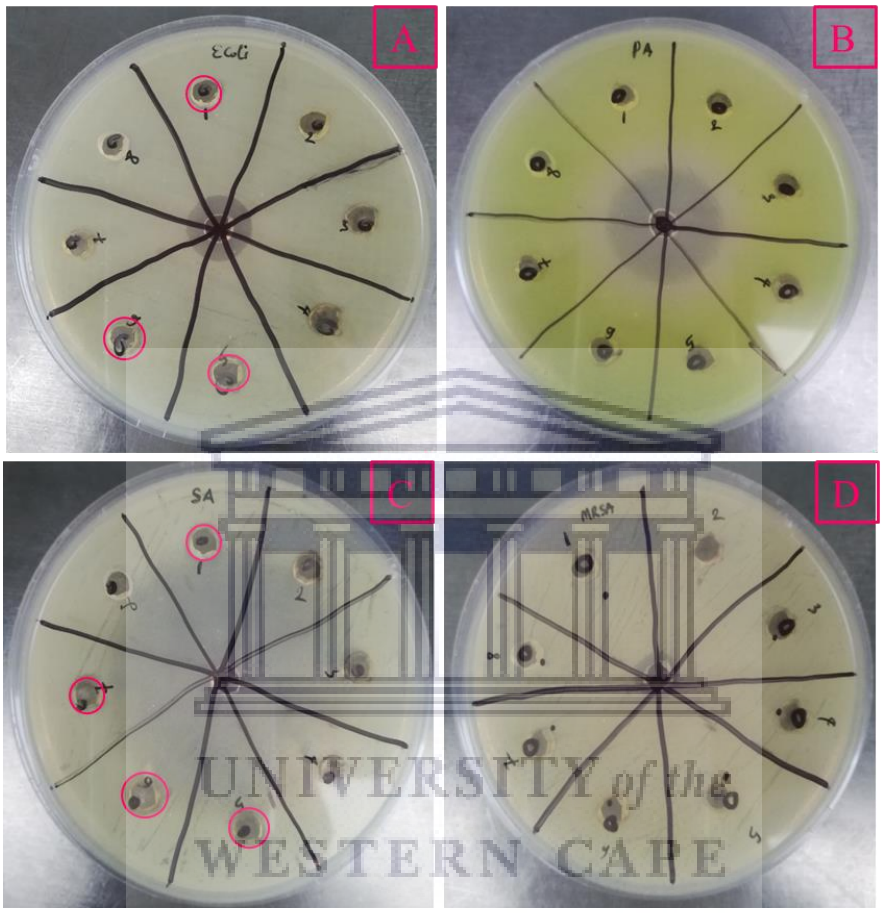

Figure 3. 20: Antibacterial activity of (1) bare-AgNPs, (2) 100% DMSO-AgNPs, (3) 1% DMSO-AgNPs, (4) 2% DMSO-AgNPs, (5) 3% DMSO-AgNPs, (6) 4% DMSO-AgNPs (7) 5% DMSO-AgNPs and (8) d(H_2O) against various human pathogenic strains of (a) *E. coli*, (b) *P. aeruginosa* (c) *S. aureus* and (d) *MRSA.*

Table 3. 2: Antibacterial activity of various AgNPs against 4 different bacterial isolates.

		Antibacterial activity against:			
Labels	**Treatments**	***E. coli***	***P. aeruginosa***	***S. aureus***	***MRSA***
0	Ciprofloxacin (+)	✓	✓	✓	✓
1	Bare-AgNPs	✓	×	✓	×
2	100%DMSO-AgNPs	×	×	×	×
3	1% DMSO-AgNPs	×	×	×	×
4	2% DMSO-AgNPs	×	×	×	×
5	3% DMSO-AgNPs	✓	×	✓	×
6	4% DMSO-AgNPs	✓	×	✓	×
7	5% DMSO-AgNPs	×	×	✓	×
8	d(H_2O) (-)	×	×	×	×

Bare-AgNPs, 3% DMSO-AgNPs and 4% DMSO-AgNPs are the only AgNPs that demonstrated activity against *E. coli* and *S. aureus* (represented by pink circles, Figure 3.19 (A) and (C)). 5% DMSO-AgNPs was only active against the *S. aureus*. These results are summarised in Table 3.2. The 4% DMSO-AgNPs showed better activity as demonstrated by the slightly larger ZOIs, compared to that of 3% DMSO-AgNPs and bare-AgNPs. The 100% DMSO-AgNPs, 1% DMSO-AgNPs, 2% DMSO-AgNPs and 5% DMSO-AgNPs were ineffective against the test bacteria and did not show any visible ZOIs. It is important to note that, even in this case 4% DMSO-AgNPs showed better antibacterial activity followed by 5% DMSO-AgNPs, 3% DMSO-AgNPs and bare-AgNPs. This suggested that the 4% DMSO-AgNPs possess better antibacterial activity against selective gram-negative and gram-positive bacteria.

One of the factors that contribute to antibacterial activity is surface composition of the AgNPs, since the AgNPs were synthesized from different DMSO concentration, this meant that their surfaces differ in terms of DMSO concentration. Since the low DMSO% (1 and 2%) showed no antibacterial activity, with 3, 4 and 5% showing activity, it can be suggested that an increase in DMSO concentration in the AgNP formulation enhanced the antibacterial properties of the 3, 4 and 5% DMSO-AgNPs. The 100% DMSO-AgNPs showed no activity as well, this could be attributed to the size and surface composition as these nanoparticles were relatively larger than 3 and 4% DMSO-AgNPs. As well as the presence of some additional functional groups present in the surface of 100% DMSO-AgNPs as revealed by the FTIR, which were not

observed in the other DMSO-AgNPs (Lin et al., 2012). Huang also demonstrated the effect of size and surface composition on antibacterial properties of citrate and pear capped AgNPs. They reported differences in the FTIR spectra of their AgNPs which led to differential inhibition bacterial growth for *P. aeruginosa*, *E. coli* and *S. aureus*. The pear capped AgNPs showed better antibacterial activity across all strains due to the presence of phytochemicals decorated on the surface of the particles. They went on to investigate the effect of size by treating the above mentioned bacteria with different sizes of pear capped-AgNPs and reported that smaller sizes showed improved antibacterial activity against all strains (Huang et al., 2013).

Also, all the active AgNPs showed better antibacterial activity against *S. aureus* compared to *E. coli*. In another study, different concentrations (100 and 200 µg/mL) of biologically synthesized AgNPs from Catharanthus roseus leaf extract also showed superior antibacterial activity against *S. aureus* compared to *E. coli* (Al-Shmgani et al., 2017). There are many papers that report on the superior growth inhibition of gram positive bacteria in comparison with gram negative bacteria (Dhapte et al., 2014; Mekkawy et al., 2017; Loan Khanh et al., 2019; Baygar, 2020). This suggested that AgNPs have a better antibacterial effect on gram-positive than gram-negative bacteria. Furthermore, another review paper reported that gram positive bacteria are less susceptible to Ag, and rarely develops resistance to silver compared to the gram negative type (Maillard & Hartemann, 2012). This variation in the level of growth inhibition between the gram-positive and gram-negative bacteria develops as a result of the difference in cell wall composition. The cell wall of gram-negative bacteria is very complex since it has a lean peptidoglycan layer made up of 5 to 20% cell wall constituents. This layer is found between the cytoplasmic and outer membranes, resulting in higher protection of the cytoplasm, since it is guarded by two layers. On the other hand, gram-positive bacteria exhibit stronger activity since (50-90%) of its cell wall composition is represented mainly by peptidoglycan, meaning that the cytoplasm is protected by one layer only. Moreover, it is easy to inhibit the growth of *S. aureus* because it does not contain molecules such as lipids, proteins and lipopolysaccharides in its cell wall which act as protective layer against biocides as in the case of *E. coli* (Ziabka, Dziadek & Królicka, 2019). Lastly, this observed antibacterial activity can be further enhanced by varying the concentration and volume of the AgNPs since it was reported that antibacterial activity of AgNPs is dose dependant (Pazos-Ortiz et al., 2017; Martínez-Rodríguez et al., 2020).

3.4. Evaluation of the cytotoxicity of AgNPs

High concentrations of AgNPs have been linked with toxic effects towards human cells, as a result many scientists choose to expose a reasonable amount of AgNPs to cells and monitor changes in cellular morphology (You et al., 2012). Cytotoxicity of the AgNPs was evaluated using MTT assay at various AgNP concentrations for 24, 48 and 72 hours. The working principle behind MTT is that, the tetrazolium salt will be reduced to purple formazan by metabolically active cells, hence the intensity of the absorption of the dye at 570 nm reflects the number of live cells (Lin et al., 2012; Mohanty et al., 2012). Dosage, time, nanoparticle sizes, surface coatings and type of cells are some of the many factors that influence AgNP toxicity (Gurunathan et al., 2013; Wei et al., 2015). Thus, in the present study, different doses of various AgNPs were evaluated at different time points using different cell types i.e. human skin fibroblasts (KMST-6), skin keratinocytes (Hacat) and the Chinese hamster ovary cells (CHO). Dox and allantoin were used as the positive controls, to retard and enhance cell growth, respectively. Pure DMSO also served a control since the AgNPs were prepared in 0, 3, 4 and 100% solutions of the aprotic solvent. The results are presented in Figure 3. 22 for AgNPs (bare-AgNPs, 3% DMSO-AgNPs, 4% DMSO-AgNPs and 100% DMSO-AgNPs) and Figure 3.23 for allantoin, Dox and DMSO.

The lower concentrations up to 1.75 µg/mL of bare-AgNPs were non-toxic to the CHO cells after 24 - 48 hours post treatment, cell viability at these were >70%. The ISO10993-5 states that if the cell viability of a formulation at a specific concentration is greater than 70%, then the formulation can be regarded as non-cytotoxic (Loan Khanh et al., 2019). Treatment with 3.5 µg/mL of bare-AgNPs decreased the percentage of viable cells by 45% after 24 hours then to 54% at 48 hours and 36% at 72 hours, indicating that this concentration was toxic to the CHO cells from 24 hours and persisted through the 72 hours of treatment. At 72 hours, 1.75 µg/mL bare-AgNPs induced cytotoxicity to the cells, with viabilities of 65. For this cell line, the imposed toxicity at higher concentrations was both dose and time dependant since the cell viability decreased with an increase in concentration and time.

The CHO cells treated with 3% DMSO-AgNPs at the concentrations up to 1.75 µg/mL showed no observable cytotoxicity, with the cell viabilities >70% at all time points. Furthermore, increased cell viabilities of 118 and 108% were observed for the two lowest concentrations at 72 hours. On the other hand, treatment with 3.5 µg/mL 3% DMSO-AgNPs reduced cell viability to < 50% indicating that at 24 hours, this concentration was toxic to the cells. The 4%

and 100% DMSO-AgNPs did not have any cytotoxic effect on CHO cells, as demonstrated by the cell viabilities percentages >70% at all concentrations at 24 and 48 hours, respectively. The cytotoxic effect was observed at 72 hours after treatment with the 3.5 µg/mL of the 4% DMSO-AgNPs. The cell viability at this period was 24%, indicating extreme cell death of up to 76%. While treatment with 100% DMSO-AgNPs at 48 hours, it was only the 0.2187 µg/mL dose that showed a reasonable percentage of viable cells, all the other concentrations had significantly lower viable cells, suggesting their toxicity at this time point. The same trend was observed at 72 hours for 100% DMSO-AgNPs. Thus, low concentrations of 100% DMSO-AgNPs were not toxic to the CHO cells, while at higher concentrations the formulation was highly toxic.

On the contrary, the AgNPs were non-toxic to the KMST-6 cells imposed to various concentrations for 24 – 72 hours. Subsequently, the cell viabilities of the various concentrations of the bare-AgNPs at 48 hours increased above 100%. Suggesting that not only are the bare-AgNPs treatments nontoxic, they also induced cell proliferation at this point in time. Furthermore, this nontoxic and cell proliferating behaviour was observed at 72 hours since the number of viable cells increased by 21, 27, 28, 29 and 30% compared to the untreated cells. Thus, it was also suggested that the bare-AgNPs operated in a time and dose dependant manner for KMST-6 cells.

The DMSO-AgNPs also exhibited no cytotoxicity towards the KMST-6 cells treated with various concentrations of the DMSO-AgNPs at all the time points. Cells treated with 3% DMSO-AgNPs demonstrated cell viabilities that were either insignificantly lower or greater than 100%. Enhanced cell proliferation was observed at 48 – 72 hours with cell viabilities >100% compared to the untreated cells. This proliferation was significantly for treatments ≤ 1.75µg/mL of 3% DMSO-AgNPs. All the tested concentrations of 4% and 100% DMSO-AgNPs did not have a toxic effect on the KMST-6 cells, rather they demonstrated proliferation at the various time frames, > 100% cell proliferation at each concentration during each time point. This increase in cell viability did not seem dose nor time dependant.

Similar to KMST-6 cells, none of the bare-AgNPs treatment demonstrated any cytotoxicity towards the HaCaT cells at 24 hours, since all the cell viabilities were >80%. At 48 hours, the recorded cell viability for the treatment with 3.5 µg/mL was 66%, suggesting that this concentration was toxic to the cells at this time point. While all the lower concentrations (0.2187 – 1.75 µg/mL) showed increased cell viabilities compared to 24 hours. At 72 hours, all

the cell viabilities were >100%, not only indicating no cytotoxicity but enhanced cell proliferation. Although the cell viabilities show an increase over time, except for the 3.5 µg/mL at 48 hours, this increase was not dose dependent. Contrary to the bare-AgNPs, differential effects on the HaCat cells exposed to the DMSO-AgNPs were observed. The 4% DMSO-AgNPs did not exhibit any cytotoxicity towards the HaCaT cells, their proliferation was > 100 % after 48 hours. After 24 hours, the 3% and 100% DMSO-AgNPs reduced the cell viability of the HaCat cells, indicating their toxicity towards the cells at this time point. Interestingly, all the concentrations showed an increase in cell viabilities from 48 hours. This increase was more pronounced at 72 hours, with cell viabilities above 100 % in the two AgNPs. To note, the cells treated with the lower concentrations up to 0.875 µg/mL showed no cytotoxicity at all the time frames. This might indicate that the DMSO-AgNPs are nontoxic and are capable of proliferating HaCaT cells and the cells recover over time.

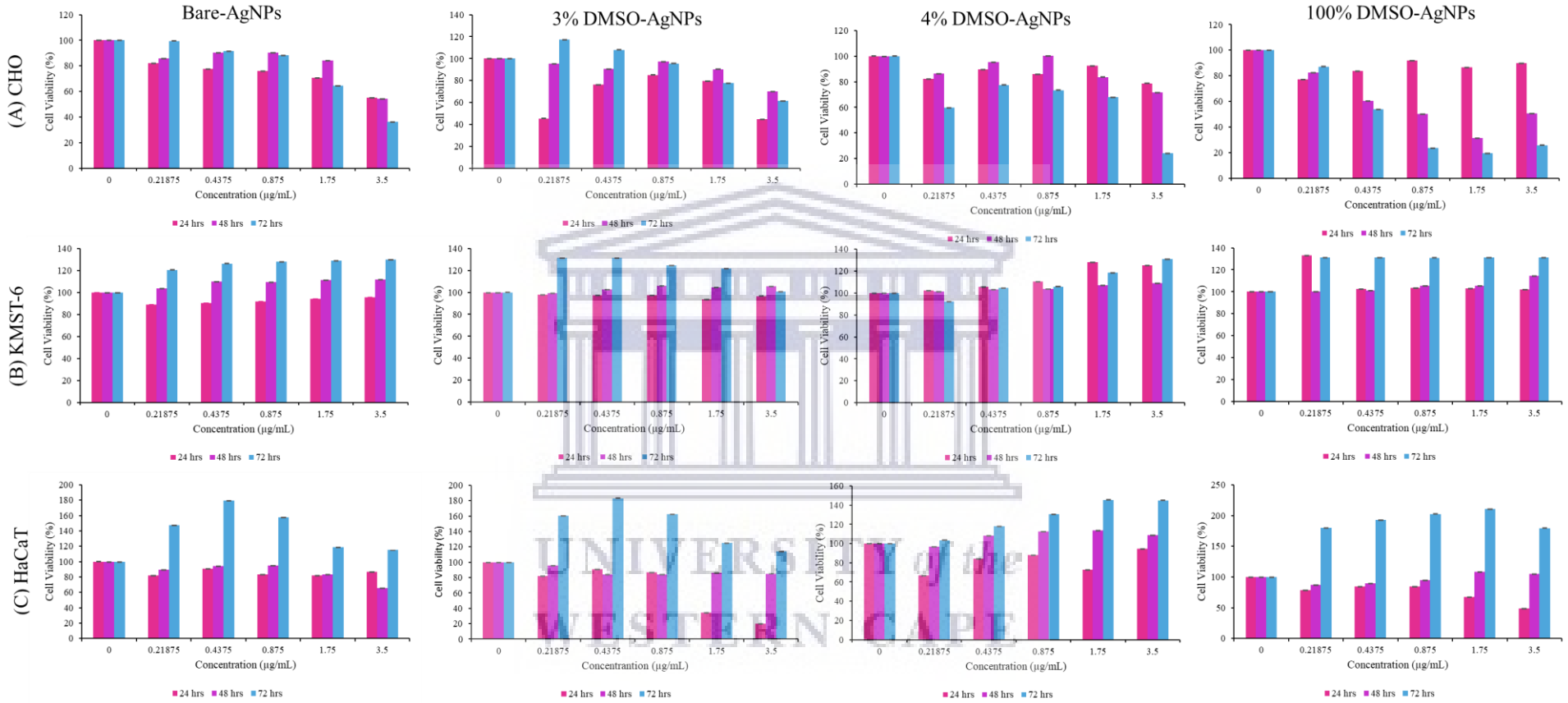

Figure 3. 21: Cell viability of (a) CHO, (b) KMST-6 and (c) HaCaT cells against various concentrations of bare-AgNPs and DMSO-AgNPs (3%, 4% and 100%) at 24, 48 and 72 hours.

Allantoin was used a positive control which is known to enhance cell growth at a particular concentrations (Savic et al., 2015). However, in this study the concentration of the allantoin and Dox were used to match the concentrations of the AgNPs. Allantoin resulted in enhanced cell viability at 0.109375 and 0.21875 µg/mL used, indicating no cytotoxicity but lived to its function of enhancing cell proliferation. Surprisingly, treatments from 0.4375µg/mL showed cell viabilities below 100%, suggesting that cell death occurred at this concentration. Although the cell viabilities at 0.109375 and 0.4375 µg/mL were lower, they were still high enough to be considered nontoxic. At 48 hours, all the treatments showed no observable toxicity, since the cell viabilities were >70%. This trend continued even at the following time point of 72 hours. At 72 hours, all the allantoin treatments exhibited cell viabilities ≥98%, further demonstrating the nontoxic nature of the compound towards KMST-6 cells. Overall, it can be suggested that allantoin does not exhibit any toxic effect on CHO cells.

Dox exhibited dose dependant toxicity towards the CHO and HaCaT cells at all time points (Figure 3.22(A)), as expected the CHO cells viability was below 50% for various concentrations of the drug. While varying degrees of toxicity was observed on the KMST-6 cells. At 24 hours, the cytotoxicity exhibited by Dox on the KMST-6 cells was 68% for 0.437 µg/mL. At tested concentration, the KMST-6 showed some resistance towards the effects of Dox, a cytotoxic anti-cancer drug. Instead, various concentrations of Dox promoted cell proliferation in the cells. The highest concentration at 72 hours demonstrated insignificant cytotoxicity. Thus, the cytotoxicity of dox in KMST-6 cells was dose dependant for various concentrations at 24, 48 and 72 hours. The known cytotoxic effect of dox was not well represented in this study since low concentrations were used. A previous study done on the cytotoxicity of this drug against three cell lines suggested that Dox was ineffective at lower concentrations. There was no evident reduction in cell viability (5.9 ± 6%) of the CHO cells exposed to 3 µM Dox for 24 hours. The cytotoxic effect was increased by 2.5 and 7.19 times when the drug was conjugated to tat and pene proteins respectively (Aroui et al., 2010).

Overall, the three cell lines, DMSO treatments showed a notable decrease in cell viability especially in KMST-6 and HaCaT cells at all time points. 6% DMSO significantly reduced cell viability of the CHO and cells to 36%, indicating extreme levels of toxicity. For KMST-6, at lower concentrations there was no remarkable cytotoxicity exhibited by DMSO to the cells since their viabilities were >70%, however at 6%, the cell viability was lower than 60% indicating that at this concentration it was toxic. At 48 hours, the lowest concentrations had cell viabilities >70% as observed at 24 hours. Enhanced cytotoxicity was observed for 3 and 6% DMSO with cell viabilities ≤49%. At 24 hours, ≤0.75% of DMSO did not exhibit any remarkable cytotoxicity since their cell viabilities were >70% except for concentrations ≥1.756% which had cell viability below 49%. Extreme cytotoxicity was observed for 1.5, 3 and 6% DMSO as indicated by a decrease in cell viabilities ≤48%. This trend persisted until 72 hours for the three cell lines.

Figure 3. 21: Cell viability of (a) CHO, (b) KMST-6 and (c) HaCaT cells against various concentrations of allantoin, 1% DMSO and Dox at 24, 48 and 72 hours.

There are many reports in literature on the high cytotoxic effect exhibited by various types of AgNPs on different cell lines (Eom & Choi, 2010; Lee et al., 2011; Jeyaraj et al., 2013; Nymark et al., 2013), and other that report on their biocompatibility (Martínez-Rodríguez et al., 2020). For instance, various AgNPs capped with tyrosine, namely $AgNPs^{Y}$, $AgNPs^{Y@PMA}$ and $AgNPs^{Y@PTA}$, were reported to be non- cytotoxic on prostate (PC3) cells even at 10 µM (Daima et al., 2014). Another study investigated the cytotoxic activity of AgNPs stabilized by different polymers on HepG2 and L929 cells. The cells were exposed to various concentrations between 10-100 ppm of POEM-AgNPs, SMA-AgNPs and PVA-AgNPs for 24 hours. The SMA-AgNPs showed slight cytotoxicity to the cell lines compared to the highly cytotoxic effect exhibited by POEM-AgNPs and PVA-AgNPs (Lin et al., 2012). Another study, bifunctional silver (II) pyridoxine silver nanoparticles (SPN) were reported to exhibit no cytotoxicity to the 3T3-L1 fibroblast and HaCaT keratinocytes but enhanced their proliferation by 49-50 fold compared to the untreated controls at concentrations of ≤5 µM (Rangasamy et al., 2016).

Similarly, the AgNPs in the present study showed no overall significant cytotoxicity, rather proliferation at some instances. It has been reported previously that cell type is one of the factors that affect AgNP cytotoxicity. It was observed that the AgNPs had better biocompatibility with KMST-6 followed by HaCaT cells. Generally, the CHO cells were the most susceptible to the AgNPs. Furthermore, the 4% DMSO-AgNPs exhibited better cell proliferation effects to all the cells as evident by the higher cell viability at each tested concentration and time point, followed by the 100% DMSO-AgNPs, 3% DMSO-AgNPs and bare-AgNPs, respectively. The cell proliferative effect imposed by 4% and 100% DMSO-AgNPs was independent of dose, overall these were considered non-toxic to the cell lines, mostly the KMST-6 and HaCaT cells. The improved cell growth enhancement in the case of 4 and 100% DMSO-AgNPs may be attributed to the presence of DMSO, since it has been reported that the solvent is capable of promoting cell proliferation in various cells.

DMSO has been reported to promote cell proliferation and growth, however, at very low concentrations (Astley & Levine, 1976; Yuan et al., 2014; Wen, Tong & Zu, 2015; De Abreu Costa et al., 2017; Guo et al., 2020). The cell growth and cell proliferation of DMSO were not observed in this study, since for all the cell lines, at all the concentrations and various time points, the cell viability of DMSO was not greater than the untreated controls. Rather, it was observed that low DMSO concentrations were non-cytotoxic, while cell death of ±50% cells were observed for both 3 and 6% DMSO concentrations. It was also observed that this cytotoxic behaviour worsens with time, since for all cell lines (72 hours) resulting in extremely

reduced cell viability at these concentrations. Thus, the noncytotoxic and cell proliferation ability of 3% DMSO-AgNP, 4% DMSO-AgNPs and 100% DMSO-AgNPs cannot be attributed to just the presence of DMSO. Furthermore, bare-AgNPs showed less biocompatibility compared to the DMSO-AgNPs indicating that cell proliferation and noncytotoxic behaviour of DMSO-AgNPs cannot be attributed to just the AgNPs component, rather the two work in synergy to improve the cytotoxic effect of DMSO-AgNPs.

3.5. Cellular Uptake of AgNPs by Dark field microscopy

The skin serves as a protective barrier for cells and other sub epithelial tissues against invasion by toxins and pathogenic species, making it difficult for topically administered drugs to penetrate or interact with it in the wound healing process. It is believed that only small hydrophobic materials are successfully carried into or across the skin (Chen, Li & Chen, 2017). Thus, it is important to find out whether the AgNPs can be internalized before they can participate in the wound healing process. Also, as a result of their cytotoxicity, the cellular uptake of AgNPs needs to be quantified since it has been reported that upon their internalization, they can travel to intracellular targets such as mitochondria, nucleus, endoplasmic reticulum and cytoskeleton and associate with them in different ways (Medici et al., 2019b). Cellular uptake differs from cell to cell and may be influenced by external factors such as size, agglomeration state, surface coating and surface charges of the AgNPs. Internalization of MNPs may occur through different routes such as diffusion, endocytosis or phagocytosis. It is also possible for AgNPs in the same sample to be internalized in different ways for examples aggregated AgNPs would enter human cells through phagocytic routes since the cells would view them as toxins and single AgNPs would enter through different routes (Akter et al., 2018; Medici et al., 2019b).

Herein, the cellular uptake of bare-AgNPs, 3% DMSO-AgNPs, 4% DMSO-AgNPs and 100% DMSO-AgNPs at 3.5 µg/mL was evaluated on CHO (Figure 3.23), KMST-6 (Figure 3.24) and HaCaT (Figure 3.25) cells by DF microscopy. The nuclei stain (DAPI) was used to associate the internalized AgNPs inside the cells, and also to study changes in the nuclear morphology induced by the different AgNPs. The nucleus is identified by the blue colour of the DAPI fluorescent dye. In the DF images, the bright yellow spots in the images represent the AgNPs (Jeong *et.al.*) since their spectra showed peaks around the SPR peak at 470 and 550 nm for single AgNPs and aggregated AgNPs, respectively (Jeong et al., 2018). Pinto *et.al.* also

attributed yellow bright spots in DF images to AuNPs and AgNPs since their UV analysis revealed a broad spectrum with a low relative intensity that was observed at the same absorption as the MNPs (Pinto et al., 2020). Thus, MNPs would appear as bright yellow spots in DF microscopy.

The AgNPs in the CHO cells were identified as brown regions in the DF images (Zhao et al., 2019) especially for those treated with the AgNPs. Nanospheres scatter green or yellow light under a DF microscope since both the surface plasmon oscillation and scattered light are in the visible region of the electromagnetic spectrum. Hence in the case of bare-AgNPs there was no green or yellow spots present indicating that these NPs were not taken up by the cells. 100% DMSO-AgNPs were taken up in minimal amounts as represented by the pink circles (Figure 3.23) in the DF images. The AgNPs were taken up by the cells as confirmed in the overlay images, which shows the yellow colour around the nucleus (blue florescent stain). This means that the AgNPs are internalized by the cells and might interact and penetrate other cellular components. This was not observed in the case of bare-AgNPs and the untreated controls, showing that these AgNPs are not internalized by the CHO cells. The amount of internalized 3% and 4% DMSO-AgNPs was extremely high as visualized by the DF images. Both the DMSO-AgNPs penetrated the cells and accumulated in the cytoplasmic region and not the nucleus although are seen to be in close proximity with the nucleus. This optimal penetration can be explained by the presence of 3% and 4% DMSO contained in the cells, since this solvent's ability to penetrate cellular membranes has been briefly mentioned previously. The reason why this uptake was not as quite observable in 100% DMSO-AgNPs can be attributed to the concentration of the solvent in 100% DMSO-AgNPs, and their aggregating state as illustrated by the HR-TEM images since concentration and aggregation are some of the factors that affect cellular uptake (Moore et al., 2019). Furthermore, changes in the cellular morphology were observed in the 3%, 4% and 100% DMSO-AgNPs. The cells became bigger in size and their tails appear elongated. In the latter, the cells seemed to have proliferated since more nuclei were observed, and the size of the nucleus seems to be reduced. Changes in cellular morphology using DF microscopy were also observed by Kumar and his co-workers when they were evaluating the cellular uptake of different sized MNPs in various ovarian cancer cells (Kumar et al., 2017). They reported that cellular uptake was influenced by the cell type, size and concentration. They reported that larger MNPs caused the cells to be more scattered, as observed in the case of 100% DMSO-AgNPs compared to the control samples.

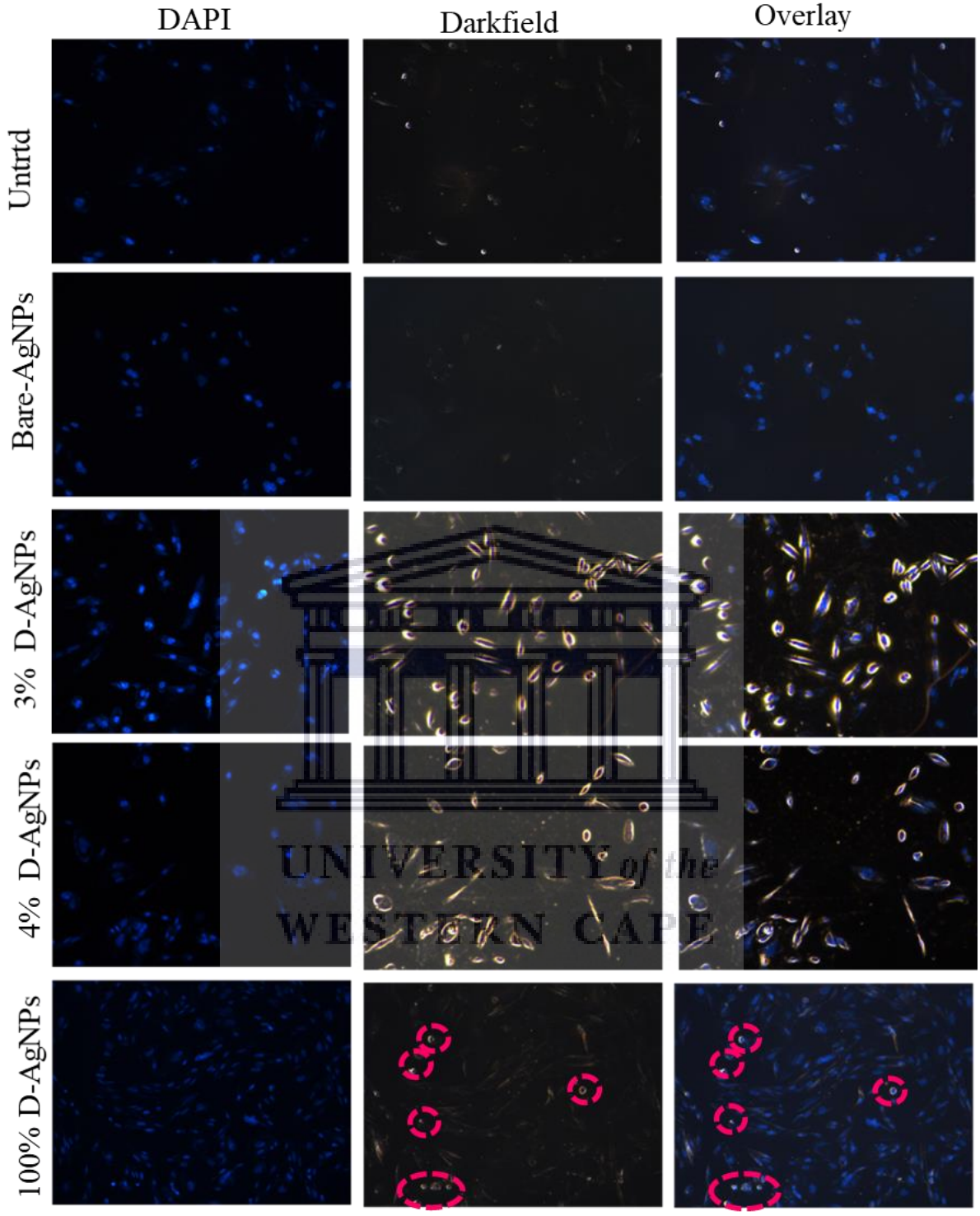

Figure 3. 22: Cellular uptake of AgNPs by CHO cell line under DF and fluorescent microscopy. The scale was set at 100 µm for all images.

The KMST-6 cells did not show any improved internalization of the AgNPs as compared to the CHO cells. Except for the case of bare-AgNPs, at least this cell line was able to take up a few particles as indicated by the pink circles in the DF images (Figure 3.24). The DF images

presents tiny bright spots (Zhao et al., 2019; Pinto et al., 2020) that were assigned to the 3%, 4% and 100% DMSO-AgNPs. Some of the 3% and 4% DMSO-AgNPs were found in the cytoplasm as in the case of CHO cells but at a reduced rate (Ashton et al., 2018). A study on the internalization of diamond nanoparticles (NPs) on mammalian cells reported that the NPs which are taken up intracellularly by the endocytic vesicles are larger in size while smaller sized NPs accumulated the cytoplasm freely (Saldmann, Saldmann & Lemaire, 2020). Since all the AgNPs in this study are polydispersed, it was then considered that the tiny bright spots were the smaller NPs while those surrounding the nucleus are larger in size. However, further cellular uptake studies need to be done to identify which parts of the cells were involved in the internalization of these AgNPs. Moreover, the AgNP cellular uptake was quite improved in the 4% DMSO-AgNPs, indicating that these NPs are much more internalized by the KMST-6 cells, and this could improve its activity in the wound healing process since these NPs are in close proximity with the nucleus and can afford better interaction with it. There were no obvious changes in cellular morphology for all the treatments, just that the 100% DMSO-AgNPs appeared to have higher proliferation rate.

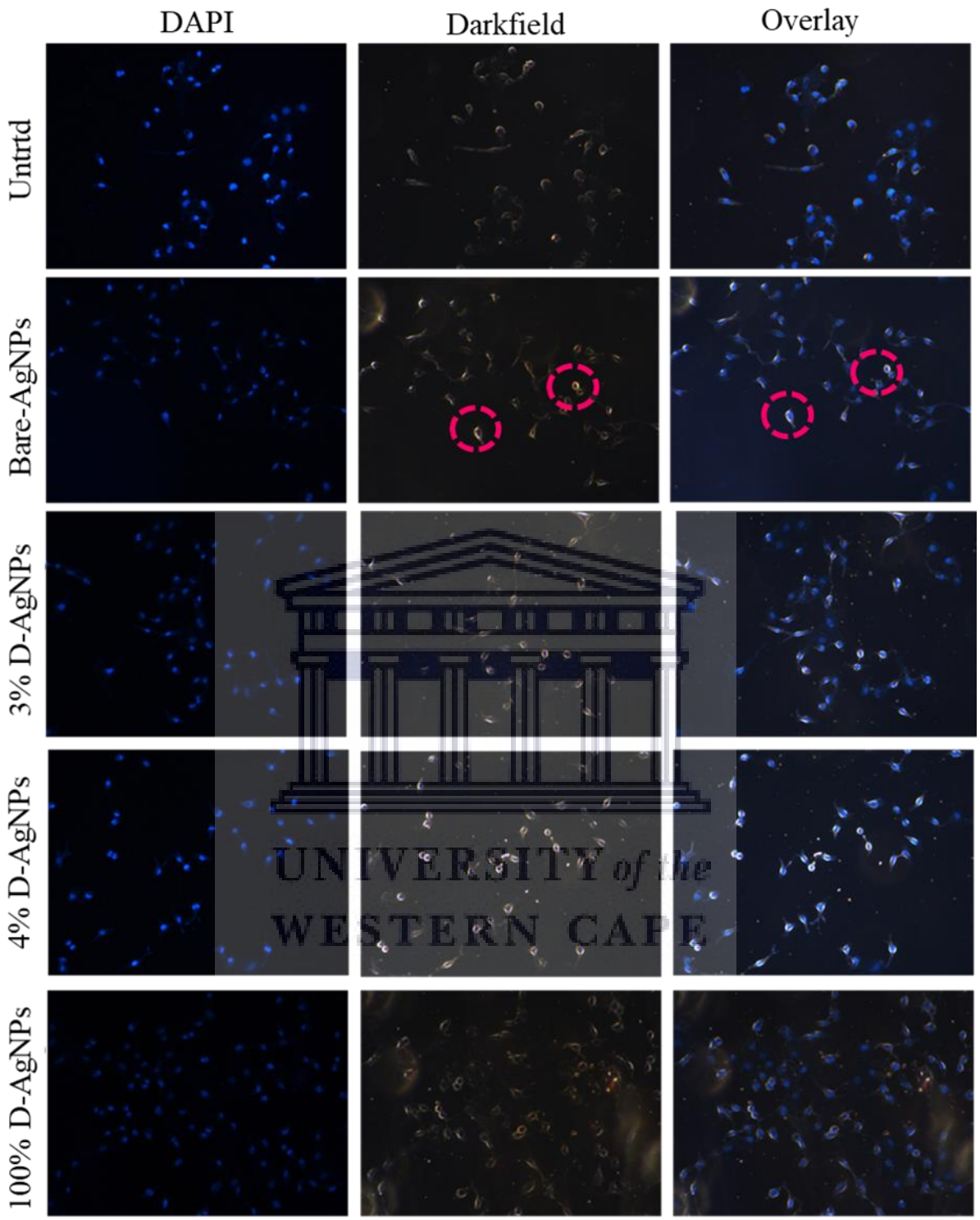

Figure 3. 23: Cellular uptake of AgNPs by KMST-6 cells under the Dark field and fluorescent microscopy. The scale was set at 100 µm for all images.

The keratinocytes (HaCaT cells) showed the least cellular uptake of all the AgNPs, AgNP internalization depends on a lot of factors including cell type thus different outcomes for the various cell lines were expected. Furthermore, Chen and his colleagues reported nanoparticles

are easily taken up by cancerous cells (HePG2 and T-47D) than normal fibroblast cells (NIH3T3) (Chen, Kandasamy & Chen, 2019; Zhao et al., 2019). The HaCaT cells were visualized as hollow circles with weak brown outlines, while various AgNPs were visualized as tiny bright spots that formed aggregates outside the nucleus in HaCaT cells. It was suspected that 4% DMSO-AgNPs would beng taken up more as in the previous cases with the CHO and KMST-6 cells, and that the AgNPs would accumulate in the cytoplasm. However, the 4% DMSO-AgNPs were internalized as aggregates intracellularly while only a few was seen by the cytoplasm (pink circle in Figure 3.25). Better internalization was observed for 100% DMSO-AgNPs rather, since the bright yellow spots were not presented as clumps but single dots indicating little or no aggregation as in the case of 4% DMSO-AgNPs. This comparison is clearly visible in the overlay images. This led to the suggestion that 100% DMSO-AgNPs were taken up better by the keratinocytes, followed by 4% DMSO-AgNPs, 3% DMSO-AgNPs and lastly the bare-AgNPs. In all treatments, there were no distinct changes in cellular morphology. Overall, the CHO cells showed better cellular internalization of the AgNPs compared to the KMST-6 and HaCaT cells. The 4% DMSO-AgNPs were better internalized by both the CHO and KMST-6 cells followed by the 3% DMSO-AgNPs, 100% DMSO-AgNPs and bare-AgNPs, respectively. But cellular uptake with HaCaT cells showed a different outcome with the 100% DMSO-AgNPs taken up more efficiently followed by the 4% DMSO-AgNPs, 3% DMSO-AgNPs and bare-AgNPs. This could be attributed to the cell type, since each cell line will behave differently.

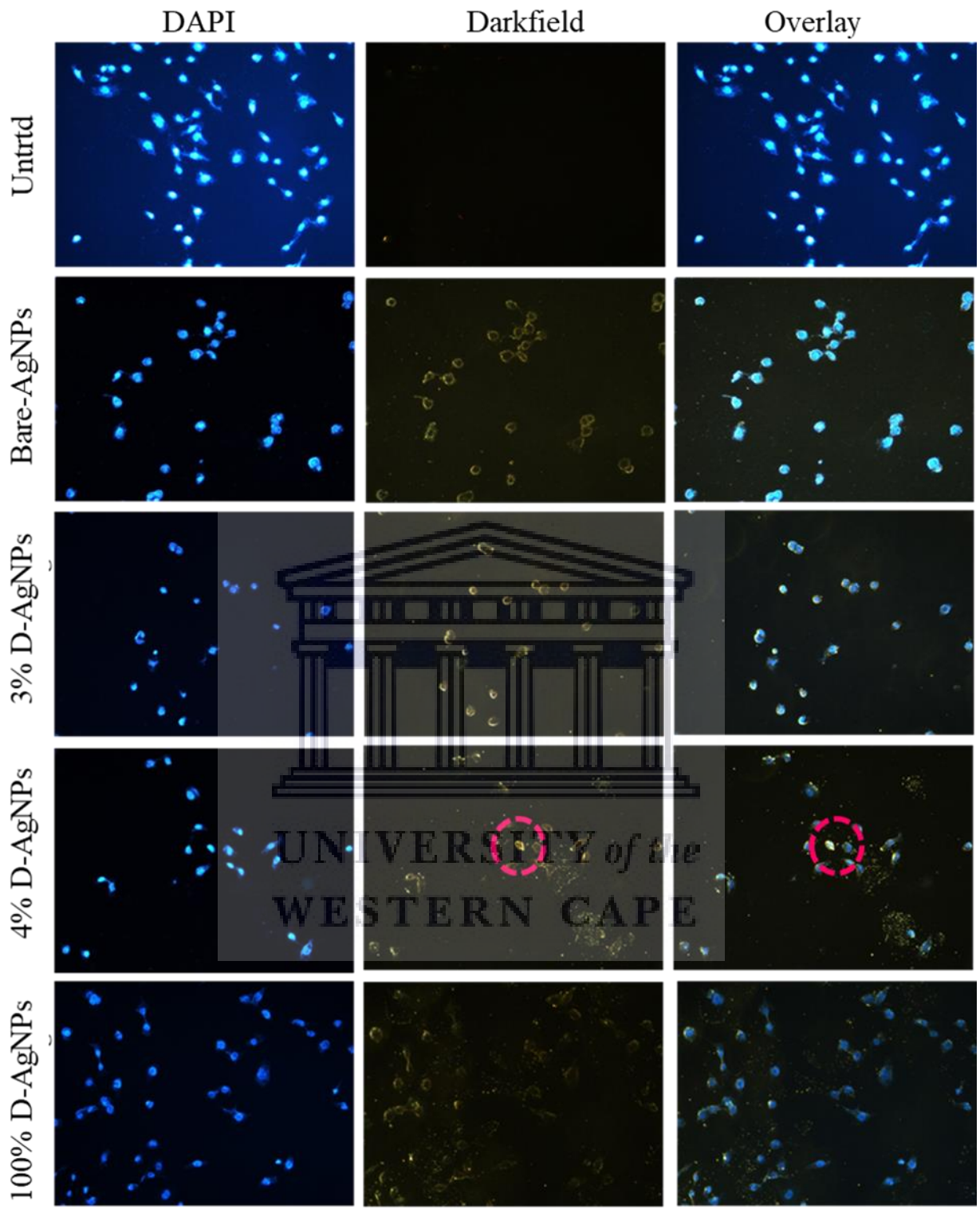

Figure 3. 24: The cellular uptake of AgNPs by HaCaT cell line using DF and fluorescent microscopy. The scale was set at 100 µm for all images.

3.6. Wound Scratch Assay

Skin wound healing is a very important, yet fragile process that is susceptible to interruptions and failures mainly due to infections on the wound. These interruptions and failures which appear in section 1.3 above arise as a result of the factors that affect wound healing. The mechanisms involved in the process are very complex, yet crucial to avoid delayed healing and other complications (Ather & Harding, 2009; Orlowski et al., 2018; Ceresa et al., 2019; Mahmoud et al., 2019; Makvandi et al., 2019). Scratch assay is an often used to model wounds *in vitro* in order to test cell migration and rate of closure following treatments (Grada et al., 2017; Giri et al., 2019). In this assay, a 2-dimensional confluent monolayer is scratched by a sharp object to create the wound which is then exposed to test compounds (Neibert et al., 2012; Jonkman et al., 2014; Grada et al., 2017; Giri et al., 2019). The migration of cells from the wound edges is then monitored throughout time and the rate at which the scratch closes in the monolayer cells is measured and quantified as the rate of wound healing (Jonkman et al., 2014; Kumar, Houreld & Abrahamse, 2020).

Keratinocytes and fibroblasts are among the top 2% of cells frequently used *in vitro* for wound healing assays (Mahmoud et al., 2019). In the present study, KMST-6 cells were chosen to carry out this assay because fibroblast cells play a very crucial role in normal wound healing. Also, the KMST-6 cells grew at the faster rate than the keratinocytes (HaCaT), further making them the cell line of choice for the rest of the biological assays involved in this study. KMST-6 cells are also implicated in vital processes including the breakdown of fibrin cloth, generation of new collagen and extracellular matrix (ECM), which supports other cell types that are involved in the wound contraction and healing process (Bainbridge, 2013; Orlowski et al., 2018). Furthermore, the fibroblasts demonstrate a collective cellular movement known as sheet migration (Grada et al., 2017). The nanoscale size of AgNPs provides them with distinctive properties that are useful in wound healing and they can also be used as transport vehicles for a variety of wound healing agents. They can penetrate deeper into the wounded area and interact with biological targets leading to enhanced wound healing. AgNPs enhance wound closure by increasing cell proliferation and migration of cells and can lead to the transformation of myofibroblast through fibroblast, resulting in the contraction of the wound. Thus many reports of the wound healing capabilities of AgNPs and AgNPs decorated scaffolds are found in literature (Neibert et al., 2012; Franková et al., 2016; Rangasamy et al., 2016; Ai et al., 2017; Giri et al., 2019; Kaur et al., 2019). Some affording complete wound closure after a short period

of time such as the Aloe arborescens synthesized AgNPs reported by Dhilip *et.al.*, which demonstrated complete wound closure at 48 hours on diabetic and non-diabetic WS1 cells (Kumar, Houreld & Abrahamse, 2020). On the other hand, low concentrations of DMSO have exhibited wound healing properties such as the enhanced proliferation and migration of fibroblasts in an *in vitro* wound healing model (Wen, Tong & Zu, 2015; Guo et al., 2020). Hence, the combination of DMSO and AgNPs was envisaged to lead to accelerated wound healing. Thus, the 3, 4 and 100% DMSO-AgNPs used in this study were expected to show enhanced healing properties compared to bare-AgNPs, DMSO and the positive control (allantoin).

The cellular morphology (Figure 3.26) and migration rate (Figure 3.27) of KMST-6 cells treated with DMSO (1%), and 3.5 µg/mL of allantoin, bare-AgNPs, and DMSO-AgNPs were investigated using the scratch assay. The wound area was measured at 0, 24, 48 and 72 hours post treatment and analysed using MRI wound healing tool on the imageJ software. The time points between 0–24 hours did not retain any observable changes. A spindle-like shape was observed for all the wounded KMST-6 cells as shown in Figure 3.26, this change in morphology occurred as the cells were moving towards the gap, they do so by elongating themselves in an attempt to maximise wound healing (Mahmoud et al., 2019; Kumar, Houreld & Abrahamse, 2020). Furthermore, Bainbridge explained that the migration route of fibroblast cells occurs via contact guidance. Meaning that, they do not move in an unplanned manner or through the fastest route, rather they move along the position of the collagen already present in the wounded area. They attach and move towards the fibronectin already in place (Bainbridge, 2013).

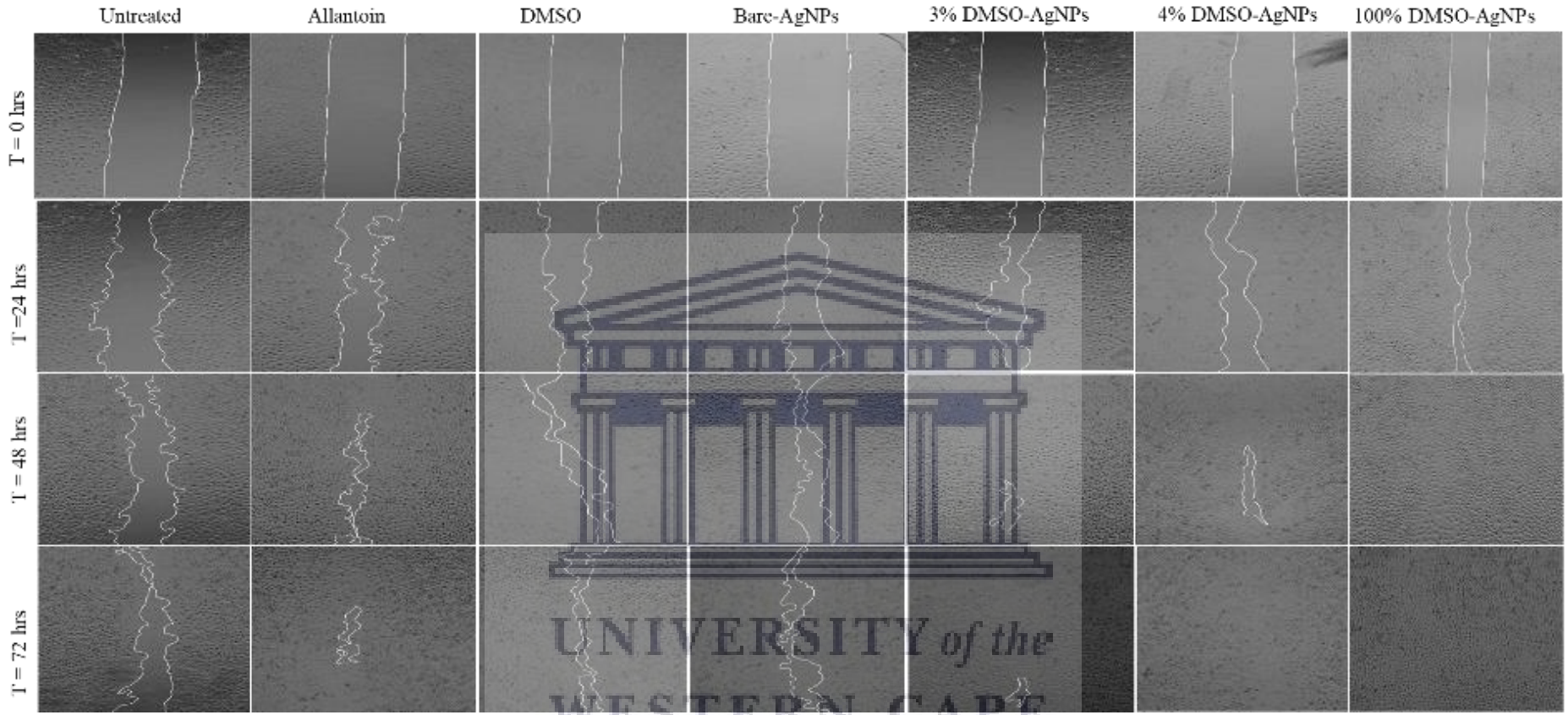

Figure 3. 25: Cellular Morphology of KMST-6 untreated cells, treated with 1% DMSO and 3.5 µg/mL allantoin at 24, 48 and 72 hours.

The migration rate which is the speed at which treatment with AgNPs can achieved complete wound closure was calculated as described by equation (1) in chapter 2. Compared to the untreated cells, the rate of migration increased in the following order at 24hours: 3% DMSO-AgNPs > bare-AgNPs > 1% DMSO > allantoin > 4% DMSO-AgNPs >100% DMSO-AgNPs. This indicated that the 3% DMSO-AgNPs followed by bare-AgNPs treatments accelerated cell migration, while cell migration in cells treated with allantoin, DMSO and 4% DMSO-AgNPs was significantly lower than the untreated control group. The 100% DMSO-AgNPs treated cells migrated at a significantly lower rate than all of the samples after 24 hours. At 48 hours there was a significant increase in the rate of migration for the 4% DMSO-AgNPs treated cells compared to the control and all the other groups, 3% DMSO-AgNPs treated cells also showed a migration rate that was higher than the controls. While all the other treatments showed a reduced cell migration rate compared to the untreated control in the order: Allantoin = bare-AgNPs > DMSO >100% DMSO-AgNPs. At 72 hours, treatment with 4% DMSO-AgNPs showed a speedy rate of migration compared to the other treated groups, followed by 3% DMSO-AgNPs. Allantoin showed a migration rate similar to the untreated controls while the migration rate of bare-AgNPs, 1% DMSO and 100% DMSO-AgNPs was significantly slower than the untreated samples. Thus, 4% DMSO-AgNPs affords an overall faster migration rate, followed by 3% DMSO-AgNPs, Allantoin, bare-AgNPs, DMSO and lastly the 100-DMSO-AgNPs.

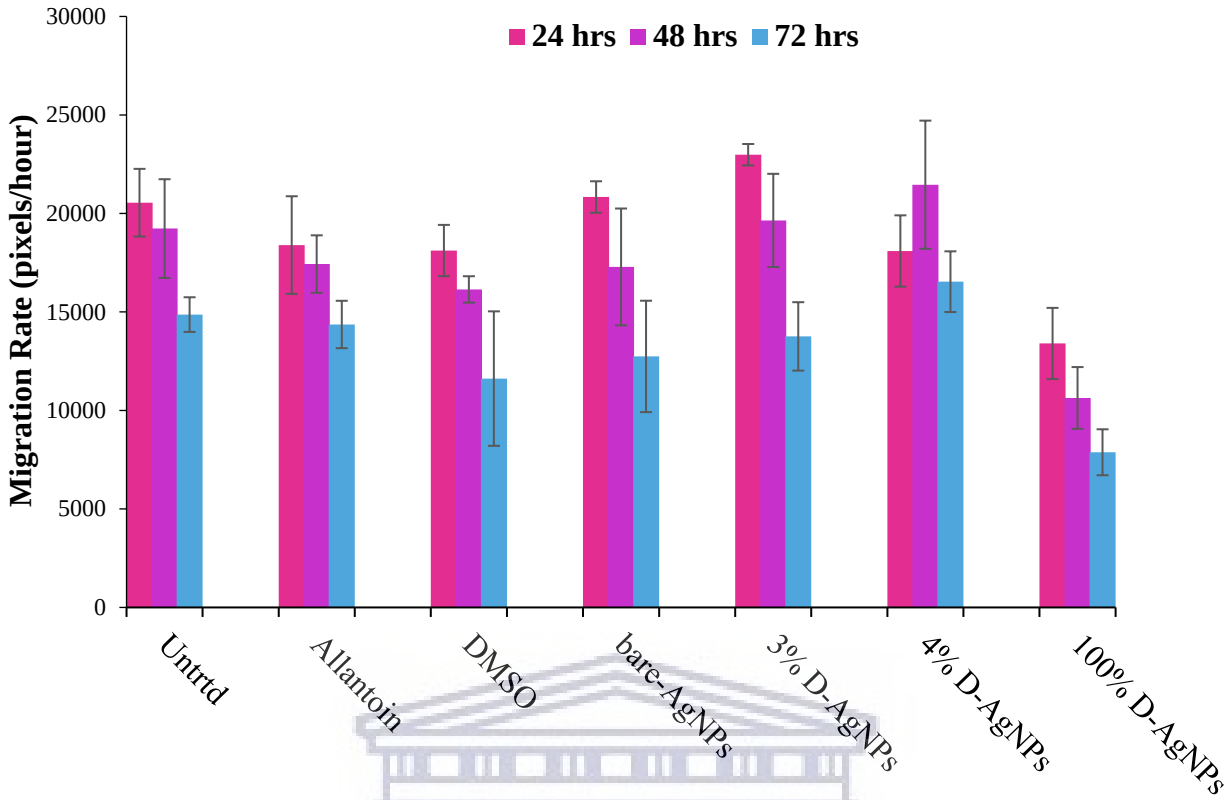

Figure 3. 26: Migration rate of KMST-6 cells after exposure to various treatments for 24, 48 and 72 hours.

After the wound healing migration assay, the cell density in all treatments was counted using the trypan blue exclusion method, which is based on the notion that the live cells with intact cellular membranes will exclude the blue dye and be visualised with bright white centres under microscope while the dead cells will take up the dye and appear dark blue (Nymark et al., 2013). Compared to the untreated samples, the cell density of the cells treated with 1% DMSO was less than the untreated, the allantoin was slightly higher, while the cell viability all the AgNPs were extremely higher. The 100% DMSO-AgNPs showed the lowest viable cells among the AgNPs followed by bare-AgNPs, 3% DMSO-AgNPs and 4% DMSO-AgNPs, respectively. The 4% DMSO-AgNPs showed an extremely high number of live cells after the wound closure compared to other test AgNPs. Thus, 4% DMSO-AgNPs, followed by 3% DMSO-AgNPs showed enhanced proliferation and growth of the fibroblast cells.

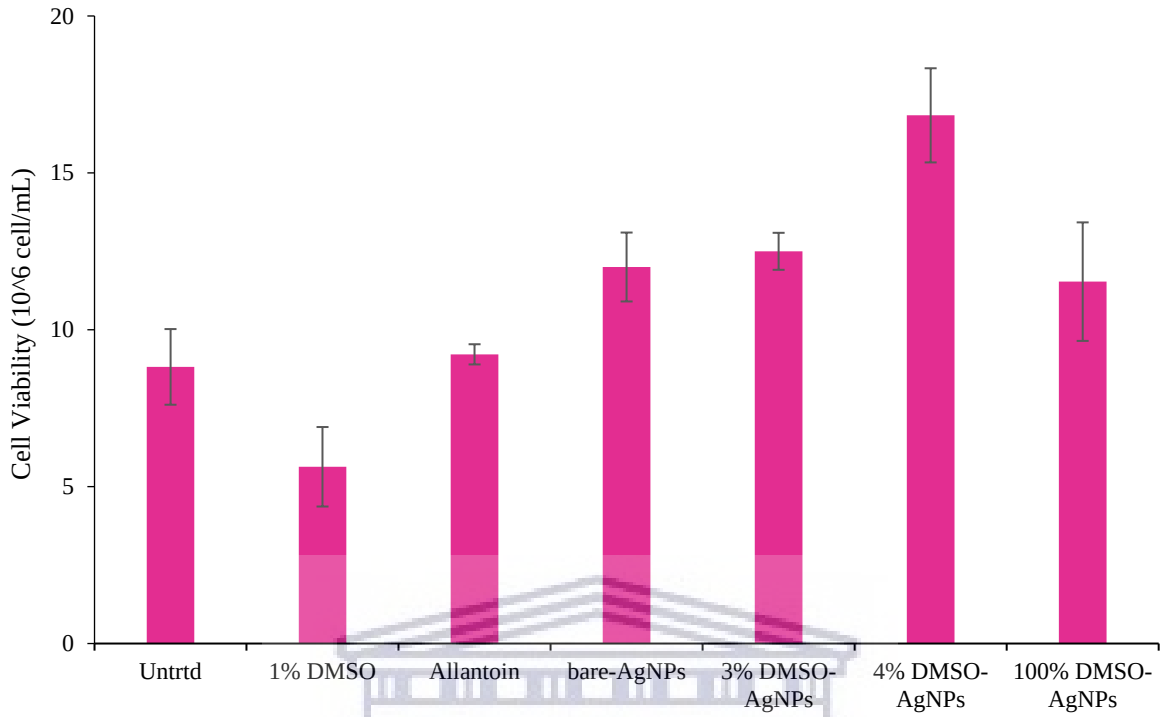

Figure 3. 27: Cell viability assay after scratch assay termination using trypan blue exclusion method**.**

The 4% DMSO-AgNPs followed by the 3% DMSO-AgNPs behaved better in the wound healing assay in terms of migration rate and cell viability. These formulations also showed better cell migration and enhanced cell viability than the untreated and positive controls. This indicates that both the 3% and 4% DMSO-AgNPs are able to speed up the rate of healing. The improved cell proliferation, growth and migration rate observed for both 3% and 4 % DMSO-AgNPs could be attributed to the presence of the low concentration of DMSO contained therein. Since these features were not pronouncedly observable in the high concentrated DMSO AgNPs i.e (100% DMSO-AgNPs) and the bare-AgNPs which do not contain any traces of DMSO. Even at lower concentrations, 1% DMSO alone was incapable of demonstrating these enhanced wound closures as reported by the current study as well as Tsung-Jung Ho *et.al*, who reported wound closures of ~44% in HMEC-1 cells treated with DMSO (Ho et al., 2016). Other scientific papers have reportedly used low concentrated DMSO in the wound healing assay as a positive control since it has been established that this solvent was capable of promoting cell growth (Lee et al., 2012; Guo et al., 2020). Thus, this enhanced activity cannot be attributed to the presence of low DMSO levels alone, but the AgNP component as well. Since it was the nanoscale dimension that brought out the properties such as larger SA/V ratios and antibacterial

properties. Thus, the low concentrations of DMSO and the AgNPs present in these formulations work in synergy to speed up the wound healing process. Since both 3% DMSO-AgNPs and 4% DMSO-AgNPs were better internalized by the KMST-6 cells, they had improved overall biological activities because they were in close proximity with the cellular components. This can be attributed to their smaller sizes in comparison to the bare and 100% DMSO AgNPs as reported by HR-TEM, SAXS and DLS. Furthermore, the presence of the low concentration of DMSO also enhanced their bioactivity dues to the solvent's abilities to permeate extracellular membranes.

3.7. Investigation of the effect of AgNPs on cellular integrity

Mitochondria are the powerhouses of the cells, and provide the cells with necessary energy required for cellular functions and survival. One of their major contributions to cellular survival and growth is the generation of chemical energy through the electron transport (ET) chain (Maurer & Meyer, 2016). The bactericidal properties of AgNPs are very well known, which makes mitochondria an easy target for AgNPs induced toxicity. Upon their internalization, AgNPs can travel across cell membranes through various pathways and interact with intracellular organelles such as the mitochondria and nuclues (Chen & Schluesener, 2008). Interactions of AgNPs with these organelles, more especially the mitochondria will alter their normal functions (Chen & Schluesener, 2008; Golinska et al., 2014) could lead to insufficient energy production and disruption of the ET chain which will result in the cell's inability to carryout basic functions. AgNPs were reported to interfere with mitochondrial membrane proteins, altering the permeability of the membrane and changing mitochondrial functions. It is the powerful oxidative ability of AgNPs that causes the release of Ag^{+} ions which leads to oxidative stress in eukaryotic cells and tissues by generating ROS and exhaustion of MMP. The end result of oxidative stress leads to severe effects such as cytotoxicity, cell death, genotoxicity, activation or suppression of the immune system. Thus, it is very important to investigate the mode of AgNP induced mitochondrial function for specific applications. In this study, the effect of the AgNPs on the intracellular ROS generation and depolarization of MMP were evaluated by the 5-(and-6)-chloromethyl-2',7'-dichlorodihydrofluorescein diacetate, acetyl ester (CM-H_2DCFDA) and tetramethylrhodamine ethyl ester perchlorate (TMRE) assays, respectively.

3.7.1. Measurement of Intracellular ROS

ROS are naturally occurring by-products of cellular oxygen metabolism generated through mitochondrial respiration in eukaryotic cells (Kim & Ryu, 2013; Holmila et al., 2018). Singlet oxygen ($^1O_2$), superoxide ($O_2^{\bullet-}$), hydroxyl ($HO^{\bullet}$), perhydroxyl ($HO_2^{\bullet}$), carbonate ($CO_3^{\bullet-}$), peroxyl ($RO_2^{\bullet}$), alkoxyl ($RO^{\bullet}$) and carbon dioxide radical ($CO_2^{\bullet-}$) are some of the biologically noteworthy free radicals of ROS elements while nonradical forms include hydrogen peroxide (H_2O_2), hypobromous acid (HOBr), hypochlorous acid (HOCl), ozone (O_3), organic peroxides (ROOH), peroxynitrite ($ONOO^-$), peroxynitrate (O_2NOO^-), peroxynitrous acid (ONOOH), peroxomonocarbonate ($HOOCO_2^-$), nitric oxide (NO), and hypochlorite (OCl^-) (Kim & Ryu, 2013). Although other external factors such as drugs and ionization radiation among others can generate intracellular ROS, the mitochondrial respiratory chain is the primary root of intracellular ROS generation. ROS have a vital task in cellular activities such as differentiation, signalling, inflammation-related factor generation, regulation of viability and death. Thus, intracellular oxidants and antioxidants need to always be in equilibrium in order for the cell to grow, adapt, regulate and function properly. When this equilibrium state is breached, and there is an imbalance between ROS levels and the antioxidants which regulates them, oxidative stress is induced. The most common kind of ROS produced by mitochondria is superoxide which is transformed to both H_2O_2 and oxygen by the mitochondrial manganese-dependant superoxide dismutase (SOD_2, MnSOD).

AgNPs may react with proteins and thiol bearing enzymes which are vital elements of the antioxidant defence mechanism of eukaryotic cells (Sadowska-Bartosz et al., 2013). This defence mechanism is in charge of regulating oxidative stress induced by mitochondrial ROS generation. Excess ROS is responsible for inducing an inflammatory response which then results in adverse cellular injuries such as mitochondrial damage and dysfunction. Oxidative stress is the most anticipated mechanism of AgNPs induced cytotoxicity (Chen & Schluesener, 2008; Eom & Choi, 2010; Kim & Ryu, 2013; Akter et al., 2018). Cancer, Alzheimer's and Parkinson's diseases are some of many human diseases that occur as a result of elevated intracellular ROS levels, mitochondrial impairment and destruction (Gonzalez-Carter et al., 2017).

Herein, generation of intracellular ROS was investigated using the cell permeant, non-florescent CM-H_2DCFDA compound, which is transformed to the extremely florescent form, dichlorofluorescein (DCF), by cellular peroxides. After the cells were exposed to various

AgNPs for 24 hours, intracellular ROS levels were measured as DFC intensities. The fluorescent intensities generated by treatments resulted from their oxidation which led to the formation of superoxide radical $O_2^{\bullet-}$, a precursor of other ROS such as $HO^{\bullet}$, $RO_2^{\bullet}$ and $HO_2^{\bullet}$, which are detectable through CM-H_2DCFDA assay. Formation of these radicals led to higher levels of ROS which was quantified by flow cytometer. Thus, higher DFC intensities was corelated to higher levels of ROS production.

The florescent intensities generated by the cells treated with the bare-AgNPs, 1% allantoin, 1% DMSO and untreated cells were compared against those of cells treated with 1% H_2O_2 a ROS inducer. In comparison, the treatment with 1% allantoin exhibited low florescent intensities than the untreated controls, suggesting that this compound does not generate intracellular ROS (Figure 3.29). DMSO has been reported to generate intracellular ROS levels in a dose dependant fashion in yeast *Saccharomyces cerevisiae* when exposed to 0-14% concentrations of DMSO (Sadowska-Bartosz et al., 2013). The treatment with 1% DMSO showed no statistical difference compared to the untreated control, this supports the results of the present study since no noteworthy difference was established. The quantitative analysis in a study conducted by Gao *et.al.* also showed no significant increase in intracellular ROS levels generated in the astrocytes treated with 1% DMSO compared to the control sample, the increase was rather observed at 5% DMSO exposure. Other papers have also reported the dose dependant increase of intracellular ROS generation following exposure to different concentrations (0.01-100%) and (0-2%) of DMSO on various cells (Mannan et al., 2010; Dludla et al., 2018).

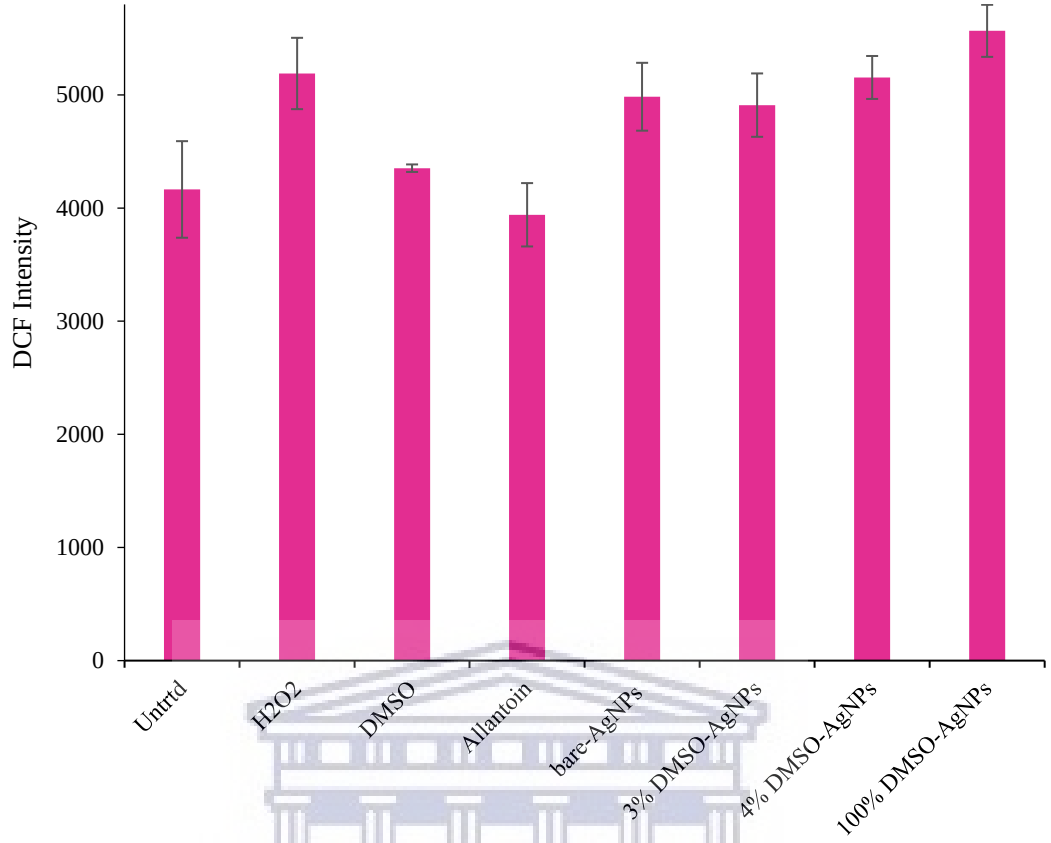

Figure 3. 28: Modulation of ROS generation post AgNPs treatment on KMST-6 cells.

Contrary, treatment with the AgNPs generated intracellular ROS levels in the cells (Lee et al., 2011; Roy et al., 2013; Batchelor-McAuley et al., 2014; Dayem et al., 2014; Paul et al., 2015; Singh, 2016), however according to the MTT assay results, a decrease in intracellular ROS levels was expected since the prepared AgNPs showed no significant toxicity towards the KMST-6 cells, rather increased proliferation at some instances. The bare-AgNPs, and the DMSO-AgNPs (3%, 4% and 100%) showed elevated ROS levels compared to the controls, the 100% DMSO-AgNPs was even higher than 1% H_2O_2. Although bare-AgNPs, 3% DMSO-AgNPs and 4% DMSO-AgNPs exhibited lower intensities than 1% H_2O_2, the decrease in ROS levels was lower than the 100% DMSO-AgNPs. This was due to the combined effects of both the AgNPs and higher concentrations of DMSO which individually contributed to extreme levels of ROS production. Moreover, ROS levels increased in a DMSO dose dependant manner for cells exposed to the DMSO-AgNPs, i.e. 3% < 4% <100%.

Cellular uptake and localization play a vital role in the intracellular events since without internalization these events would not occur. Thus, there has to be a direct link of the degree

of cellular uptake and generation of the intracellular ROS levels (Jeong et al., 2018; Vuković et al., 2020). The AgNPs were internalized as visualized by the DF microscope in the cytoplasm and around the nucleus (Figure 3.24), suggesting that the AgNPs had a better chance of interacting with the internal organelles and the respiratory enzymes. However, the ROS levels in cells treated with the 3% and 4% DMSO-AgNPs were lower than ROS levels generated by the H_2O_2 and the 100% DMSO-AgNPs, indicating that they might still be within the accepted range needed by the cells. The ROS generated by both bare-AgNPs and DMSO-AgNPs, do not lead to apoptosis since there was no extreme cytotoxicity induced via MTT evaluation. Thus, the oxidative stress induced by the AgNPs does not always lead to cytotoxicity. In fact, several papers have reported high cytotoxicity via MTT assay but no generation of intracellular ROS, indicating that oxidative stress in some instances does not have a direct impact on cytotoxic effects. Since no ROS was generated, the cytotoxic effect was attributed to various features such as size, agglomeration and surface charge (Gonzalez-Carter et al., 2017). This was also demonstrated in the present study, however, no cytotoxicity was observed at the tested concentrations up to 72 hours but there was a clear indication of intracellular ROS generation at 24 hours. The ROS generated by the bare-AgNPs and DMSO-AgNPs might be required for the cells to adapt to the presence of the AgNPs for their survival and growth, since ROS is also vital for such cellular processes.

3.7.2. Measurement of MMP, $\Delta\Psi_m$

Separations in electric charges between cellular compartments divided by membranes causes an electric potential difference across both sides of the membrane. This difference is caused by electrogenic pumps embedded in both the plasma and inner mitochondrial membranes. Such that the inner compartment e.g. cytoplasm or mitochondrial matrix is always more negatively charged than the outer compartments. Therefore, mitochondrial membrane potentials (MMPs) are physiologically higher than those across the cell membrane, ranging between 150–200 mV, while the cell membrane has potentials across 50–100 mV (Zorova et al., 2018). Subsistence of these potentials is crucial for physiological processes of the cell, thus their alteration leads to cellular dysfunction (Nicholls, 2004).

Upon their internalization, AgNPs diffuse towards the mitochondrial membrane and interact with the respiratory enzymes and accumulate around the mitochondrial membrane, where they disturb the protons in that vicinity, affecting the ET chain (Gonzalez-Carter et al., 2017). This usually cause the lipid peroxidation in the mitochondrial membrane, decoupling of oxidative

phosphorylation and decrease in MMP (Golinska et al., 2014). In the current study, the MMP potential (MMP, $\Delta\Psi_m$) was evaluated by TMRE, a red-orange cell permeant fluorescent dye. It is a positively charged lipophilic dye that is secluded by negatively charged healthy mitochondria upon its cellular entrance. Reduction of MMP in damaged mitochondria makes them lose their negative charge and capability to take up TMRE. Thus, depolarization of the MMP can be evaluated by the measuring intensities exhibited by the fluorescent dye inside the cells. Active mitochondria would exhibit higher fluorescent intensities due to their ability to take up TMRE, while depolarized mitochondria will show less intensity. The intensities generated by various AgNPs in this study were normalized as percentages relative to the untreated control. Therefore, a decrease in percentage is regarded as an increase in depolarization of MMP.

The MMP of the cells treated with 1% DMSO and 3.5 µg/mL allantoin was comparable to the untreated controls. This suggested that these treatments are not damaging or toxic to the mitochondria and consequently do not result in the depolarization of the MMP (Figure 3.30). This was expected because the two treatments did not cause elevated ROS levels (Figure 3.29), which is the culprit in mitochondrial dysfunction. Depolarization of MMP in cells treated with DMSO increased with an increase in concentrations of the DMSO (Sadowska-Bartosz et al., 2013; Yuan et al., 2014; Dludla et al., 2018). The DMSO concentration used in this study was relatively low (1%), therefore no depolarization of MMP was expected, Yuan et.al also reported that 1% DMSO did not show significant changes in MMP compared to their control, change was rather observed at 5% DMSO. Exposure of various human cells to AgNPs has been linked with altering $\Delta\Psi_m$ (Singh & Ramarao, 2012; Rosarin et al., 2013; Aueviriyavit, Phummiratch & Maniratanachote, 2014; Auguste et al., 2018; Fanti et al., 2018).

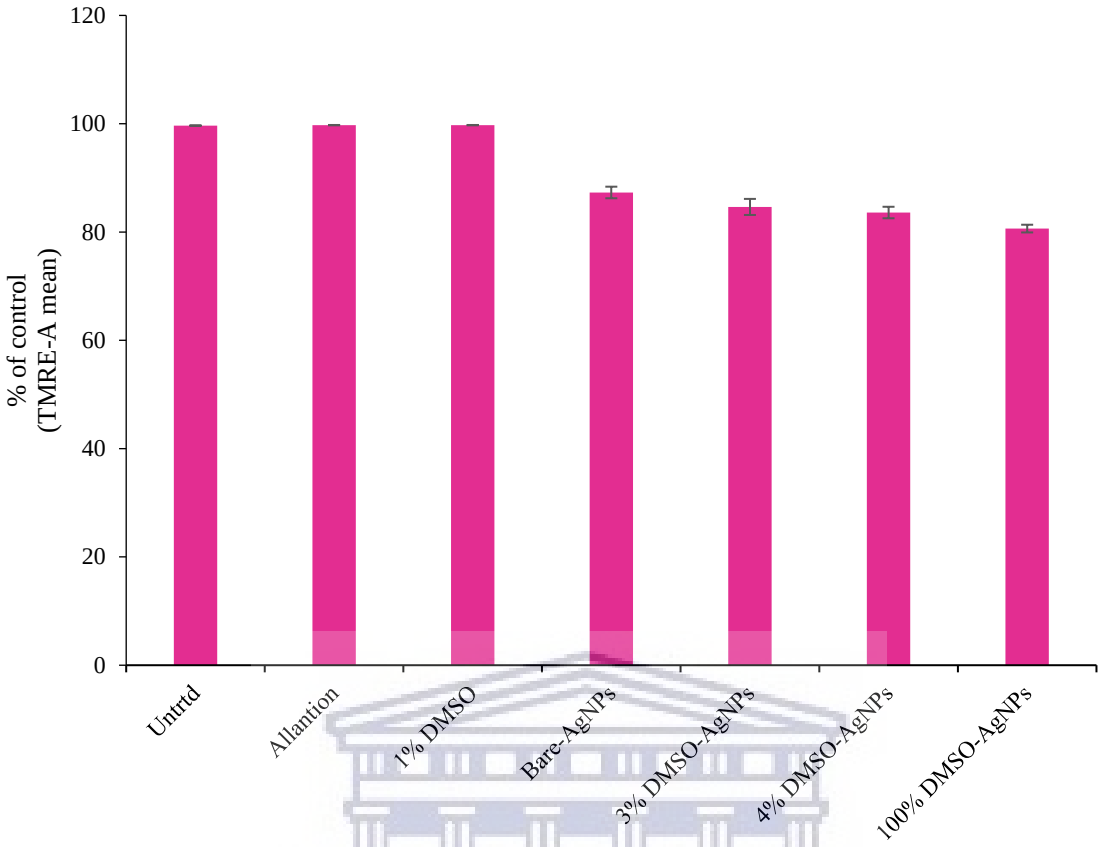

Figure 3. 29: Measurement of $\Delta\Psi_m$ on untreated cells, 1% DMSO, Allantoin and various AgNPs after 24 hours of exposure.

For the AgNPs treated cells in this study, the increase in MMP depolarization was observed in the order: bare-AgNPs < 3% DMSO-AgNPs < 4% DMSO-AgNPs < 100% DMSO-AgNPs. This indicated that the bare-AgNPs altered mitochondrial integrity less than DMSO-AgNPs. Furthermore, among the DMSO-AgNPs, the depolarization of MMP increased with DMSO concentration i.e. 3% DMSO-AgNPs < 4% DMSO-AgNPs < 100% DMSO-AgNPs. This was expected since it was already reported that elevated concentrations of DMSO increase $\Delta\Psi_m$. Also, the ROS levels of the DMSO-AgNPs increased in the same order. Indicating a direct link between generation of intracellular ROS and the increased depolarization of $\Delta\Psi_m$. This relationship was demonstrated by an independent study that reported on the cell viability, generation of ROS and MMP qualification in N9 microglial cells after exposure to trisodium citrate reduced-AgNPs. It was reported that after 24 hours of exposure, the AgNPs showed insignificantly lower cytotoxicity, low levels of intracellular ROS generation and absolutely no decrease in MMP even at higher concentrations of 50 µg/mL. These amazing results were attributed to the internalization and dissolution of AgNPs into an unreactive silver sulphide

compound (Ag_2S). Analytical microscopy revealed that Ag_2S was presented in the surface of the AgNPs and acted as a coating that blocked AgNPs cytotoxic effects (Gonzalez-Carter et al., 2017). Inversely, the ROS formation led to oxidative stress which in turn caused an increase in the depolarization of the MMP leading to their cytotoxicity. Damaged mitochondria form more ROS, while overaccumulation of ROS leads to depolarization of MMP, which results in the disturbance of oxidative phosphorylation. Thus, oxidation following treatment with AgNPs plus damaged mitochondria might be the course of the high levels of intracellular ROS as explained by Vukovic et al. (Vuković et al., 2020). However, the mitochondria of the cells treated with bare-AgNPs and DMSO-AgNPs was not entirely dysfunctional, because if it was that would have led to severe cytotoxicity. Therefore, decrease in MMPs might not always mean mitochondrial dysfunction since the cells undergoing apoptosis and necrosis also show reduced MMP (Dykens & Will, 2014).

CHAPTER 4

Conclusions and Recommendations

4.1. Conclusions

Various AgNPs were successfully synthesized using different solvents i.e dH_2O and DMSO, denoted bare-AgNPs and DMSO-AgNPs respectively via the chemical reduction route with $NaBH_4$. To confirm and monitor the synthesis as well as determining the physicochemical properties such as size, shape, distribution, stability etc, various characterizations techniques were employed. UV-vis spectra confirmed the successful synthesis by showing SPR bands within the specified range for AgNPs. The SPR bands were observed at 395, 400, 402 and 422 nm for bare-AgNPs, 3% DMSO-AgNPs, 4% DMSO-AgNPs and 100% DMSO-AgNPs respectively. FTIR spectra of all AgNPs showed a similar profile with peaks around 3300 and 1630 cm^{-1} attributed to an O−H stretch and/or N−H bend and an amine (N−H) bend respectively, characteristic of AgNPs. While 100% DMSO-AgNPs showed extra peaks at 1438 (asymmetric vibrations of $-CH_3$ groups), 1320 (symmetric vibrations of $-CH_3$ groups), 1011 (S=O bond vibration stretching modes), 951 (C−S stretch or bend), and 675 (C−S stretch or bend) cm^{-1} denoting that DMSO was adsorbed on the surface of the 100% DMSO-AgNPs. The bare-AgNPs and DMSO-AgNPs were all spherical in nature and unevenly distributed in terms of size, volume and intensity as confirmed by SAXS in conjunction with HR-TEM. With average sizes of 15, 14, 13 and 26 nm for bare-AgNPs, 3% DMSO-AgNPs, 4% DMSO-AgNPs and 100% DMSO-AgNPs respectively. DLS analysis showed that the AgNPs were polydisperse and of moderate stability with PDI values of 0992, 09599, 0937, 0.399 and zeta potentials of 20.8, 26.1, 25.5 and 16.1 mV for bare-AgNPs, 3% DMSO-AgNPs, 4% DMSO-AgNPs and 100% DMSO-AgNPs respectively.

After successfully determining the physicochemical properties of bare-AgNPs and DMSO-AgNPs, they were evaluated for their biological activities. All the AgNPs showed no anti-bacterial activity against *P. aeruginosa* and *MRSA* in the agar well diffusion method. Bacterial inhibition was only observed for bare-AgNPs, 3% DMSO-AgNPs and 4% DMSO-AgNPs against *E. coli* and *S. aureus*. 100% DMSO-AgNPs showed no anti-bacterial action against all four strands. MTT results confirmed the biocompatibility and safety of bare-AgNPs and DMSO-AgNPs since they all demonstrated no notable cytotoxicity against various human skin cells (KMST-6 and HaCaT) and Chinese hamster ovarian (CHO) cells. DF microscopy

revealed that 3% DMSO-AgNPs and 4% DMSO-AgNPs were successfully taken up by CHO, KMST-6 and HaCaT cells through endocytosis and localized in the cytoplasm, while 100% was mainly internalized in the cytoplasm and in close proximity to the nucleus. Cellular uptake of bare-AgNPs by various cells was insignificant. Bare-AgNPs and DMSO-AgNPs accelerated the rate of wound healing in KMST-6 cells by demonstrating faster cell migration rate in the scratch assay within 72 hours. Bare-AgNPs and DMSO-AgNPs did not cause a loss of cellular integrity of the KMST-6 cells since the generated intracellular ROS levels were within the accepted range and the decrease in MMP levels was insignificant. Thus, the aims and objectives of the studies were all met.

Furthermore, the 4% DMSO-AgNPs behaved better in the overall study, these AgNPs showed accelerated healing rate as demonstrated by a faster wound migration rate as well as better antibacterial activity which are the main desirable characteristics of a wound treatment therapy. Therefore, through 4% DMSO-AgNPs the goal of the study to combine both DMSO and AgNPs to create a better wound treatment formulation was achieved. DMSO and AgNPs showed their synergic antibacterial effect against various strains of bacteria and promoted cell growth of various cells. Furthermore, they were better internalized as a result of DMSO's ability to permeate membranes in synergy with the nanosize of the AgNPs. This superior cellular uptake resulted in improved interaction with the cells leading to accelerated healing an indication that the formulation might be safe to use on human cells.

4.2. Recommendations

To improve the moderate stability, wide size distribution and highly polydisperse nature of bare-AgNPs and DMSO-AgNPs, they should be synthesized in the presence of stabilizing agents such as Polyvinyl alcohol (PVA), Polyvinylpyrrolidone (PVP) etc. For example, PVA plays an important role in biomedical devices because of its good water solubility, biodegradability in human tissue, biocompatibility, low protein absorption property, and chemical resistance thus its choice. Furthermore, different concentrations as well as different time points should be evaluated to monitor the mitochondrial toxicity, cellular uptake and cell migration of these particles over time. Since time and concentration are two of the major factors that influences AgNP biological activities. Nevertheless, it is recommended that further evaluations be done with 4% DMSO-AgNPs since they show better wound healing abilities than the rest of the DMSO-AgNPs.

4.3. Future work

- MIC and MBC values of DMSO-AgNPs should be determined to identify suitable dosages for further evaluations in wound healing and management.
- Improve antibacterial properties of DMSO-AgNPs by doping with other microbial agents such as zinc, copper, cobalt or conventional antibiotics.
- Quantify cellular uptake of DMSO-AgNPs with other techniques such as inductive coupled plasma optical emission spectroscopy (ICP-OES) and/or atomic absorption spectroscopy (AAS).
- Enhance wound healing abilities of DMSO-AgNPs by embedding on a suitable polymeric scaffold to create a potential wound dressing material.

4.4. References

Adeyemi, O.S. & Adewumi, I. 2014. Biochemical Evaluation of Silver Nanoparticles in Wistar Rats. *International Scholarly Research Notices*. 2014:1–8. DOI: 10.1155/2014/196091.

Ai, X.Y., Liu, H.J., Lu, C., Liang, C.L., Sun, Y., Chen, S., Sun, B., Li, Y., et al. 2017. Phenytoin silver: A new nanocompound for promoting dermal wound healing via comprehensive pharmacological action. *Theranostics*. 7(2):425–435. DOI: 10.7150/thno.17073.

Akter, M., Sikder, M.T., Rahman, M.M., Ullah, A.K.M.A., Hossain, K.F.B., Banik, S., Hosokawa, T., Saito, T., et al. 2018. A systematic review on silver nanoparticles-induced cytotoxicity: Physicochemical properties and perspectives. *Journal of Advanced Research*. 9:1–16. DOI: 10.1016/j.jare.2017.10.008.

Al-Shmgani, H.S.A., Mohammed, W.H., Sulaiman, G.M. & Saadoon, A.H. 2017. Biosynthesis of silver nanoparticles from Catharanthus roseus leaf extract and assessing their antioxidant, antimicrobial, and wound-healing activities. *Artificial Cells, Nanomedicine and Biotechnology*. 45(6):1234–1240. DOI: 10.1080/21691401.2016.1220950.

Alexander, J.W. 2009. History of the Medical Use of Silver *. 10(3).

Aroui, S., Brahim, S., Waard, M. De & Kenani, A. 2010. Cytotoxicity, intracellular distribution and uptake of doxorubicin and doxorubicin coupled to cell-penetrating peptides in different cell lines: A comparative study. *Biochemical and Biophysical Research Communications*. 391(1):419–425. DOI: 10.1016/j.bbrc.2009.11.073.

Ashton, J.R., Castle, K.D., Qi, Y., Kirsch, D.G., West, J.L. & Badea, C.T. 2018. T h e r a n o s t i c s Dual-Energy CT Imaging of Tumor Liposome Delivery After Gold Nanoparticle-Augmented Radiation Therapy. (February). DOI: 10.7150/thno.22621.

Astley, J.P. & Levine, M. 1976. Effect of dimethyl sulfoxide on permeability of human skin In vitro. *Journal of Pharmaceutical Sciences*. 65(2):210–215. DOI: 10.1002/jps.2600650210.

Ather, S. & Harding, K.G. 2009. Wound management and dressings. *Advanced Textiles for Wound Care: A Volume in Woodhead Publishing Series in Textiles*. 3–19. DOI: 10.1533/9781845696306.1.3.

Atiba, A. & Ghazy, A. 2015. The Effects of Topical Dimethyle Sulfoxide on Second-Degree

Burn Wound Healing in Dogs. 6–12. DOI: 10.5455/ajvs.177583.

Aueviriyavit, S., Phummiratch, D. & Maniratanachote, R. 2014. Mechanistic study on the biological effects of silver and gold nanoparticles in Caco-2 cells - Induction of the Nrf2/HO-1 pathway by high concentrations of silver nanoparticles. *Toxicology Letters*. 224(1):73–83. DOI: 10.1016/j.toxlet.2013.09.020.

Auguste, M., Ciacci, C., Balbi, T., Brunelli, A., Caratto, V., Marcomini, A., Cuppini, R. & Canesi, L. 2018. Effects of nanosilver on Mytilus galloprovincialis hemocytes and early embryo development. *Aquatic Toxicology*. 203(July):107–116. DOI: 10.1016/j.aquatox.2018.08.005.

Bainbridge, P. 2013. Wound healing and the role of fibroblasts. *Journal of Wound Care*. 22(8):407–412. DOI: 10.12968/jowc.2013.22.8.407.

Bansod, S.D., Bawaskar, M.S., Gade, A.K. & Rai, M.K. 2015. Development of shampoo, soap and ointment formulated by green synthesised silver nanoparticles functionalised with antimicrobial plants oils in veterinary dermatology: Treatment and prevention strategies. *IET Nanobiotechnology*. 9(4):165–171. DOI: 10.1049/iet-nbt.2014.0042.

Barillo, D.J. & Marx, D.E. 2014. ScienceDirect Silver in medicine : A brief history BC 335 to. *Burns*. 40:S3–S8. DOI: 10.1016/j.burns.2014.09.009.

Batchelor-McAuley, C., Tschulik, K., Neumann, C.C.M., Laborda, E. & Compton, R.G. 2014. Why are silver nanoparticles more toxic than bulk silver? Towards understanding the dissolution and toxicity of silver nanoparticles. *International Journal of Electrochemical Science*. 9(3):1132–1138.

Baygar, T. 2020. Characterization of silk sutures coated with propolis and biogenic silver nanoparticles (AgNPs); an eco-friendly solution with wound healing potential against surgical site infections (SSIs). *Turkish Journal of Medical Sciences*. 50(1):258–266. DOI: 10.3906/sag-1906-48.

Becaro, A.A., Jonsson, C.M., Puti, F.C., Siqueira, M.C., Mattoso, L.H.C., Correa, D.S. & Ferreira, M.D. 2015. Toxicity of PVA-stabilized silver nanoparticles to algae and microcrustaceans. *Environmental Nanotechnology, Monitoring and Management*. 3:22–29. DOI: 10.1016/j.enmm.2014.11.002.

Bell, G. & Dn, C.D. 2017. In this issue The use of silver-based dressings in wound care. 19:56–59.

Berthet, M., Gauthier, Y., Lacroix, C., Verrier, B. & Monge, C. 2017. Nanoparticle-Based Dressing: The Future of Wound Treatment? *Trends in Biotechnology*. 35(8):770–784. DOI: 10.1016/j.tibtech.2017.05.005.

Bhatia, S. 2016. *Natural polymer drug delivery systems: Nanoparticles, plants, and algae*. DOI: 10.1007/978-3-319-41129-3.

Bhosale, M.A., Chenna, D.R. & Bhanage, B.M. 2017. Ultrasound Assisted Synthesis of Gold Nanoparticles as an Efficient Catalyst for Reduction of Various Nitro Compounds. *ChemistrySelect*. 2(3):1225–1231. DOI: 10.1002/slct.201601851.

Biranje, S.S., Madiwale, P. V., Patankar, K.C., Chhabra, R., Dandekar-Jain, P. & Adivarekar, R. V. 2019. Hemostasis and anti-necrotic activity of wound-healing dressing containing chitosan nanoparticles. *International Journal of Biological Macromolecules*. 121:936–946. DOI: 10.1016/j.ijbiomac.2018.10.125.

Capek, I. 2019. Nanotechnology and nanomaterials. *Nanocomposite Structures and Dispersions*. 1–93. DOI: 10.1016/b978-0-444-63748-2.00001-8.

Capriotti, K. & Capriotti, J.A. 2012. Dimethyl sulfoxide: History, chemistry, and clinical utility in dermatology. *Journal of Clinical and Aesthetic Dermatology*. 5(9):24–26.

Ceresa, C., Fracchia, L., Marchetti, A., Rinaldi, M. & Bosetti, M. 2019. Injectable scaffolds enriched with silver to inhibit bacterial invasion in tissue regeneration. *Materials*. 12(12). DOI: 10.3390/ma12121931.

Chakrabarti, S., Chattopadhyay, P., Islam, J., Ray, S., Raju, P.S. & Mazumder, B. 2019. Aspects of Nanomaterials in Wound Healing. 26–41. DOI: 10.2174/1567201815666180918110134.

Chen, X. & Schluesener, H.J. 2008. Nanosilver: A nanoproduct in medical application. *Toxicology Letters*. 176(1):1–12. DOI: 10.1016/j.toxlet.2007.10.004.

Chen, H., Lan, G., Ran, L., Xiao, Y., Yu, K., Lu, B., Dai, F., Wu, D., et al. 2018. A novel wound dressing based on a Konjac glucomannan/silver nanoparticle composite sponge

effectively kills bacteria and accelerates wound healing. *Carbohydrate Polymers*. 183(July 2017):70–80. DOI: 10.1016/j.carbpol.2017.11.029.

Chen, J., Li, H. & Chen, J. 2017. International Journal of Biological Macromolecules Human epidermal growth factor coupled to different structural classes of cell penetrating peptides : A comparative study. 105:336–345.

Chen, W.J., Kandasamy, K. & Chen, Y.C. 2019. Functional Gold Nanoparticles as Sensing Probes for Concanavalin A and as Imaging Agents for Cancer Cells. *ACS Applied Nano Materials*. 2(6):3348–3357. DOI: 10.1021/acsanm.9b00220.

Clement, J.L. & Jarrett, P.S. 1869. Antibacterial silver. (13):467–482.

Coates, J. 2006. Interpretation of Infrared Spectra, A Practical Approach. *Encyclopedia of Analytical Chemistry*. 1–23. DOI: 10.1002/9780470027318.a5606.

Crowley, T.E. 2020. Absorption of ultraviolet, visible, and infrared radiation. *Purification and Characterization of Secondary Metabolites*. 33–48. DOI: 10.1016/b978-0-12-813942-4.00004-8.

Daima, H.K., Selvakannan, P.R., Kandjani, A.E., Shukla, R., Bhargava, S.K. & Bansal, V. 2014. Synergistic influence of polyoxometalate surface corona towards enhancing the antibacterial performance of tyrosine-capped Ag nanoparticles. *Nanoscale*. 6(2):758–765. DOI: 10.1039/c3nr03806h.

Dayem, A.A., Kim, B., Gurunathan, S., Choi, H.Y., Yang, G., Saha, S.K., Han, D., Han, J., et al. 2014. Biologically synthesized silver nanoparticles induce neuronal differentiation of SH-SY5Y cells via modulation of reactive oxygen species, phosphatases, and kinase signaling pathways. *Biotechnology Journal*. 9(7):934–943. DOI: 10.1002/biot.201300555.

De Abreu Costa, L., Ottoni, M.H.F., Dos Santos, M.G., Meireles, A.B., De Almeida, V.G., De Fátima Pereira, W., De Avelar-Freitas, B.A. & Brito-Melo, G.E.A. 2017. Dimethyl sulfoxide (DMSO) decreases cell proliferation and TNF-α, IFN-, and IL-2 cytokines production in cultures of peripheral blood lymphocytes. *Molecules*. 22(11):1–10. DOI: 10.3390/molecules22111789.

Dhapte, V., Kadam, S., Moghe, A. & Pokharkar, V. 2014. Probing the wound healing potential

of biogenic silver nanoparticles. *Journal of Wound Care*. 23(9):431–441. DOI: 10.12968/jowc.2014.23.9.431.

Dludla, P. V., Jack, B., Viraragavan, A., Pheiffer, C., Johnson, R., Louw, J. & Muller, C.J.F. 2018. A dose-dependent effect of dimethyl sulfoxide on lipid content, cell viability and oxidative stress in 3T3-L1 adipocytes. *Toxicology Reports*. 5(September):1014–1020. DOI: 10.1016/j.toxrep.2018.10.002.

Duimel-Peeters, I., Houwing, R., Teunissen, C., Berger, M., Snoeckx, L. & Halfens., R. 2003. *A Systematic Review of the Efficacy of Topical Skin Application of Dimethyl Sulfoxide on Wound Healing and as an Anti- Inflammatory Drug*. V. 9. DOI: 10.12968/jowc.2000.9.1.25939.

Dykens, J.A. & Will, Y. 2014. *Mitochondrial Toxicity*. Third Edit ed. V. 3. Elsevier. DOI: 10.1016/B978-0-12-386454-3.00967-2.

Egerton, R.F. 2016. *Physical principles of electron therapy*. V. 7.

Egypt, Ptolemy X (XI), ancient coins index with thumbnails - WildWinds.com. n.d. Available: https://www.wildwinds.com/coins/greece/egypt/ptolemy_X/t.html [2020, September 22].

Eom, H.J. & Choi, J. 2010. p38 MAPK activation, DNA damage, cell cycle arrest and apoptosis as mechanisms of toxicity of silver nanoparticles in Jurkat T cells. *Environmental Science and Technology*. 44(21):8337–8342. DOI: 10.1021/es1020668.

European Medicines Agency. 2019. ICH guideline Q3C (R6) on impurities: Guideline for Residual Solvents. *International Conference on Harmonization of Technical Requirements for Registration of Pharmaceuticals for Human Use*. 31(December 2016):24.

Fanti, J.R., Tomiotto-Pellissier, F., Miranda-Sapla, M.M., Cataneo, A.H.D., Andrade, C.G.T. de J., Panis, C., Rodrigues, J.H. da S., Wowk, P.F., et al. 2018. Biogenic silver nanoparticles inducing Leishmania amazonensis promastigote and amastigote death in vitro. *Acta Tropica*. 178(May 2017):46–54. DOI: 10.1016/j.actatropica.2017.10.027.

Franková, J., Pivodová, V., Vágnerová, H., Juráňová, J. & Ulrichová, J. 2016. Effects of silver nanoparticles on primary cell cultures of fibroblasts and keratinocytes in a wound-healing model. *Journal of Applied Biomaterials and Functional Materials*. 14(2):e137–e142. DOI:

10.5301/jabfm.5000268.

Ghavaminejad, A., Park, C.H. & Kim, C.S. 2016. In Situ Synthesis of Antimicrobial Silver Nanoparticles within Antifouling Zwitterionic Hydrogels by Catecholic Redox Chemistry for Wound Healing Application. *Biomacromolecules*. 17(3):1213–1223. DOI: 10.1021/acs.biomac.6b00039.

GhavamiNejad, A., Rajan Unnithan, A., Ramachandra Kurup Sasikala, A., Samarikhalaj, M., Thomas, R.G., Jeong, Y.Y., Nasseri, S., Murugesan, P., et al. 2015. Mussel-Inspired Electrospun Nanofibers Functionalized with Size-Controlled Silver Nanoparticles for Wound Dressing Application. *ACS Applied Materials and Interfaces*. 7(22):12176–12183. DOI: 10.1021/acsami.5b02542.

Giri, V.P., Pandey, S., Kumari, M., Paswan, S.K., Tripathi, A., Srivastava, M., Rao, C.V., Katiyar, R., et al. 2019. Biogenic silver nanoparticles as a more efficient contrivance for wound healing acceleration than common antiseptic medicine. *FEMS Microbiology Letters*. 366(16):1–10. DOI: 10.1093/femsle/fnz201.

Goldblum, O.M., Alvarez, O.M., Mertz, P.M. & Eaglstein, W.H. 1983. Dimethyl Sulfoxide (DMSO) Does Not Affect Epidermal Wound Healing. *Proceedings of the Society for Experimental Biology and Medicine*. 172(3):301–307. DOI: 10.3181/00379727-172-41561.

Golinska, P., Wypij, M., Ingle, A.P., Gupta, I., Dahm, H. & Rai, M. 2014. Biogenic synthesis of metal nanoparticles from actinomycetes: biomedical applications and cytotoxicity. *Applied Microbiology and Biotechnology*. 98(19):8083–8097. DOI: 10.1007/s00253-014-5953-7.

Gonzalez-Carter, D.A., Leo, B.F., Ruenraroengsak, P., Chen, S., Goode, A.E., Theodorou, I.G., Chung, K.F., Carzaniga, R., et al. 2017. Silver nanoparticles reduce brain inflammation and related neurotoxicity through induction of H 2 S-synthesizing enzymes. *Scientific Reports*. 7(June 2016):1–14. DOI: 10.1038/srep42871.

Grada, A., Otero-Vinas, M., Prieto-Castrillo, F., Obagi, Z. & Falanga, V. 2017. Research Techniques Made Simple: Analysis of Collective Cell Migration Using the Wound Healing Assay. *Journal of Investigative Dermatology*. 137(2):e11–e16. DOI: 10.1016/j.jid.2016.11.020.

Gunasekaran, T., Nigusse, T. & Dhanaraju, M.D. 2011. Silver nanoparticles as real topical

bullets for wound healing. *Journal of the American College of Clinical Wound Specialists*. 3(4):82–96. DOI: 10.1016/j.jcws.2012.05.001.

Guo, W., Qiu, W., Ao, X., Li, W., He, X., Ao, L., Hu, X., Li, Z., et al. 2020. Low-concentration DMSO accelerates skin wound healing by Akt/mTOR-mediated cell proliferation and migration in diabetic mice. *British Journal of Pharmacology*. 177(14):3327–3341. DOI: 10.1111/bph.15052.

Gupta, S., Gupta, S., Jindal, N., Jindal, A. & Bansal, R. 2013. Nanocarriers and nanoparticles for skin care and dermatological treatments. *Indian Dermatology Online Journal*. 4(4):267. DOI: 10.4103/2229-5178.120635.

Gurunathan, S., Lee, K.J., Kalishwaralal, K., Sheikpranbabu, S., Vaidyanathan, R. & Eom, S.H. 2009. Antiangiogenic properties of silver nanoparticles. *Biomaterials*. 30(31):6341–6350. DOI: 10.1016/j.biomaterials.2009.08.008.

Gurunathan, S., Han, J.W., Eppakayala, V., Jeyaraj, M. & Kim, J.H. 2013. Cytotoxicity of biologically synthesized silver nanoparticles in MDA-MB-231 human breast cancer cells. *BioMed Research International*. 2013. DOI: 10.1155/2013/535796.

Hamdan, S., Pastar, I., Drakulich, S., Dikici, E., Tomic-canic, M., Deo, S. & Daunert, S. 2017. Nanotechnology-Driven Therapeutic Interventions in Wound Healing: Potential Uses and Applications. DOI: 10.1021/acscentsci.6b00371.

Hasan, S. 2014. A Review on Nanoparticles : Their Synthesis and Types. *Research Journal of Recent Sciences Res . J . Recent . Sci . Uttar Pradesh (Lucknow Campus)*. 4:1–3.

Hasan, S. 2015. A Review on Nanoparticles : Their Synthesis and Types A Review on Nanoparticles : Their Synthesis and Types. (March):7–10.

Hebeish, A., El-Rafie, M.H., EL-Sheikh, M.A., Seleem, A.A. & El-Naggar, M.E. 2014. Antimicrobial wound dressing and anti-inflammatory efficacy of silver nanoparticles. *International Journal of Biological Macromolecules*. 65:509–515. DOI: 10.1016/j.ijbiomac.2014.01.071.

Henglein, A. & Giersig, M. 1999. Formation of Colloidal Silver Nanoparticles: Capping Action of Citrate Arnim Henglein. *Journal of Physical Chemistry B*. 103(44):9533–9539. DOI:

10.1021/jp9925334.

Ho, T.-J., Jiang, S.-J., Lin, G.-H., Li, T.S., Yiin, L.-M., Yang, J.-S., Hsieh, M.-C., Wu, C.-C., et al. 2016. The In Vitro and In Vivo Wound Healing Properties of the Chinese Herbal Medicine (Jinchuang Ointment). DOI: 10.1155/2016/1654056.

Hoet, P.H.M., Brüske-Hohlfeld, I. & Salata, O. V. 2004. Nanoparticles - Known and unknown health risks. *Journal of Nanobiotechnology*. 2:1–15. DOI: 10.1186/1477-3155-2-12.

Holmila, R.J., Vance, S.A., Chen, X., Wu, H., Shukla, K., Bharadwaj, M.S., Mims, J., Wary, Z., et al. 2018. Mitochondria-targeted Probes for Imaging Protein Sulfenylation. *Scientific Reports*. 8(1):1–14. DOI: 10.1038/s41598-018-24493-x.

Hong, N.H. 2019. *Introduction to Nanomaterials : Basic Properties , Synthesis , and Characterization*. Elsevier Inc. DOI: 10.1016/B978-0-12-813934-9.00001-3.

Huang, J.T., Yang, X.X., Zeng, Q.L. & Wang, J. 2013. A simple green route to prepare stable silver nanoparticles with pear juice and a new selective colorimetric method for detection of cysteine. *Analyst*. 138(18):5296–5302. DOI: 10.1039/c3an00901g.

Huq, M.A. 2020. Green synthesis of silver nanoparticles using pseudoduganella eburnea MAHUQ-39 and their antimicrobial mechanisms investigation against drug resistant human pathogens. *International Journal of Molecular Sciences*. 21(4). DOI: 10.3390/ijms21041510.

ICH International Conference on Harmon. 2009. ICH Topic Q3C (R4) Impurities: Guideline for Residual Solvents. CPMP/ICH/283/95. 44(February 2009):1–22. Available: www.ema.europa.eu.

Jacob, S.W. & Wood, D.C. 1967. Dimethyl sulfoxide (DMSO) toxicology, pharmacology, and clinical experience. *The American Journal of Surgery*. 114(3):414–426. DOI: 10.1016/0002-9610(67)90166-3.

Jeong, J., Song, T., Chatterjee, N., Choi, I., Cha, Y.K. & Choi, J. 2018. Developing adverse outcome pathways on silver nanoparticle-induced reproductive toxicity via oxidative stress in the nematode Caenorhabditis elegans using a Bayesian network model. *Nanotoxicology*. 12(10):1182–1197. DOI: 10.1080/17435390.2018.1529835.

Jeong, Y., Lim, D.W. & Choi, J. 2014. Assessment of size-dependent antimicrobial and

cytotoxic properties of silver nanoparticles. *Advances in Materials Science and Engineering*. 2014. DOI: 10.1155/2014/763807.

Jeyaraj, M., Sathishkumar, G., Sivanandhan, G., MubarakAli, D., Rajesh, M., Arun, R., Kapildev, G., Manickavasagam, M., et al. 2013. Biogenic silver nanoparticles for cancer treatment: An experimental report. *Colloids and Surfaces B: Biointerfaces*. 106:86–92. DOI: 10.1016/j.colsurfb.2013.01.027.

Jm, H., Mn, S., Dt, U. & Sj, W. 2007. Topical silver for treating infected wounds (Review). DOI: 10.1002/14651858.CD005486.pub2.www.cochranelibrary.com.

Jonkman, J.E.N., Cathcart, J.A., Xu, F., Bartolini, M.E., Amon, J.E., Stevens, K.M. & Colarusso, P. 2014. Cell Adhesion & Migration An introduction to the wound healing assay using livecell microscopy An introduction to the wound healing assay using livecell microscopy. *Cell adhesion and migration*. 8(5):440–451. DOI: 10.4161/cam.36224.

Kalashnikova, I. & Seal, S. 2015. Nanomaterials for wound healing : scope and advancement.

Kasuya, A. & Tokura, Y. 2014. Attempts to accelerate wound healing. *Journal of Dermatological Science*. 76(3):169–172. DOI: 10.1016/j.jdermsci.2014.11.001.

Kaur, P., Sharma, A.K., Nag, D., Das, A., Datta, S., Ganguli, A., Goel, V., Rajput, S., et al. 2019. Novel nano-insulin formulation modulates cytokine secretion and remodeling to accelerate diabetic wound healing. *Nanomedicine: Nanotechnology, Biology, and Medicine*. 15(1):47–57. DOI: 10.1016/j.nano.2018.08.013.

Khan, A.U., Malik, N., Khan, M. & Hwan, M. 2017. Fungi-assisted silver nanoparticle synthesis and their applications. *Bioprocess and Biosystems Engineering*. DOI: 10.1007/s00449-017-1846-3.

Khan, A.U., Malik, N., Khan, M., Cho, M.H. & Khan, M.M. 2018. Fungi-assisted silver nanoparticle synthesis and their applications. *Bioprocess and Biosystems Engineering*. 41(1):1–20. DOI: 10.1007/s00449-017-1846-3.

Khan, S.U., Saleh, T.A., Wahab, A., Khan, M.H.U., Khan, D., Khan, W.U., Rahim, A., Kamal, S., et al. 2018. Nanosilver: New ageless and versatile biomedical therapeutic scaffold. *International Journal of Nanomedicine*. 13:733–762. DOI: 10.2147/IJN.S153167.

Khorrami, S., Zarrabi, A., Khaleghi, M., Danaei, M. & Mozafari, M.R. 2018. Selective cytotoxicity of green synthesized silver nanoparticles against the MCF-7 tumor cell line and their enhanced antioxidant and antimicrobial properties. *International Journal of Nanomedicine*. 13:8013–8024. DOI: 10.2147/IJN.S189295.

Kim, S. & Ryu, D.Y. 2013. Silver nanoparticle-induced oxidative stress, genotoxicity and apoptosis in cultured cells and animal tissues. *Journal of Applied Toxicology*. 33(2):78–89. DOI: 10.1002/jat.2792.

Kinam Park. 2014. 基因的改变NIH Public Access. *Bone*. 23(1):1–7. DOI: 10.1038/jid.2014.371.

Klasen, H.J. 2000. DOI: 10.1016/S0305-4179(99)00108-4.

Konop, M., Damps, T., Misicka, A. & Rudnicka, L. 2016. Certain Aspects of Silver and Silver Nanoparticles in Wound Care: A Minireview. *Journal of Nanomaterials*. 2016. DOI: 10.1155/2016/7614753.

Kotakadi, V.S., Gaddam, S.A., Subba Rao, Y., Prasad, T.N.V.K.V., Varada Reddy, A. & Sai Gopal, D.V.R. 2014. Biofabrication of silver nanoparticles using Andrographis paniculata. *European Journal of Medicinal Chemistry*. 73:135–140. DOI: 10.1016/j.ejmech.2013.12.004.

Kumar, D., Mutreja, I., Chitcholtan, K. & Sykes, P. 2017. Cytotoxicity and cellular uptake of different sized gold nanoparticles in ovarian cancer cells. *Nanotechnology*. 28(47). DOI: 10.1088/1361-6528/aa935e.

Kumar, S.S.D., Houreld, N.N. & Abrahamse, H. 2020. Selective laser efficiency of green-synthesized silver nanoparticles by aloe arborescens and its wound healing activities in normal wounded and diabetic wounded fibroblast cells: In vitro studies. *International Journal of Nanomedicine*. 15:6855–6870. DOI: 10.2147/IJN.S257204.

Lai, D., Liu, T., Gu, X., Chen, Y., Niu, J., Yi, L. & Chen, W. 2015. Suspension Synthesis of Surfactant-Free Cuprous Oxide Quantum Dots. *Journal of Nanomaterials*. 2015. DOI: 10.1155/2015/825021.

Lee, S.H. & Jun, B.H. 2019. Silver nanoparticles: Synthesis and application for nanomedicine. *International Journal of Molecular Sciences*. 20(4). DOI: 10.3390/ijms20040865.

Lee, H.J., Lee, S.G., Oh, E.J., Chung, H.Y., Han, S.I., Kim, E.J., Seo, S.Y., Ghim, H. Do, et al. 2011. Antimicrobial polyethyleneimine-silver nanoparticles in a stable colloidal dispersion. *Colloids and Surfaces B: Biointerfaces*. 88(1):505–511. DOI: 10.1016/j.colsurfb.2011.07.041.

Lee, J.H., Kim, H.L., Lee, M.H., You, K.E., Kwon, B.J., Seo, H.J. & Park, J.C. 2012. Asiaticoside enhances normal human skin cell migration, attachment and growth in vitro wound healing model. *Phytomedicine*. 19(13):1223–1227. DOI: 10.1016/j.phymed.2012.08.002.

Lee, S.M., Song, K.C. & Lee, B.S. 2010. Antibacterial activity of silver nanoparticles prepared by a chemical reduction method. *Korean Journal of Chemical Engineering*. 27(2):688–692. DOI: 10.1007/s11814-010-0067-0.

Li, Y., Chang, Y., Lian, X., Zhou, L., Yu, Z., Wang, H. & An, F. 2018. Silver nanoparticles for enhanced cancer theranostics: In vitro and in vivo perspectives. *Journal of Biomedical Nanotechnology*. 14(9):1515–1542. DOI: 10.1166/jbn.2018.2614.

Liang, D., Lu, Z., Yang, H., Gao, J. & Chen, R. 2016. Novel Asymmetric Wettable AgNPs/Chitosan Wound Dressing: In Vitro and in Vivo Evaluation. *ACS Applied Materials and Interfaces*. 8(6):3958–3968. DOI: 10.1021/acsami.5b11160.

Lin, J.J., Lin, W.C., Dong, R.X. & Hsu, S.H. 2012. The cellular responses and antibacterial activities of silver nanoparticles stabilized by different polymers. *Nanotechnology*. 23(6). DOI: 10.1088/0957-4484/23/6/065102.

Liu, X., Lee, P.Y., Ho, C.M., Lui, V.C.H., Chen, Y., Che, C.M., Tam, P.K.H. & Wong, K.K.Y. 2010. Silver nanoparticles mediate differential responses in keratinocytes and fibroblasts during skin wound healing. *ChemMedChem*. 5(3):468–475. DOI: 10.1002/cmdc.200900502.

Loan Khanh, L., Thanh Truc, N., Tan Dat, N., Thi Phuong Nghi, N., van Toi, V., Thi Thu Hoai, N., Ngoc Quyen, T., Thi Thanh Loan, T., et al. 2019. Gelatin-stabilized composites of silver nanoparticles and curcumin: characterization, antibacterial and antioxidant study. *Science and Technology of Advanced Materials*. 20(1):276–290. DOI: 10.1080/14686996.2019.1585131.

Loomba, L. & Scarabelli, T. 2013. Metallic nanoparticles and their medicinal potential. Part II: Aluminosilicates, nanobiomagnets, quantum dots and cochleates. *Therapeutic Delivery*. 4(9):1179–1196. DOI: 10.4155/tde.13.74.

Lu, Z., Gao, J., He, Q., Wu, J., Liang, D., Yang, H. & Chen, R. 2017. Enhanced antibacterial and wound healing activities of microporous chitosan-Ag/ZnO composite dressing. *Carbohydrate Polymers*. 156:460–469. DOI: 10.1016/j.carbpol.2016.09.051.

Mahmoud, N.N., Al-Kharabsheh, L.M., Khalil, E.A. & Abu-Dahab, R. 2019. Interaction of gold nanorods with human dermal fibroblasts: Cytotoxicity, cellular uptake, and wound healing. *Nanomaterials*. 9(8):18–20. DOI: 10.3390/nano9081131.

Maillard, J. & Hartemann, P. 2012. Silver as an antimicrobial : Facts and gaps in knowledge. (January 2014). DOI: 10.3109/1040841X.2012.713323.

Makvandi, P., Ali, G.W., Della Sala, F., Abdel-Fattah, W.I. & Borzacchiello, A. 2019. Biosynthesis and characterization of antibacterial thermosensitive hydrogels based on corn silk extract, hyaluronic acid and nanosilver for potential wound healing. *Carbohydrate Polymers*. 223(June):115023. DOI: 10.1016/j.carbpol.2019.115023.

Mannan, A., Liu, C., Arsenault, P.R., Towler, M.J., Vail, D.R., Lorence, A. & Weathers, P.J. 2010. DMSO triggers the generation of ROS leading to an increase in artemisinin and dihydroartemisinic acid in Artemisia annua shoot cultures. *Plant Cell Reports*. 29(2):143–152. DOI: 10.1007/s00299-009-0807-y.

Martínez-Rodríguez, M.A., Madla-Cruz, E., Urrutia-Baca, V.H., de la Garza-Ramos, M.A., González-González, V.A. & Garza-Navarro, M.A. 2020. Influence of Polysaccharides' Molecular Structure on the Antibacterial Activity and Cytotoxicity of Green Synthesized Composites Based on Silver Nanoparticles and Carboxymethyl-Cellulose. *Nanomaterials*. 10(6):1164. DOI: 10.3390/nano10061164.

Maurer, L.L. & Meyer, J.N. 2016. A systematic review of evidence for silver nanoparticle-induced mitochondrial toxicity. *Environmental Science: Nano*. 3(2):311–322. DOI: 10.1039/c5en00187k.

Medici, S., Peana, M., Nurchi, V.M. & Zoroddu, M.A. 2019a. Medical Uses of Silver : History , Myths , and Scienti fi c Evidence. *Journal of Medicinal Chemistry*. 62:5923–5943. DOI: 10.1021/acs.jmedchem.8b01439.

Medici, S., Peana, M., Nurchi, V.M. & Zoroddu, M.A. 2019b. Medical Uses of Silver: History, Myths, and Scientific Evidence. *Journal of Medicinal Chemistry*. 62(13):5923–5943. DOI:

10.1021/acs.jmedchem.8b01439.

Mekkawy, A.I., El-Mokhtar, M.A., Nafady, N.A., Yousef, N., Hamad, M., El-Shanawany, S.M., Ibrahim, E.H. & Elsabahy, M. 2017. In vitro and in vivo evaluation of biologically synthesized silver nanoparticles for topical applications: Effect of surface coating and loading into hydrogels. *International Journal of Nanomedicine*. 12:759–777. DOI: 10.2147/IJN.S124294.

Mihai, M.M., Dima, M.B., Dima, B. & Holban, A.M. 2019. Infection Control. 1–16.

Mohanty, S., Mishra, S., Jena, P., Jacob, B., Sarkar, B. & Sonawane, A. 2012. An investigation on the antibacterial, cytotoxic, and antibiofilm efficacy of starch-stabilized silver nanoparticles. *Nanomedicine: Nanotechnology, Biology, and Medicine*. 8(6):916–924. DOI: 10.1016/j.nano.2011.11.007.

Mohseni, M., Shamloo, A., Aghababaie, Z., Afjoul, H., Abdi, S., Moravvej, H. & Vossoughi, M. 2019. A comparative study of wound dressings loaded with silver sulfadiazine and silver nanoparticles: In vitro and in vivo evaluation. *International Journal of Pharmaceutics*. 564(April):350–358. DOI: 10.1016/j.ijpharm.2019.04.068.

Moore, T.L., Urban, D.A., Rodriguez-Lorenzo, L., Milosevic, A., Crippa, F., Spuch-Calvar, M., Balog, S., Rothen-Rutishauser, B., et al. 2019. Nanoparticle administration method in cell culture alters particle-cell interaction. *Scientific Reports*. 9(1):1–9. DOI: 10.1038/s41598-018-36954-4.

Mugade, M., Patole, M. & Pokharkar, V. 2017. Bioengineered mannan sulphate capped silver nanoparticles for accelerated and targeted wound healing: Physicochemical and biological investigations. *Biomedicine and Pharmacotherapy*. 91:95–110. DOI: 10.1016/j.biopha.2017.04.017.

Mukherji, S., Bharti, S., Shukla, G. & Mukherji, S. 2019. Synthesis and characterization of size- And shape-controlled silver nanoparticles. *Physical Sciences Reviews*. 4(1):1–73. DOI: 10.1515/psr-2017-0082.

Murugan, K., Senthilkumar, B., Senbagam, D. & Al-Sohaibani, S. 2014. Biosynthesis of silver nanoparticles using Acacia leucophloea extract and their antibacterial activity. *International Journal of Nanomedicine*. 9(1):2431–2438. DOI: 10.2147/IJN.S61779.

Naraginti, S., Kumari, P.L., Das, R.K., Sivakumar, A., Patil, S.H. & Andhalkar, V.V. 2016. Amelioration of excision wounds by topical application of green synthesized, formulated silver and gold nanoparticles in albino Wistar rats. *Materials Science and Engineering C*. 62:293–300. DOI: 10.1016/j.msec.2016.01.069.

Nath, D. & Banerjee, P. 2013. Green nanotechnology - A new hope for medical biology. *Environmental Toxicology and Pharmacology*. 36(3):997–1014. DOI: 10.1016/j.etap.2013.09.002.

Neibert, K., Gopishetty, V., Grigoryev, A., Tokarev, I., Al-Hajaj, N., Vorstenbosch, J., Philip, A., Minko, S., et al. 2012. Wound-healing with mechanically robust and biodegradable hydrogel fibers loaded with silver nanoparticles. *Advanced Healthcare Materials*. 1(5):621–630. DOI: 10.1002/adhm.201200075.

Nethi, S.K., Das, S., Patra, C.R. & Mukherjee, S. 2019. Biomaterials Science. 2652–2674. DOI: 10.1039/c9bm00423h.

Nicholls, D.G. 2004. Mitochondrial membrane potential and aging. *Aging Cell*. 3(1):35–40. DOI: 10.1111/j.1474-9728.2003.00079.x.

Niska, K., Zielinska, E., Radomski, M.W. & Inkielewicz-Stepniak, I. 2018. Metal nanoparticles in dermatology and cosmetology: Interactions with human skin cells. *Chemico-Biological Interactions*. 295:38–51. DOI: 10.1016/j.cbi.2017.06.018.

Nymark, P., Catalán, J., Suhonen, S., Järventaus, H., Birkedal, R., Clausen, P.A., Jensen, K.A., Vippola, M., et al. 2013. Genotoxicity of polyvinylpyrrolidone-coated silver nanoparticles in BEAS 2B cells. *Toxicology*. 313(1):38–48. DOI: 10.1016/j.tox.2012.09.014.

Orlowski, P., Zmigrodzka, M., Tomaszewska, E., Ranoszek-Soliwoda, K., Czupryn, M., Antos-Bielska, M., Szemraj, J., Celichowski, G., et al. 2018. Tannic acid-modified silver nanoparticles for wound healing: The importance of size. *International Journal of Nanomedicine*. 13:991–1007. DOI: 10.2147/IJN.S154797.

Oryan, A., Alemzadeh, E., Tashkhourian, J. & Nami Ana, S.F. 2018. Topical delivery of chitosan-capped silver nanoparticles speeds up healing in burn wounds: A preclinical study. *Carbohydrate Polymers*. 200(March):82–92. DOI: 10.1016/j.carbpol.2018.07.077.

Ovais, M., Ahmad, I., Khalil, A.T., Mukherjee, S., Javed, R., Ayaz, M., Raza, A. & Shinwari, Z.K. 2018. Wound healing applications of biogenic colloidal silver and gold nanoparticles: recent trends and future prospects. *Applied Microbiology and Biotechnology*. 102(10):4305–4318. DOI: 10.1007/s00253-018-8939-z.

Pacioni, N.L., Borsarelli, C.D., Rey, V. & Veglia, A. V. 2015. *Silver Nanoparticle Applications*. DOI: 10.1007/978-3-319-11262-6.

Pal, S., Nisi, R., Stoppa, M. & Licciulli, A. 2017. Silver-Functionalized Bacterial Cellulose as Antibacterial Membrane for Wound-Healing Applications. *ACS Omega*. 2(7):3632–3639. DOI: 10.1021/acsomega.7b00442.

Paladini, F. & Pollini, M. 2019. Antimicrobial silver nanoparticles for wound healing application: Progress and future trends. *Materials*. 12(16). DOI: 10.3390/ma12162540.

Parani, M., Lokhande, G., Singh, A. & Gaharwar, A.K. 2016. Engineered Nanomaterials for Infection Control and Healing Acute and Chronic Wounds. *ACS Applied Materials and Interfaces*. 8(16):10049–10069. DOI: 10.1021/acsami.6b00291.

Pastar, I., Stojadinovic, O., Yin, N.C., Ramirez, H., Nusbaum, A.G., Sawaya, A., Patel, S.B., Khalid, L., et al. 2014. Epithelialization in Wound Healing : A Comprehensive Review. 3(7):445–464. DOI: 10.1089/wound.2013.0473.

Paul, A., Ju, H., Rangasamy, S., Shim, Y. & Song, J.M. 2015. Nanosized silver (II) pyridoxine complex to cause greater inflammatory response and less cytotoxicity to RAW264.7 macrophage cells. *Nanoscale Research Letters*. 10(1). DOI: 10.1186/s11671-015-0848-9.

Pazos-Ortiz, E., Roque-Ruiz, J.H., Hinojos-Márquez, E.A., López-Esparza, J., Donohué-Cornejo, A., Cuevas-González, J.C., Espinosa-Cristóbal, L.F. & Reyes-López, S.Y. 2017. Dose-Dependent Antimicrobial Activity of Silver Nanoparticles on Polycaprolactone Fibers against Gram-Positive and Gram-Negative Bacteria. *Journal of Nanomaterials*. 2017. DOI: 10.1155/2017/4752314.

Pham, T.N., Jiang, Y.S., Su, C.F. & Jan, J.S. 2020. In situ formation of silver nanoparticles-contained gelatin-PEG-dopamine hydrogels via enzymatic cross-linking reaction for improved antibacterial activities. *International Journal of Biological Macromolecules*. 146:1050–1059. DOI: 10.1016/j.ijbiomac.2019.09.230.

Pinto, R.J.B., Bispo, D., Vilela, C., Botas, A.M.P., Ferreira, R.A.S., Menezes, A.C., Campos, F., Oliveira, H., et al. 2020. Field Imaging.

Polte, J., Tuaev, X., Wuithschick, M., Fischer, A., Thuenemann, A.F., Rademann, K., Kraehnert, R. & Emmerling, F. 2012. Formation mechanism of colloidal silver nanoparticles: Analogies and differences to the growth of gold nanoparticles. *ACS Nano*. 6(7):5791–5802. DOI: 10.1021/nn301724z.

Prakash, P., Gnanaprakasam, P., Emmanuel, R., Arokiyaraj, S. & Saravanan, M. 2013. Green synthesis of silver nanoparticles from leaf extract of Mimusops elengi, Linn. for enhanced antibacterial activity against multi drug resistant clinical isolates. *Colloids and Surfaces B: Biointerfaces*. 108:255–259. DOI: 10.1016/j.colsurfb.2013.03.017.

Raj, S., Singh, H., Trivedi, R. & Soni, V. 2020. Biogenic synthesis of AgNPs employing Terminalia arjuna leaf extract and its efficacy towards catalytic degradation of organic dyes. *Scientific reports*. 10(1):9616. DOI: 10.1038/s41598-020-66851-8.

Rajendran, N.K., Kumar, S.S.D., Houreld, N.N. & Abrahamse, H. 2018. A review on nanoparticle based treatment for wound healing. *Journal of Drug Delivery Science and Technology*. 44(January):421–430. DOI: 10.1016/j.jddst.2018.01.009.

Rangasamy, S., Tak, Y.K., Kim, S., Paul, A. & Song, J.M. 2016. Bifunctional therapeutic high-valence silver-pyridoxine nanoparticles with proliferative and antibacterial wound-healing activities. *Journal of Biomedical Nanotechnology*. 12(1):182–196. DOI: 10.1166/jbn.2016.2179.

Rashid, M.U., Bhuiyan, M.K.H. & Quayum, M.E. 2013. Synthesis of silver nano particles (Ag-NPs) and their uses for quantitative analysis of vitamin C tablets. *Dhaka University Journal of Pharmaceutical Sciences*. 12(1):29–33. DOI: 10.3329/dujps.v12i1.16297.

Roddick, J. n.d. *Open Wound: Types, Treatments, and Complications*. Available: https://www.healthline.com/health/open-wound [2021, February 22].

Rodríguez-Gattorno, G., Díaz, D., Rendón, L. & Hernández-Segura, G.O. 2002. Metallic nanoparticles from spontaneous reduction of silver(I) in DMSO. Interaction between nitric oxide and silver nanoparticles. *Journal of Physical Chemistry B*. 106(10):2482–2487. DOI: 10.1021/jp012670c.

Rosarin, F.S., Arulmozhi, V., Nagarajan, S. & Mirunalini, S. 2013. Antiproliferative effect of silver nanoparticles synthesized using amla on Hep2 cell line. *Asian Pacific Journal of Tropical Medicine*. 6(1):1–10. DOI: 10.1016/S1995-7645(12)60193-X.

Ross, D.A., Phipps, A.J. & Clarke, J.A. 1993. The use of cerium nitrate-silver sulphadiazine as a topical burns dressing. 582–584.

Roy, N., Gaur, A., Jain, A., Bhattacharya, S. & Rani, V. 2013. Green synthesis of silver nanoparticles: An approach to overcome toxicity. *Environmental Toxicology and Pharmacology*. 36(3):807–812. DOI: 10.1016/j.etap.2013.07.005.

Russell, A.D. & Hugo, W.B. 1994. 7 Antimicrobial Activity and Action of. 31.

S Sibuyi, N.R., Thovhogi, N., Gabuza, K.B., Meyer, M.D., Drah, M., Onani, M.O., Skepu, A., Madiehe, A.M., et al. 2017. Peptide-functionalized nanoparticles for the selective induction of apoptosis in target cells. *Nanomedicine*. 12(14):1631–1645. DOI: 10.2217/nnm-2017-0085.

Sadowska-Bartosz, I., Paczka, A., Moloń, M. & Bartosz, G. 2013. Dimethyl sulfoxide induces oxidative stress in the yeast Saccharomyces cerevisiae. *FEMS Yeast Research*. 13(8):820–830. DOI: 10.1111/1567-1364.12091.

Saldmann, F., Saldmann, A. & Lemaire, M.C. 2020. Characterization and internalization of nanodiamond – trehalose conjugates into mammalian fibroblast cells of naked mole rat. 151–157.

Sasidharan, S., Raj, S. & Sonawane, S. 2019. *Nanomaterial Synthesis : Chemical and Biological Route and Applications*. Elsevier Inc. DOI: 10.1016/B978-0-12-815751-0.00002-X.

Savic, V.L., Nikolic, V.D., Arsic, I.A., Stanojevic, L.P., Najman, S.J., Stojanovic, S. & Mladenovic-Ranisavljevic, I.I. 2015. Comparative Study of the Biological Activity of Allantoin and Aqueous Extract of the Comfrey Root. *Phytotherapy Research*. 29(8):1117–1122. DOI: 10.1002/ptr.5356.

Schnablegger, H. & Singh, Y. 2013. The SAXS Guide. *Anton Paar GmbH*. 1–99.

Sciences, O.H. 2005. DMSO: Applications in Plastic Surgery. 201–209.

Shanmuganathan, R., Karuppusamy, I., Saravanan, M., Muthukumar, H., Ponnuchamy, K., Ramkumar, V.S. & Pugazhendhi, A. 2019. Synthesis of Silver Nanoparticles and their Biomedical Applications - A Comprehensive Review. *Current Pharmaceutical Design*. 25(24):2650–2660. DOI: 10.2174/1381612825666190708185506.

Shao, J., Wang, B., Li, J., Jansen, J.A., Walboomers, X.F. & Yang, F. 2019. Antibacterial effect and wound healing ability of silver nanoparticles incorporation into chitosan-based nanofibrous membranes. *Materials Science and Engineering C*. 98(January):1053–1063. DOI: 10.1016/j.msec.2019.01.073.

Singh, M. 2016. Elucidation of biogenic silver nanoparticles susceptibility towards Escherichia coli: An investigation on the antimicrobial mechanism. *IET Nanobiotechnology*. 10(5):276–280. DOI: 10.1049/iet-nbt.2015.0063.

Singh, R.P. & Ramarao, P. 2012. Cellular uptake, intracellular trafficking and cytotoxicity of silver nanoparticles. *Toxicology Letters*. 213(2):249–259. DOI: 10.1016/j.toxlet.2012.07.009.

Singla, R., Soni, S., Kulurkar, P.M., Kumari, A., Mahesh, S., Patial, V., Padwad, Y.S. & Yadav, S.K. 2017. In situ functionalized nanobiocomposites dressings of bamboo cellulose nanocrystals and silver nanoparticles for accelerated wound healing. *Carbohydrate Polymers*. 155:152–162. DOI: 10.1016/j.carbpol.2016.08.065.

Sood, R. & Chopra, D.S. 2018. Optimization of reaction conditions to fabricate Ocimum sanctum synthesized silver nanoparticles and its application to nano-gel systems for burn wounds. *Materials Science and Engineering C*. 92(October 2017):575–589. DOI: 10.1016/j.msec.2018.06.070.

Srikar, S.K., Giri, D.D., Pal, D.B., Mishra, P.K. & Upadhyay, S.N. 2016. Green Synthesis of Silver Nanoparticles: A Review. *Green and Sustainable Chemistry*. 06(01):34–56. DOI: 10.4236/gsc.2016.61004.

Syafiuddin, A., Salmiati, Salim, M.R., Beng Hong Kueh, A., Hadibarata, T. & Nur, H. 2017. A Review of Silver Nanoparticles: Research Trends, Global Consumption, Synthesis, Properties, and Future Challenges. *Journal of the Chinese Chemical Society*. 64(7):732–756. DOI: 10.1002/jccs.201700067.

Tejiram, S., Kavalukas, S.L., Shupp, J.W. & Barbul, A. 2016. *Wound healing*. V. 1. Elsevier

Ltd. DOI: 10.1016/B978-1-78242-455-0.00001-X.

The Skin and Wound Healing - Physiopedia. n.d. Available: https://www.physiopedia.com/The_Skin_and_Wound_Healing [2020, October 18].

Tonda-Turo, C., Ruini, F., Argentati, M., Di Girolamo, N., Robino, P., Nebbia, P. & Ciardelli, G. 2016. Porous CS based membranes with improved antimicrobial properties for the treatment of infected wound in veterinary applications. *Materials Science and Engineering C*. 60:416–426. DOI: 10.1016/j.msec.2015.11.065.

Tran, Q.H., Nguyen, V.Q. & Le, A. n.d. Corrigendum : Silver nanoparticles : synthesis , properties , toxicology ,.

Vanitha, G., Rajavel, K., Boopathy, G., Veeravazhuthi, V. & Neelamegam, P. 2017. Physiochemical charge stabilization of silver nanoparticles and its antibacterial applications. *Chemical Physics Letters*. 669(3):71–79. DOI: 10.1016/j.cplett.2016.11.037.

Venugopal, K., Rather, H.A., Rajagopal, K., Shanthi, M.P., Sheriff, K., Illiyas, M., Rather, R.A., Manikandan, E., et al. 2017. Synthesis of silver nanoparticles (Ag NPs) for anticancer activities (MCF 7 breast and A549 lung cell lines) of the crude extract of Syzygium aromaticum. *Journal of Photochemistry and Photobiology B: Biology*. 167(January):282–289. DOI: 10.1016/j.jphotobiol.2016.12.013.

Vijayakumar, V., Samal, S.K., Mohanty, S. & Nayak, S.K. 2019. Recent advancements in biopolymer and metal nanoparticle-based materials in diabetic wound healing management. *International Journal of Biological Macromolecules*. 122:137–148. DOI: 10.1016/j.ijbiomac.2018.10.120.

Vowden, P. 2011. Hard- to- heal Wounds. *Wound International*. 2(4):1–6. Available: http://www.woundsinternational.com/media/issues/514/files/content_10140.pdf.

Vuković, B., Milić, M., Dobrošević, B., Milić, M., Ilić, K., Pavičić, I., Šerić, V. & Vrček, I.V. 2020. Surface stabilization affects toxicity of silver nanoparticles in human peripheral blood mononuclear cells. *Nanomaterials*. 10(7):1–18. DOI: 10.3390/nano10071390.

Wei, L., Lu, J., Xu, H., Patel, A., Chen, Z.S. & Chen, G. 2015. Silver nanoparticles: Synthesis, properties, and therapeutic applications. *Drug Discovery Today*. 20(5):595–601. DOI:

10.1016/j.drudis.2014.11.014.

Wen, J., Tong, Y. & Zu, Y. 2015. Low Concentration DMSO Stimulates Cell Growth and In vitro Transformation of Human Multiple Myeloma Cells. *British Journal of Medicine and Medical Research*. 5(1):65–74. DOI: 10.9734/bjmmr/2015/5276.

White, R.J. & Cooper, R. 2003. Silver sulphadiazine : A review of the evidence.

World health organization. n.d. *Diabetes*. Available: https://www.who.int/news-room/fact-sheets/detail/diabetes [2021, February 17].

Worsch, P.M. 2015. Discussing the principles of SAXS. 1–85.

Wu, J., Zheng, Y., Wen, X., Lin, Q., Chen, X. & Wu, Z. 2014. Silver nanoparticle/bacterial cellulose gel membranes for antibacterial wound dressing: Investigation in vitro and in vivo. *Biomedical Materials (Bristol)*. 9(3). DOI: 10.1088/1748-6041/9/3/035005.

Xu, S., Wang, H., Cheng, M., Hu, J., Wang, C. & Han, C.C. 2013. Preparation and optimization of silver nanoparticles embedded electrospun membrane for implant associated infections prevention. *ACS Applied Materials and Interfaces*. 5(21):11014–11021. DOI: 10.1021/am403250t.

You, C., Han, C., Wang, X., Zheng, Y., Li, Q., Hu, X. & Sun, H. 2012. The progress of silver nanoparticles in the antibacterial mechanism, clinical application and cytotoxicity. *Molecular Biology Reports*. 39(9):9193–9201. DOI: 10.1007/s11033-012-1792-8.

Yu, K., Lu, F., Li, Q., Chen, H., Lu, B., Liu, J., Li, Z., Dai, F., et al. 2017. In situ assembly of Ag nanoparticles (AgNPs) on porous silkworm cocoon-based would film: Enhanced antimicrobial and wound healing activity. *Scientific Reports*. 7(1):1–13. DOI: 10.1038/s41598-017-02270-6.

Yuan, C., Gao, J., Guo, J., Bai, L., Marshall, C., Cai, Z., Wang, L. & Xiao, M. 2014. Dimethyl sulfoxide damages mitochondrial integrity and membrane potential in cultured astrocytes. *PLoS ONE*. 9(9). DOI: 10.1371/journal.pone.0107447.

Zhang, X.F., Liu, Z.G., Shen, W. & Gurunathan, S. 2016. Silver nanoparticles: Synthesis, characterization, properties, applications, and therapeutic approaches. *International Journal of Molecular Sciences*. 17(9). DOI: 10.3390/ijms17091534.

Zhao, J., Liu, P., Ma, J., Li, D., Yang, H., Chen, W. & Jiang, Y. 2019. Enhancement of radiosensitization by silver nanoparticles functionalized with polyethylene glycol and aptamer As1411 for glioma irradiation therapy. *International Journal of Nanomedicine*. 14:9483–9496. DOI: 10.2147/IJN.S224160.

Ziabka, M., Dziadek, M. & Królicka, A. 2019. Biological and physicochemical assessment of middle ear prosthesis. *Polymers*. 11(1). DOI: 10.3390/polym11010079.

Zorova, L.D., Popkov, V.A., Plotnikov, E.J., Silachev, D.N., Pevzner, I.B., Jankauskas, S.S., Zorov, S.D., Babenko, V.A., et al. 2018. Functional Significance of the Mitochondrial Membrane Potential. *Biochemistry (Moscow) Supplement Series A: Membrane and Cell Biology*. 12(1):20–26. DOI: 10.1134/S1990747818010129.